November 2015

Process-Structure-Property Relationship in Ultra High Molecular Weight Polytetrafluoroethylene and Double Network Epoxies

Ranadip Ganguly
University of Massachusetts Amherst

PROCESS-STRUCTURE-PROPERTY RELATIONSHIP IN ULTRA HIGH MOLECULAR WEIGHT PTFE AND DOUBLE NETWORK EPOXIES

A Dissertation Presented

by

RANADIP GANGULY

Submitted to the Graduate School of the
University of Massachusetts, Amherst in partial fulfillment
of the degree requirements for the degree of

DOCTOR OF PHILOSOPHY

September 2015

Polymer Science and Engineering

PROCESS-STRUCTURE-PROPERTY RELATIONSHIP IN ULTRA HIGH MOLECULAR WEIGHT PTFE AND DOUBLE NETWORK EPOXIES

A Dissertation Presented

by

RANADIP GANGULY

Approved as to style and content by:

_____

Alan J. Lesser, Chair

_____

E. Bryan Coughlin, Member

_____

H. Henning Winter, Member

_____

David Hoagland, Department Head
Polymer Science and Engineering

DEDICATION

To my beloved family

ACKNOWLEDGMENTS

I would like to express my immeasurable gratitude to Prof. Alan J. Lesser for his incredible support and mentorship. His utmost commitment to the scientific and professional development of his students is commendable. He taught me to solve complicated problems by conducting a minimum number of simple and well-structured experiments. He helped me develop an aggressive and relentless attitude towards problem solving. I immensely enjoyed the environment of intellectual freedom and flexibility that he fostered in the group.

My sincere thank goes to Prof. E. Bryan Coughlin and Prof. Henning H. Winter for serving on my committee. They provided me numerous suggestions during my work that greatly improved the quality of this dissertation and helped me to look at my research in a new light. I consider it a great privilege for me to have such accomplished scientists on my committee.

I am extremely grateful to Dr. Naveen Singh and Dr. Jan Kalfus for providing valuable inputs during my first year in Lesser group. The discussions I had with them helped me to grow as a scientist. I would like to thank past members of the Lesser group Polina and Henry for all their help. The present Lesser group Angela, Brian, Connor, Madhura, Nihal, Silas, Matt are a great bunch and we all had so much fun together both inside and outside the lab.

I would like to thank CUMIRP Cluster M, Cluster F, BASF and St. Gobain for funding my research.

Finally, I would like to thank my family-Mr. Ramen Ganguly (Dad), Mrs. Krishna Ganguly (Mom), and Rudradeep Ganguly (Brother) without whose support, encouragement and inspiration nothing would have been possible. Further, I would like to thank my wife-Sourima for her ever cheerful and ever supportive presence. She sits by me as I write.

ABSTRACT

PROCESS-STRUCTURE-PROPERTY RELATIONSHIP IN ULTRA HIGH MOLECULAR WEIGHT PTFE AND DOUBLE NETWORK EPOXIES

SEPTEMBER 2015

RANADIP GANGULY, B.S., UNIVERSITY COLLEGE OF SCIENCE AND TECHNOLOGY, CALCUTTA UNIVERSITY

M.S., UNIVERSITY OF MASSACHUSETTS AMHERST

Ph.D., UNIVERSITY OF MASSACHUSETTS AMHERST

Directed by: Professor Alan J. Lesser

The focus of this dissertation is to develop a fundamental understanding of process-structure-property relationship in two different classes of polymers: semi-crystalline Ultra High Molecular Weight Polytetrafluoroethylene (UHMWPTFE) and amorphous glassy double network (DN) epoxies. Conventional melt processing techniques such as extrusion and injection molding cannot be applied to UHMWPTFE due to its very high melt viscosity (10^{10}-10^{11} poise). Therefore, UHMWPTFE is industrially processed by a modified metallurgy technology-sintering. However, the fundamental mechanism for UHMWPTFE sintering is unknown. Further, this process is highly time consuming, cost inefficient and hinders the recyclability of the material. The first part of this dissertation aims at developing experimental techniques for studying the sintering process in-situ and thereby elucidates the molecular mechanism associated with UHMWPTFE sintering. Further, the effect of different fluoropolymer additives and process conditions on the sintering behavior will be studied. The second part of this dissertation aims at developing asymmetric double network epoxies where the two networks are distinct both in terms of chemical stiffness and crosslink density and correlating this complex network architecture with thermal and non-linear mechanical properties.

TABLE OF CONTENTS

Page

LIST OF TABLES

LIST OF FIGURES

LIST OF ABBREVIATIONS

UHMWPTFE	Ultra High Molecular Weight Polytetrafluoroethylene
SALS	Small Angle Light Scattering
DSC	Differential Scanning Calorimetry
TMA	Thermal Mechanical Analyzer
DN	Double Network
UHMWPE	Ultra High Molecular Weight
SEM	Scanning Electron Microscopy
WAXS	Wide Angle X-Ray Scattering
sPS	Syndiotactic Polystyrene
PET	Polyethylene terephthalate
GPC	Gel Permeation Chromatography
AF	Anisotropy Factor
DGEBA	Bisphenol A diglycidyl ether
DDS	4,4’ Diaminodiphenylsulfone
EDA	Ethylene diamine
ASTM	American Standard Test Method

LIST OF SYMBOLS

G_R	Strain hardening modulus
K_{IC}	Fracture Toughness
Tg	Glass transition temperature
Ec	Cohesive energy density
ΔHc	Enthalpy of crystallization
ΔHm	Enthalpy of melting
σy	Yield stress
σr	Rejuvenated stress
εb	Strain at break
Mc	Molecular weight between crosslinks
E	Young's modulus
σt	True stress
λ	Compression ratio
Kq	Fracture toughness
Pc	Critical load
f(x)	Geometric factor
Me	Epoxy equivalent weight of the epoxide monomer
Φx	Molar fraction of amine hydrogens from x-functional amine

CHAPTER 1

INTRODUCTION

1.1 Overview

The focus of this dissertation is to develop a fundamental understanding of process-structure-property relationship in two different classes of polymers: semi-crystalline Ultra High Molecular Weight Polytetrafluoroethylene (UHMWPTFE) and amorphous glassy epoxies.

Conventional melt processing techniques such as extrusion and injection molding cannot be applied to Ultra High Molecular Weight PTFE because of its high melt viscosity (10^{10}-10^{11} poise)[1]. Industrially, PTFE is processed by semi-continuous melt extrusion [2,3]or compaction (pre-forming) of PTFE molding powder at room temperature followed by sintering [4,5,6,7,8]. Preforming consists of room temperature compaction of PTFE molding powder to form a green part which has sufficient strength for proper handling. Parameters critical to the pre-forming step include pre-forming temperature and pressure. Sintering involves heating the preform above its melting temperature, dwelling at that temperature for a specified time followed by slow cooling to room temperature. This leads to the formation of a homogeneous part with improved mechanical integrity[1]. The sintering process is associated with particle coalescence and void elimination. However, the driving force behind particle coalescence and the molecular processes associated with inter-particle coalescence is not understood. Moreover, UHMWPTFE exhibits very poor re-sintering characteristics inhibiting recycling.

The first part of the dissertation develops experimental techniques for in-situ monitoring of the sintering process at different length scales and thereby elucidate the

molecular mechanism associated with sintering. Thermo-mechanical analyzer in the dynamic mode has been used to probe the complex viscoelastic response of the melt by the application of an oscillatory loading of low amplitude. Further, the evolution of residual melt order has been examined in-situ by using high temperature X-ray scattering studies and Small Angle Light Scattering studies (SALS). The melt structure evolution has simultaneously been characterized by employing a cyclic thermal loading profile within the DSC and TMA. Further, non-standard compression testing has been used as a tool for probing the sintering process at the molecular level.

The second part of the dissertation focuses on understanding the effect of different fluoropolymer additives, particle size distribution and processing conditions on the sintering kinetics of UHMWPTFE. Further, a secondary objective of this work is to identify strategies that might enhance the recyclability of UHMWPTFE. Two types of fluoropolymer additives will be studied. Firstly, a lower molecular weight PTFE fraction will be homogeneously mixed with UHMWPTFE over a composition range and the effect of the lower molecular weight fraction on the sintering kinetics of UHMWPTFE will be studied. Secondly, UHMWPTFE regrind powder will be homogeneously mixed with UHMWPTFE virgin powder and the effect of regrind fraction on the sintering kinetics will be studied. Further, the effect of reducing the particle size of regrind fraction on the sintering kinetics will be investigated. The kinetics of sintering will be studied in-situ by monitoring the storage modulus evolution as a function of sintering time and the kinetics will be quantified by the absolute value of the storage modulus and its rate of growth. Further, the dimension change of the billet in the machine direction will be monitored in-situ.

The third part of the dissertation involves developing Asymmetric Double Network (DN) epoxies where the two networks will be distinct both in terms of their chemical stiffness and crosslink density. Asymmetric Double Network (DN) epoxies have be formulated using miscible stoichiometric blends of amines following a controlled three stage cure schedule. The widely different reactivities of the aromatic and aliphatic amines aided in sequential network formation leading to the development of Double Networks where the two networks will be different both in terms of their backbone stiffness and in terms of crosslink density. The study correlates these complex network architectures with non-linear mechanical properties such as strain hardening modulus (G_R) and important engineering properties such as fracture toughness (K_{IC}) of the neat resin. Further, this study will help in understanding the effect of network polydispersity on the non-linear mechanical properties by comparing the asymmetric DNs corresponding single network shaving

1.2 Background

1.2.1 Asymmetric Double Network epoxies

Epoxies are one of the thermosets commonly employed in coatings, adhesives, electronics, and aerospace applications. They are known for their small cure shrinkage, good chemical and creep resistance, as well as broad service temperature range. However, they are susceptible to brittle failure due to highly crosslinked network structures[9]. Moreover, certain applications require high thermal stability and high fracture toughness simultaneously but conventionally it has been difficult to achieve high fracture toughness in high T_g systems[10-12].

Most epoxy formulations found in the open literature have glass transition temperatures above room temperature. The resins are typically prepared by curing a difunctional epoxide diglycidyl ether of bisphenol A (DGEBA) with a single aliphatic or aromatic diamine[9,13-16]. Few studies have investigated the use of miscible blends of amines with different molecular weights and functionalities[17-27]. For example, symmetric double network epoxies with highly tunable thermal and mechanical properties have been prepared by sequentially reacting stoichiometric blends of an aliphatic and aromatic curing agent[26]. Further, pre-stressed double network epoxies with improved fracture toughness have been developed and characterized[28]. There are even fewer reports on homogenous mixtures of epoxide monomers[29,30]. However, there is no previous work that investigates the effect of asymmetric Double Network (DN) on the thermal and mechanical properties of epoxy resins. An asymmetric DN system is one which consists of two networks having different crosslink densities.

Asymmetric DN hydrogels are developed by Gong and coworkers as a potential candidate for artificial soft tissues[31]. Formed via radical chemistry, they exhibit excellent strength and toughness even at 90 wt% water content. During their synthesis, a highly crosslinked polyelectrolyte network is swollen with an aqueous solution of monomer and crosslinker for a lightly crosslinked neutral polymer network. Due to isotropic expansion, the polyelectrolyte chains are merely extended and have no preferred orientation.

Gong and coworkers observed that a high molar ratio of second component to the first is needed to obtain the unusual synergistic effect from the two fragile polymer networks[31]. Chain entanglement has been related to load transfer within the matrix[32]. The toughening mechanism is associated with microscale fragmentation of highly crosslinked

polyelectrolyte, which improves energy dissipation during deformation[32]. The breakdown of the more brittle component has also been related to large strain hysteresis[33] and necking[34]. The approach has recently been utilized to toughen elastomers[35]. However, similar investigation using thermosets or systems with glass transition temperatures above room temperature has not been reported. The objective of the current study is to formulate asymmetric DN epoxies and correlate network architecture with non-linear mechanical properties i.e. fracture toughness and post yield response in uniaxial compression testing.

The linear, yield, and fracture behaviors of epoxies have been investigated in the past decades[10,36,37]. Shown in Figure 1.1 is a typical stress-strain curve of glassy epoxy tested in compression. The elastic modulus is a statistically averaged linear property associated with molecular packing[37]. The modulus is influenced by thermal treatment or physical aging[36]. Yielding is considered the onset of plastic deformation. The process is described as thermally activated[36]. A generalized yield criteria is proposed based on Eyring flow model and von Mises criterion to predict the effects of stress states, strain rate, test temperature, crosslinker functionalities, and crosslink densities[19]. The activation volume stays the same for all the controlled epoxy networks studied except for the most densely crosslinked. In contrast, the internal friction coefficient is insensitive to molecular structure and strain rate. The yield strength of aliphatic and aromatic epoxies with various crosslink densities collapse together when normalized by the cohesive energy density (E_c), and plotted against test temperature normalized by T_g[22,23]. The correlation suggests that E_c and T_g are molecular parameters that govern yielding.

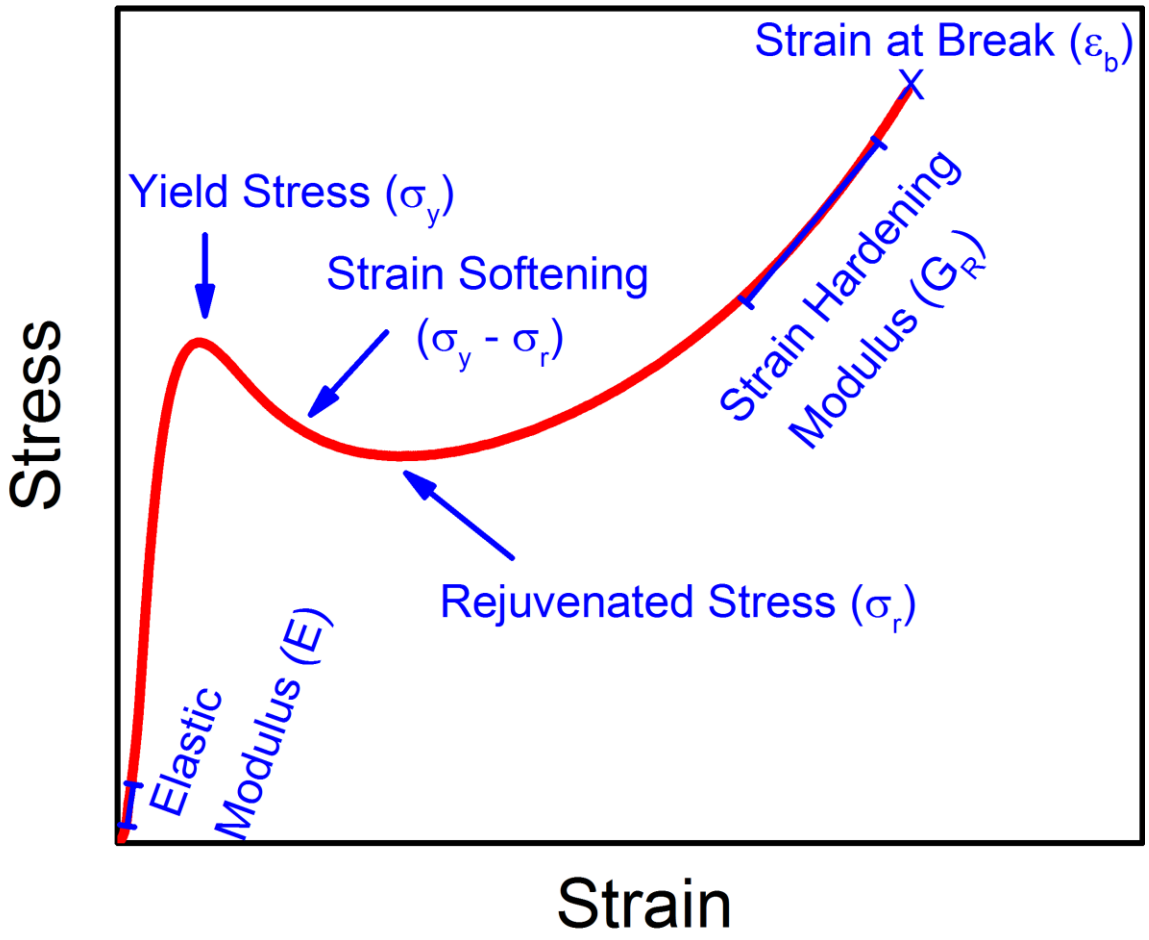

Figure-1-1: Typical stress-strain curve of glassy epoxy tested in compression

Fracture toughness is an important engineering property used to evaluate materials for structural applications[10,11]. The testing measures the energy needed to propagate a sharp precrack by unit area. A highly crosslinked epoxy tends to have high T_g and yield stress but low toughness. The diminished energy dissipation is due to small process zone or damage-accumulation region in front of the crack tip[10-12].

The evolution of yield stress, strain softening, rejuvenated stress, and strain hardening modulus during network formation has recently been reported for epoxies cured with ethylene diamine[38]. Systematic changes are also observed for epoxies cured with two miscible amines in different molar ratios[26] . However, it is unclear how these non-linear mechanical behaviors are affected by more complex network architectures such as asymmetric DNs.

The objective of the current research is to engineer asymmetric DN epoxies and correlate network architecture to non-linear mechanical properties such as strain hardening modulus and fracture toughness.

1.2.2 Sintering of Ultra High Molecular Weight polymers

Ultra High Molecular Weight (UHMW) semi-crystalline polymers e.g. UHMW Polyethylene, UHMW Polypropylene, UHMW Polytetrafluoroethylene cannot be processed by conventional melt-processing techniques such as extrusion and injection molding owing to their extremely high melt viscosities. Therefore, they are processed by powder processing technique that involves cold compaction or preforming of the polymeric powder under pressure followed by free sintering of the preforms above their melting point. There are several critical process parameters that needs to be carefully

controlled for optimum product performance. Critical pre-forming parameters include the preforming pressure, rate of application of pressure and preforming temperature. While the sintering process is governed by the sintering temperature, the dwell time and the cooling rate. Sintering of polymers is a highly complicated process as it is associated with polymer melting, inter-particle coalescence and void elimination followed by crystallization. Therefore, optimization of the sintering process necessitates careful consideration of all these processes. In other words, obtaining a fundamental understanding of the sintering process is key to efficient process optimization and ultimate product performance.

UHMWPE shows high abrasion resistance, low coefficient of friction, good chemical and stress cracking resistance and exceptional resistance at cryogenic temperatures. Consequently, it has found applications in electrical, coal and mining, shipbuilding, biomedical and textile industries[39]. Jog[39] studied the sintering behavior of two grades of UHMWPE having differences in particles characteristics i.e. both the grades had spherical particles but one had a smooth surface while the other had rough surface. The preforming parameters and the sintering parameters were kept constant. However, the two grades showed differences in green densities, sintering behavior and the ultimate strength development process. The observed differences were attributed to the differences in particle characteristics. The sintering process or the particle coalescence could not be explained on the basis of Frenkel's model that describes the early stages of viscous coalescence. The Frenkel model explains coalescence of two spheres by Newtonian viscous flow. The model assumes coalescence to occur by mutual interpenetration of chains. There are some reports where UHMWPE having weight

average molecular weight of 100,000 has been processed by under high pressures. The material was compression molded at 149-204^{o}C by applying pressure as high as 80,000 psi. The high pressure processing led to increased tensile modulus[40]. However, the most widely used processing technique for UHMWPE is cold compaction followed by elevated temperature free sintering. The sintering process is highly time-consuming and wasteful primarily due to lack of optimization i.e. improper choice of preforming and sintering parameters. Therefore, the first step towards efficient optimization involves understanding the time evolution of UHMWPE melt. It has been shown that the melting of semi-crystalline polymers is not only dependent on the crystal lamellar thickness but it also depends on the topological constraints in the amorphous regions[41].

Polytetrafluoroethylene (PTFE) is a fluoropolymer with many outstanding properties including excellent thermal stability, chemical inertness and very low coefficient of friction, making it suitable for a wide range of applications[1].

Conventional melt processing techniques such as extrusion and injection molding cannot be applied to Ultra High Molecular Weight PTFE resulting from its very high melt viscosity (10^{10}-10^{11} poise)[1]. Industrially, PTFE is processed by semi-continuous melt extrusion [2,3]or compaction (pre-forming) of PTFE molding powder at room temperature followed by sintering[4,5,6,7,8]. Preforming consists of room temperature compaction of PTFE molding powder to form a green part which has sufficient strength for proper handling. Parameters critical to the pre-forming step include pre-forming temperature and pressure. The powder is harder below the transition temperature of 19^{o}C and does not respond well to pressure leading to poor green strength and likelihood of cracking during sintering. In order to avoid these problems preforming should be done above 21^{o}C. PTFE

exhibits higher plastic flow as the temperature increases therefore it can be preformed at lower pressures. In general, the tensile strength, elongation, dielectric strength, compression ratio and specific gravity increases with increase in preforming pressure. Sintering involves heating a preform above its melting temperature, dwelling at that temperature for a specified time followed by slow cooling to room temperature. This leads to the formation of a homogeneous part with improved mechanical integrity[1]. Figure 1.1 shows a schematic of the preforming and sintering process in UHMWPTFE[1] while Figure 1.2 shows the coalescence of UHMWPTFE particles as a function of sintering time[1].

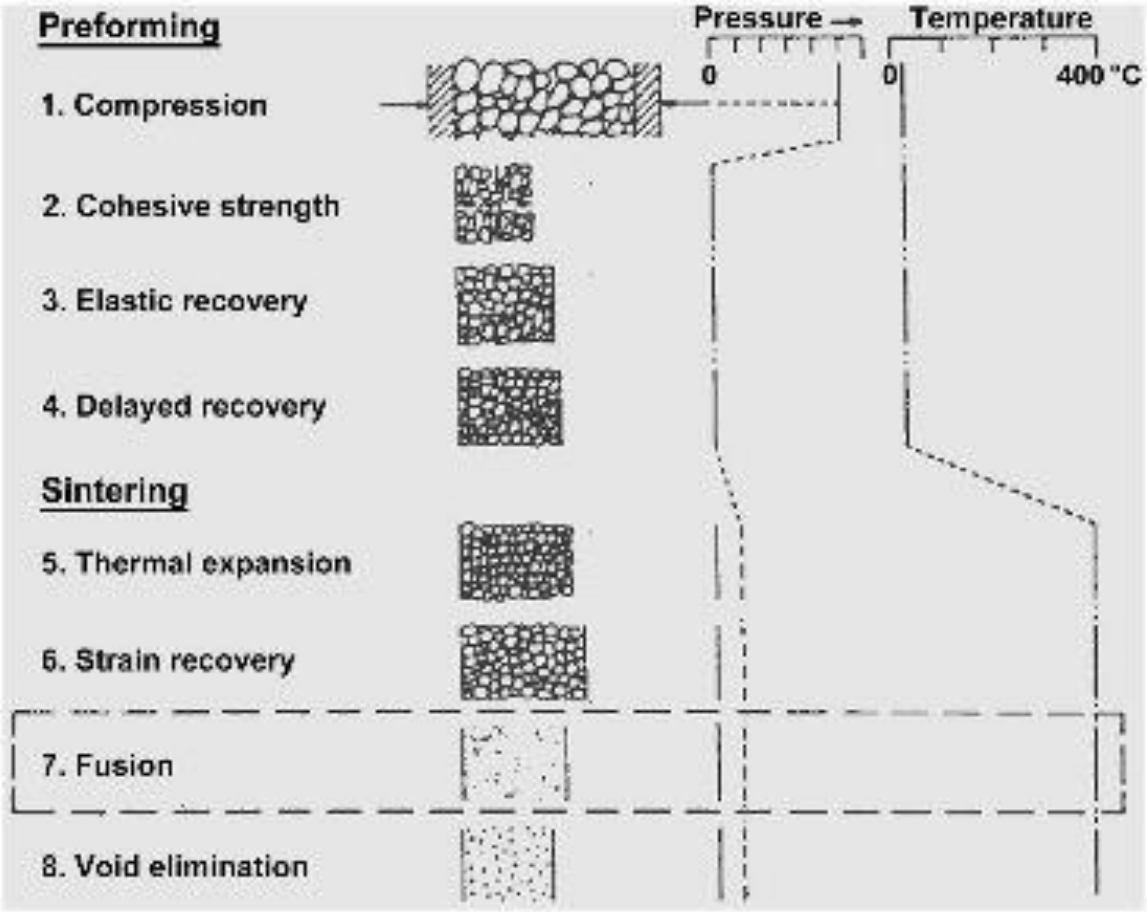

Figure 1-2: Schematic illustration of preforming and sintering process in UHMWPTFE[1]

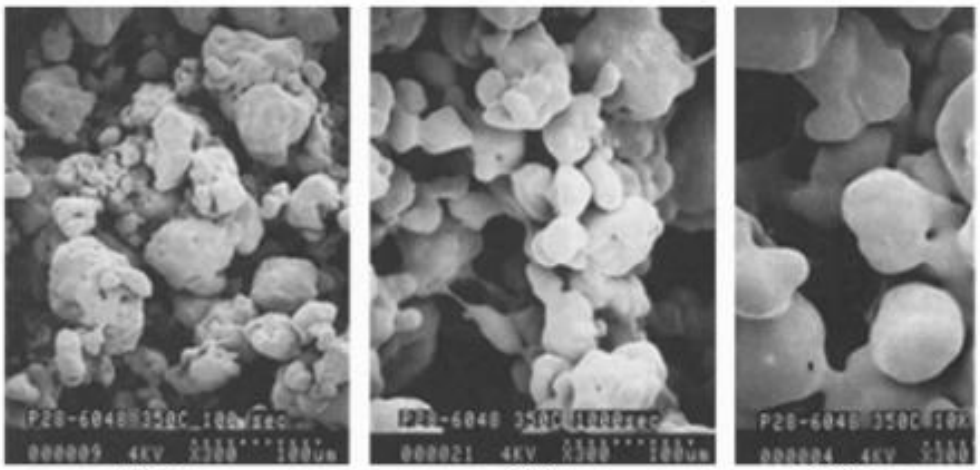

Micrographs (300×) showing evolution of the coalescence of PTFE particles over time.

Figure 1-3: SEM images of particle coalescence of UHMWPTFE as a function of sintering time[1]

Although a significant amount of work has been devoted towards developing sintering models for polymers, Frenkel's expression for sintering of glasses still serves as the basis to illustrate what are conventional materials properties that affect the sintering process[42]. It states that the thermodynamic driving force for sintering or particle coalescence is reduction in surface energy and the kinetics of this process is governed by the viscosity of the coalescing particles. Clearly, sintering of PTFE, a polymer with very low surface energy and very high melt viscosity cannot be explained on the basis of such a model. This is not unexpected when one considers the distinctive features of PTFE melt. There is extensive literature that suggests the existence of partial order in PTFE melt. Neutron scattering studies on molten PTFE has shown existence of conformational order up to 400^{o}C[43]. WAXS results on molten PTFE suggest straight chain segments arranged parallel to one another packed in a disordered manner[44]. Microscopy studies have revealed the development of a folded chain structure in the melt state which increases in perfection with sintering time[45].

Thus, the first step towards understanding the sintering process in PTFE involves an in depth study of the structure evolution of PTFE melt as a function of sintering time. In the present work, the time evolution of PTFE melt will be investigated at different length scales by using an array of in-situ experimental techniques. TMA in the dynamic mode will be used to probe the complex viscoelastic response of the melt by the application of an oscillatory loading of low amplitude. Further, the evolution of residual melt order will be examined in-situ by using high temperature X-ray scattering studies. The melt structure evolution will simultaneously be characterized by employing a cyclic thermal loading profile within the DSC and TMA. Herein, we intend to propose a

mechanism for the sintering process in UHMWPTFE based on a critical evaluation of our experimental results that probe different facets of this process.

The second part of the dissertation involves understanding the effect of temperature, particle size, lower molecular weight PTFE fraction and regrind fraction on the sintering kinetics of UHMWPTFE. Further, the effect of $scCO_2$ annealing on the sintering behavior will be studied. Another objective of this study is to identify fluoropolymer additives, processing aid and processing conditions that will aid in the recycling of UHMWPTFE. The high chemical resistance of PTFE makes waste disposal a challenge. The two major routes for PTFE decomposition are thermal and ion radiation. However, these are complicated methods leading to high disposal costs. A second reason for recycling PTFE is economic due to its high cost. A significant proportion of PTFE scrap is converted to micropowder and used as fluoroadditives. Another portion of PTFE is converted back to molding powder and referred to as "Repro" or reprocessed. The tensile strength, elongation at break and impact strength of Repro PTFE is lower than the virgin material[1,46].

An important point to mention here is that virgin and sintered PTFE has a fundamentally different crystalline structure. Virgin PTFE consists of extended chain crystals that are formed due to crystallization during polymerization but once melted and recrystallized the crystallinity drops to nearly half of its initial value and the material now consists of folded chain crystals[47]. This transition from an extended chain crystal structure to a folded chain crystal structure that occurs during the first heat treatment above its melting point is irreversible in nature. Virgin PTFE has a melting point of 342 ^{o}C while recycled PTFE has a melting point of 327^{o}C.

This study investigates the effect of regrind particle size, lower molecular weight PTFE fraction, sintering temperature and particle sizes on the sintering behavior of PTFE. Homo-composites of virgin and regrind PTFE in different proportions will be studied with regard to their sintering kinetics. The effect of regrind particle size on the re-sintering characteristics will be investigated. Further, homo-composites of virgin UHMWPTFE with lower molecular weight PTFE will be studied. Moreover, supercritical carbon dioxide will be evaluated as a processing aid for PTFE recycling. CO_2 is in its supercritical state above its critical point of 31.1^{o}C and 72.9 atm. $scCO_2$ assisted extrusion of intractable polymers like PTFE and FEP has been carried out and it was demonstrated that $scCO_2$ based on its plasticization effect aids in extrusion[22]. It has been shown that $scCO_2$ annealing increases tensile creep resistance and crystallinity of PTFE[48]. The plasticization effect of $scCO_2$ on PVDF and SBS triblock copolymer has been quantified by using a linear variable differential transducer technique[49-51]. The effect of $scCO_2$ on the viscosity and morphology of polyethylene and polystyrene and their blends has been studied[52,53]. The effect of $scCO_2$on the melting behavior of sPS and PET was investigated and it was shown that the melting temperature decreased with increase in $scCO_2$ pressure. It was also shown that the depression in melting point was not a result of gas pressure and solubility of the gas in the polymer played a crucial role[54].

CHAPTER 2

MECHANISM OF ULTRA HIGH MOLECULAR WEIGHT PTFE SINTERING

2.1 Abstract

The effect of sintering time on the melt evolution of Ultra High Molecular Weight Polytetrafluoroethylene (UHMWPTFE) was studied in-situ by high temperature Wide Angle X-ray Scattering (WAXS), high temperature Small Angle Light Scattering (SALS) and by cyclic thermal loading profiles within a Differential Scanning Calorimeter (DSC) and Thermo-Mechanical Analyzer (TMA). Further, TMA in the dynamic mode was used to probe the in-situ viscoelastic response of the melt. Moreover, non-standard compression testing was used to probe the sintering process at the molecular level. Results obtained from these techniques support the concept of simultaneous molecular ordering and entanglement formation in the melt state as a function of sintering time well above the melting temperature. TMA, which is not a conventional technique for monitoring thermal transitions, is shown to be sensitive enough for such purposes. Both DSC and TMA exhibit non-equilibrium melt behavior even 30^{o}C above its equilibrium melting temperature for long time periods. A correlation between the DSC and TMA results is established. The cyclic thermal profile leads to a dramatic growth in enthalpy of crystallization/melting. The mechanism for this growth is associated with two independent processes; isothermal annealing at the sintering temperature and lamellar thickening in the solid state. Further, UHMWPTFE is shown to exhibit a double yield phenomenon in compression.

2.2 Background

Polytetrafluoroethylene (PTFE) is a fluoropolymer with many outstanding properties including excellent thermal stability, chemical inertness and very low coefficient of friction, making it suitable for a wide range of applications[1].

Conventional melt processing techniques such as extrusion and injection molding cannot be applied to Ultra High Molecular Weight PTFE resulting from its very high melt viscosity (10^{10}-10^{11} poise)[1]. Industrially, PTFE is processed by semi-continuous melt extrusion[2,3]or compaction (pre-forming) of PTFE molding powder at room temperature followed by sintering[4,5,6,7,8]. Sintering involves heating a preform above its melting temperature, dwelling at that temperature for a specified time followed by slow cooling to room temperature. This leads to the formation of a homogeneous part with improved mechanical integrity[1].

Although a significant amount of work has been devoted towards developing sintering models for polymers, Frenkel's expression for sintering of glasses still serves as the basis to illustrate what are conventional materials properties that affect the sintering process[42]. It states that the thermodynamic driving force for sintering or particle coalescence is reduction in surface energy and the kinetics of this process is governed by the viscosity of the coalescing particles. Clearly, sintering of PTFE, a polymer with very low surface energy and very high melt viscosity cannot be explained on the basis of such a model. This is not unexpected when one considers the distinctive features of PTFE melt. There is extensive literature that suggests the existence of partial order in PTFE melt. Neutron scattering studies on molten PTFE has shown existence of conformational order up to 400^{o}C[43]. WAXS results on molten PTFE suggest straight

chain segments arranged parallel to one another packed in a disordered manner [44]. Microscopy studies have revealed the development of a folded chain structure in the melt state which increases in perfection with sintering time[45].

Thus, the first step towards understanding the sintering process in PTFE involves an in depth study of the structure evolution of PTFE melt as a function of sintering time. In the present work, the time evolution of PTFE melt was investigated at different length scales by using an array of in-situ experimental techniques. TMA in the dynamic mode was used to probe the complex viscoelastic response of the melt by the application of an oscillatory loading of low amplitude. Further, the evolution of residual melt order was examined in-situ by using high temperature X-ray scattering studies and high temperature Small Angle Light Scattering (SALS) studies. The melt structure evolution was simultaneously characterized by employing a cyclic thermal loading profile within the DSC and TMA. Non-standard compression testing was also used to provide valuable insight into the molecular processes associated with UHMWPTFE sintering. Herein, we propose a mechanism for the sintering process in UHMWPTFE based on a critical evaluation of our experimental results that probe different facets of this process.

2.3 Experimental

2.3.1 Material and Sample Preparation

M15X, a granular PTFE molding powder, supplied by Saint Gobain was used in the current work. Cylindrical green billets were compacted from the raw powder by following a controlled two-stage pre-forming strategy using Instron 5500R at room temperature. A 6mm internal diameter compression mold was employed for this purpose allowing for plane strain compaction.

In the first stage, the powder was compacted at 1 mm/min strain rate to 4MPa stress followed by a 5min dwell time. In the second stage, it is again compacted at 1mm/min strain rate to 20MPa stress and held for 5mins (Figure 2.1). The molding region was kept under vacuum during this process. This strategy was adopted after testing several other compaction methods on grounds of improved sample to sample reproducibility. After compaction, a resting time of 3 hrs or more was allowed for degassing and natural recovery. The resulting pre-forms had a density of approximately 2.15 g/c.c and an aspect ratio of approximately 5:6.

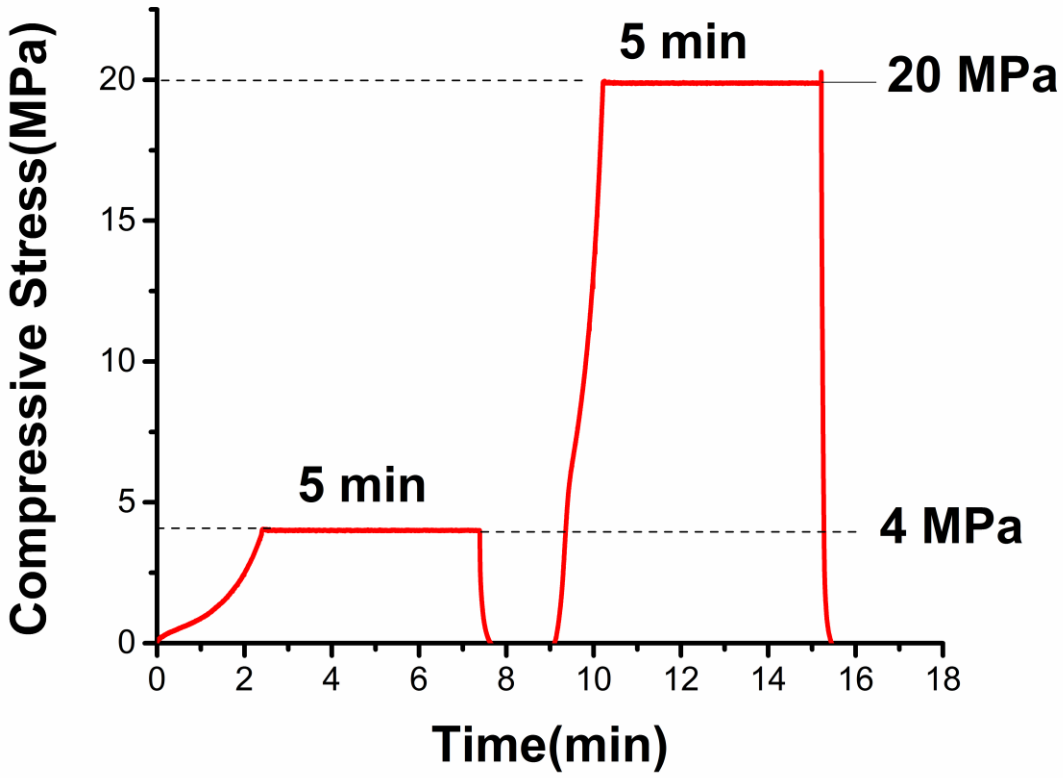

Figure 2-1: Controlled two stage preforming strategy

2.3.2 Method

Differential Scanning Calorimeter: DSC Q200 (TA Instruments, USA) was used to monitor the structure evolution of the PTFE melt by employing a cyclic thermal loading profile.

Thermo-mechanical Analyzer: TMA Q400 (TA Instruments, USA) in the dynamic mode was used to probe the storage modulus evolution of PTFE melt as a function of sintering time by applying an oscillatory force of +/- 0.002 N at 0.5 Hz frequency. A preload force of 0.01N was applied to sustain contact between the probe and the specimen surface. The dimension changes associated with the melting/crystallization transitions was also measured using this technique. Further, the structure evolution of PTFE melt was studied by using a cyclic thermal profile by harnessing this technique to monitor melting/crystallization transitions.

Wide angle X-ray scattering: WAXS was done using an in-house setup from Molecular Metrology Inc. (presently sold as Rigaku S-Max3000). It uses a 30 W microsource (Bede) with a 30×30 μm^2 spot size matched to a Maxflux® optical system (Osmic) leading to a low-divergence beam of monochromatic CuK_α radiation (wavelength λ=0.1542 nm). After passing beam-defining and guard pinholes, the beam of about 0.4 mm diameter enters the sample chamber. A Fujifilm CR HR-V image plate at a distance of L = 117 mm was used to record the scattering. L was calibrated using the q = 15.197 nm-1, (110) peak from a tricosane standard. The image plate has a maximum resolution of 50 µm. The whole system is evacuated.

WAXS studies on molten PTFE at 370^{o}C was performed inside an environmental chamber to study the evolution of melt state order as a function of sintering time.

Small Angle Light Scattering (SALS): The small angle laser scattering (SALS) setup consists of a linear polarized laser (Uniphase 1125P, HeNe λ: 632.8nm); a polarizer set parallel to the laser polarization, a heating stage (Linkam TMS93) where the sample is placed; and an image screen to collect scattered image. The image is captured from the projected scattering beams using a CCD Camera (Panasonic CCTV camera WVBP330). The scattered light intensity is measured by a photodiode. A home-made LabVIEW protocol was used to collect all information simultaneously. An illustration of the SALS setup is given in Figure 2.2.

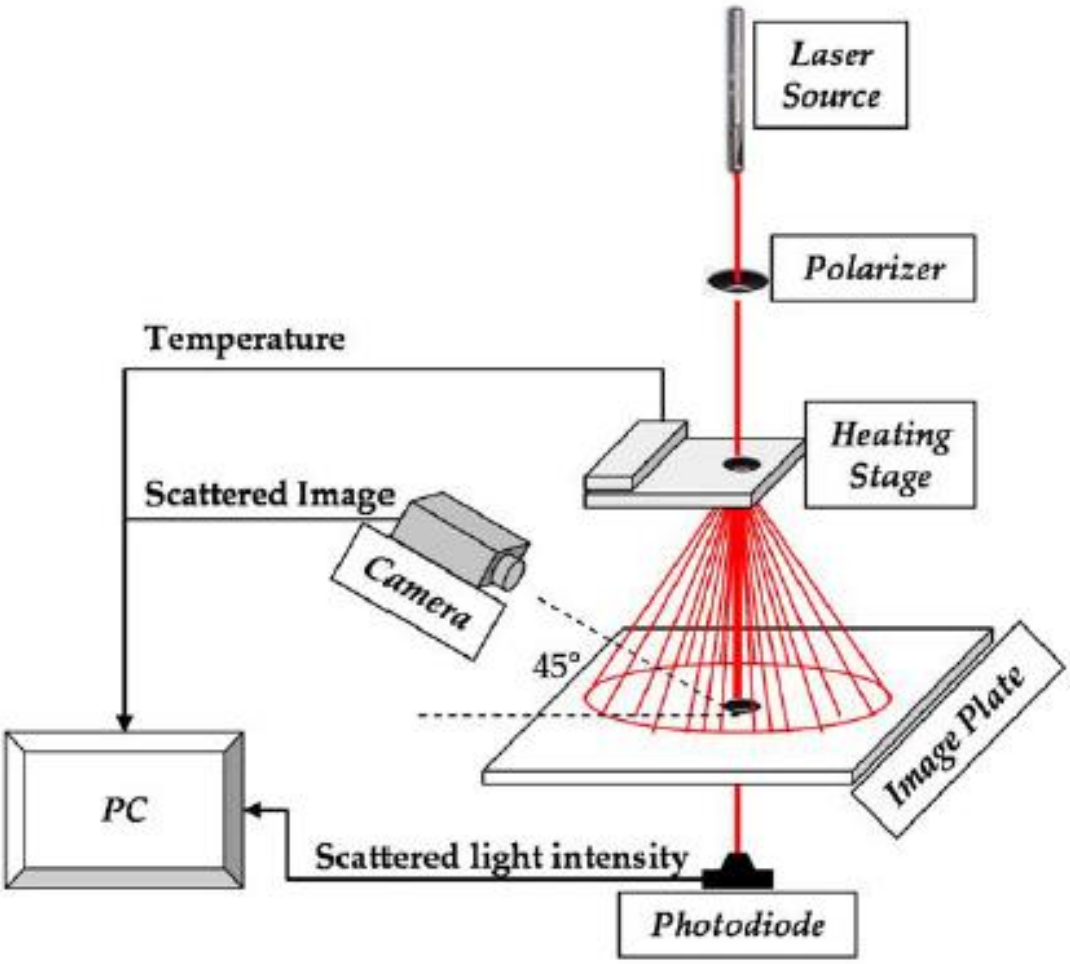

Figure 2-2: Small Angle Light Scattering set-up

Compression testing: Uniaxial compression test was conducted on an Instron 5800 universal tester at 20°C and a constant strain rate of 1 min^{-1}. Cylindrical bullets (Diameter ~ 11.3 mm) with 1:1 height-to-diameter ratio were machined. Soapy water and thin PTFE films were used for lubricating the ends of the specimens. The strain hardening modulus (G_R) was computed at 90% of the ultimate true strain using the following equation:

$$G_R = \frac{\partial \sigma_t}{\partial(\lambda^2 - 1/\lambda)} \qquad (2.1)$$

whereσ_t is the true stress, λ^2-1/λ is the Neo-hookian strain, and λ is the compression ratio.

2.4 Results and Discussion

Figure 2.3 shows the storage modulus evolution of PTFE melt at 370^{o}C as a function of sintering time. The specimen was equilibrated at 370^{o}C for 10 minutes prior to data acquisition. This relatively long equilibration time was chosen keeping in mind the low thermal conductivity of the material. As shown in Figure 2.3, the modulus keeps increasing with annealing time and does not equilibrate within the experimental time frame.

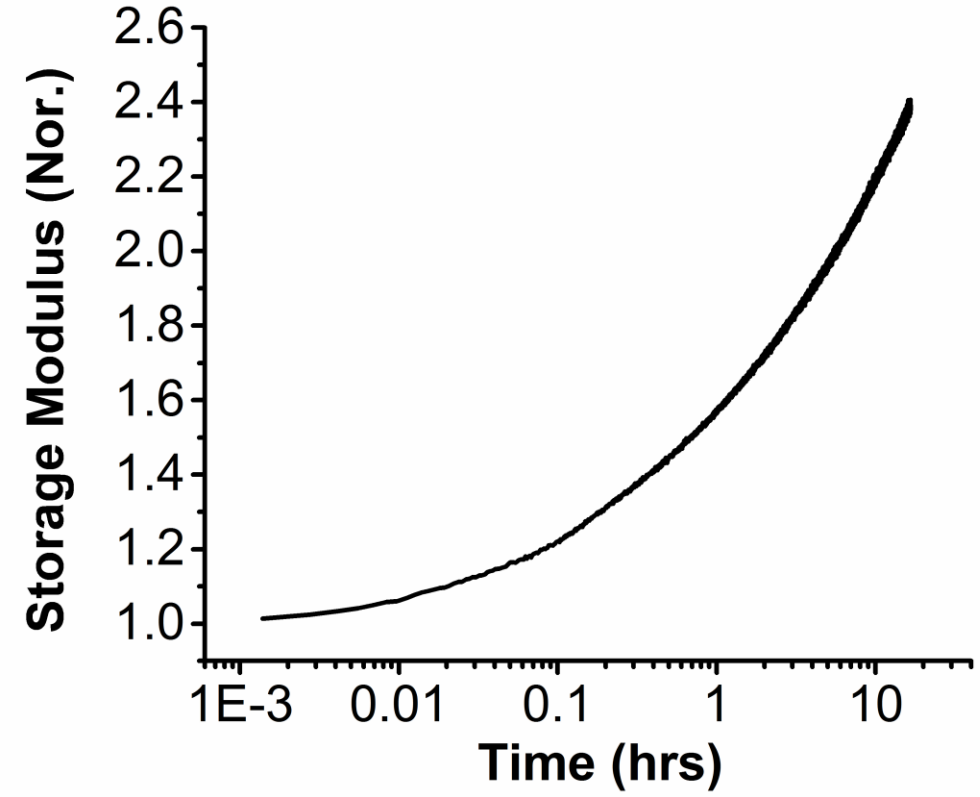

Figure 2-3: Storage modulus evolution of UHMWPTFE as a function of annealing time at 370°C

Such a slow equilibration kinetics is not unlikely when one considers the ultra-high molecular weight and the inherent stiffness of the PTFE chains[55]. However, the molecular mechanism responsible for this non-equilibrium melt evolution is one of the primary questions that this paper aims to answer.

Recently published literature on UHMWPE has shown a similar increase in elastic modulus as a function of annealing time and this increase has been attributed to entanglement formation in a disentangled polymer melt. This work further showed that the kinetics of entanglement formation is a function of polymer molecular weight and significantly longer times are required for higher molecular polymers to reach an equilibrium entanglement density which corresponds to a plateau in storage modulus [56] (Figure 2.11). This may be one of the potential mechanisms responsible for the non-equilibrium melt evolution observed in PTFE. In other words, entanglement formation might be the molecular mechanism that drives inter-particle sintering.

Next to investigate if melt equilibration is achieved in an industrial sintering process, the storage modulus evolution of a billet already sintered by St. Gobain was probed. The specimen was again annealed at 370^{o}C but for significantly longer times (approximately 12 days). However, the melt did not equilibrate even in 12 days with the modulus continuing to increase with time (Figure 2.4).

This 12 day long non-equilibrium evolution might be a mere consequence of very slow entanglement kinetics. However, this increase in storage modulus can also come from some other molecular mechanism which is not entanglement formation and further investigation is necessary to confirm or refute this hypothesis.

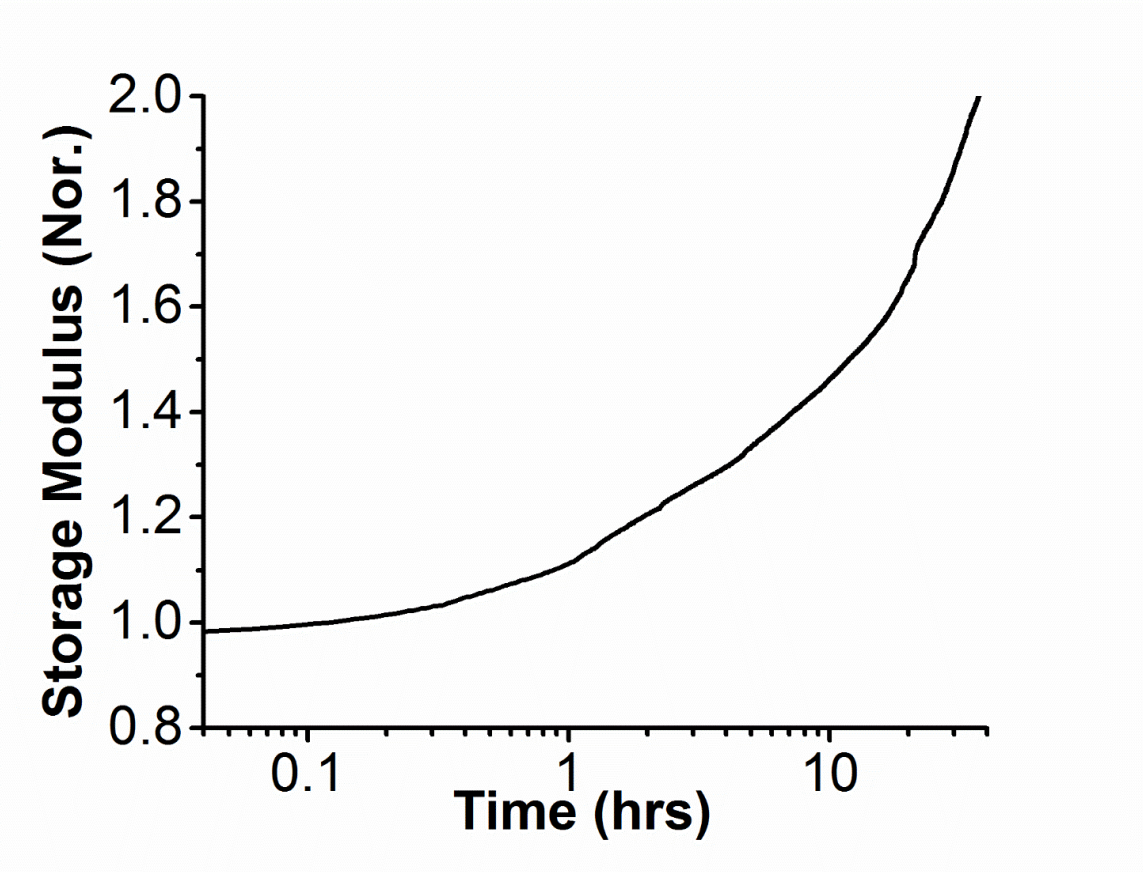

Figure 2-4: Storage modulus evolution for 280 hours (~ 12 days) of an industrially sintered UHMWPTFE billet

2.4.1 Differential Scanning Calorimetry

A cyclic DSC profile, shown in Figure 2.5 was designed to interrogate the effect of thermal memory on PTFE (M15X) melting and crystallization. Cycling was done between 0^{o} and 370^{o}C at a constant rate of 5^{o}C/min. The thermal cycling was coupled with isothermal annealing for different durations at 370^{o}C. Note that the isothermal times were chosen such that they sum up to 1000 mins with the first and last having equal times, the second and next to last having the same times, and so on. The amount of time required to erase any memory in the PTFE melt would be identified by the pair of isotherms showing the same response. For example, if PTFE has no thermal memory then all the seven heating and cooling steps would yield identical values for melting/crystallization temperatures and enthalpies. Further, if PTFE crystallization was a function solely of the preceding annealingtime, then the first and seventh cooling would be identical and the same would be true for second and sixth, third and fifth cooling**.**

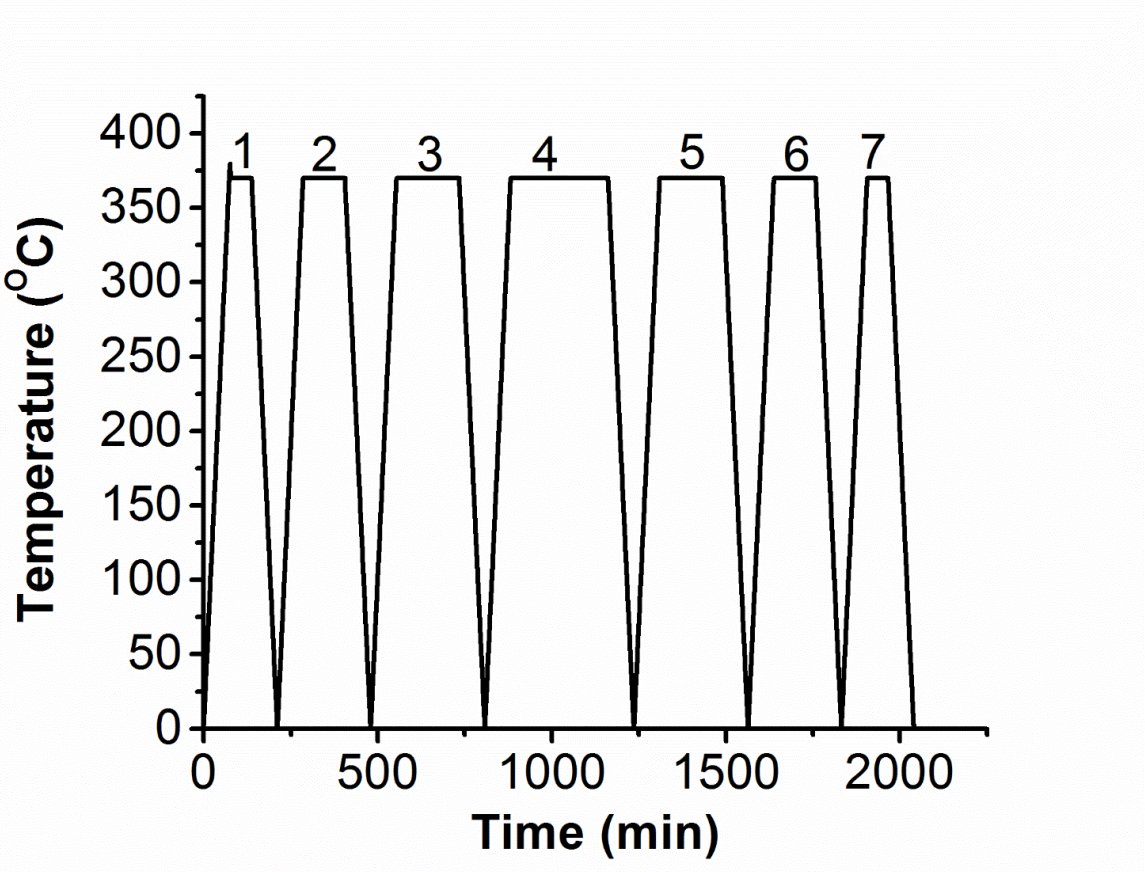

Figure 2-5: Cyclic DSC thermal loading profile

Figure 2.6 shows the melting peaks for this profile. Note that both enthalpy of melting and melting temperature increases with successive sintering steps (Figure 2.7). An increase in melting temperature might correspond to lamellar thickening as a function of sintering time. The first melting is very different from the rest because of different morphologies of virgin (extended chain) and sintered PTFE(folded Chain)[47]. The enthalpy of crystallization increased whereas, the crystallization temperature decreased with successive sintering steps (Figure 2.8 and Figure 2.9). This is counter intuitive and contradicts the initial entanglement hypothesis as these results indicate that sintering is associated with some other molecular process that leads to an increase in enthalpy of melting and crystallization. Further, we wanted to compare this unusual behavior of molecular ordering at 370^{o}C with that of UHMWPE. Both the materials show an increase in storage modulus as a function of annealing time at their respective sintering temperatures[56]. Therefore, we wanted to understand weather UHMWPE would show a similar behavior when subjected to a cyclic thermal loading in the DSC. The only difference in this experiment would be the fact that the sintering temperature was chosen to be 160^{o}C instead of 370^{o}C (Figure 2.10). The annealing temperature of 160^{o}C for UHMWPE was chosen as Rastogi did his storage modulus evolution studies at that temperature[56]. However, as in the case of UHMWPE there was absolutely no change in the enthalpy of crystallization with increase in annealing time (132 J/g for all seven cycles). Thus, UHMWPE unlike UHMWPTFE exhibits no measurable melt memory. Further, two exothermic peaks (Peak 1 & 2) to the right of the main crystallization peak were reported, one of which grew at the expense of the other as a function of sintering time (Figure 2.12 and Figure 2.13). Such, sintering time dependent disappearance and

reappearance of molecular order is again indicative of the complex time evolution of the PTFE melt.

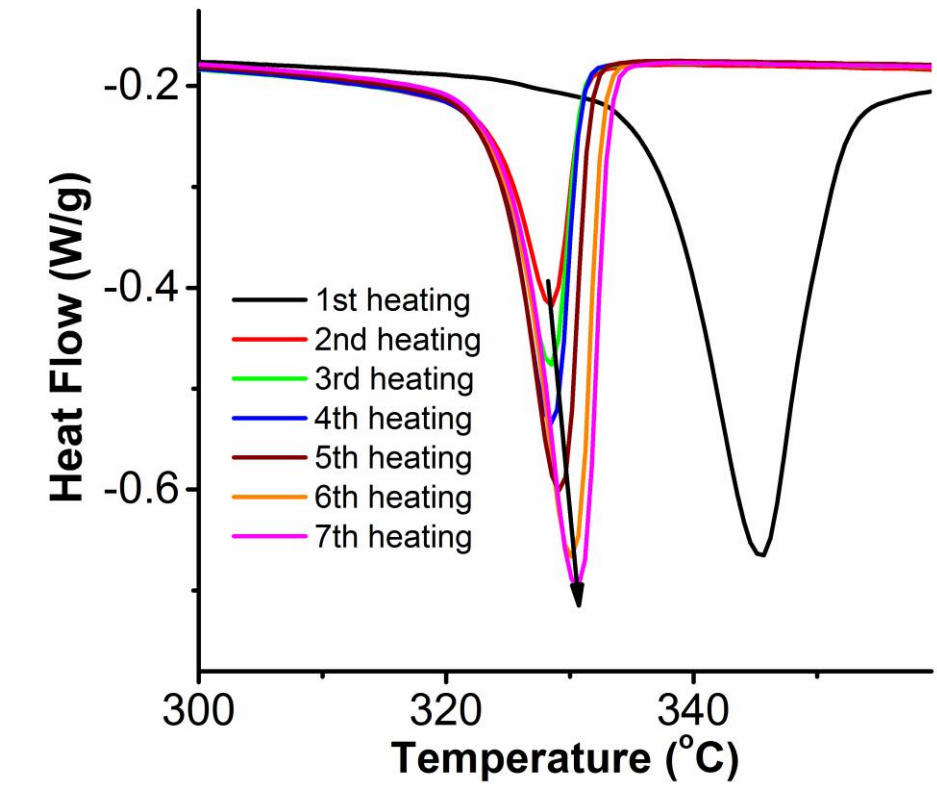

Figure 2-6: Effect of successive sintering steps on melting behavior of UHMWPTFE

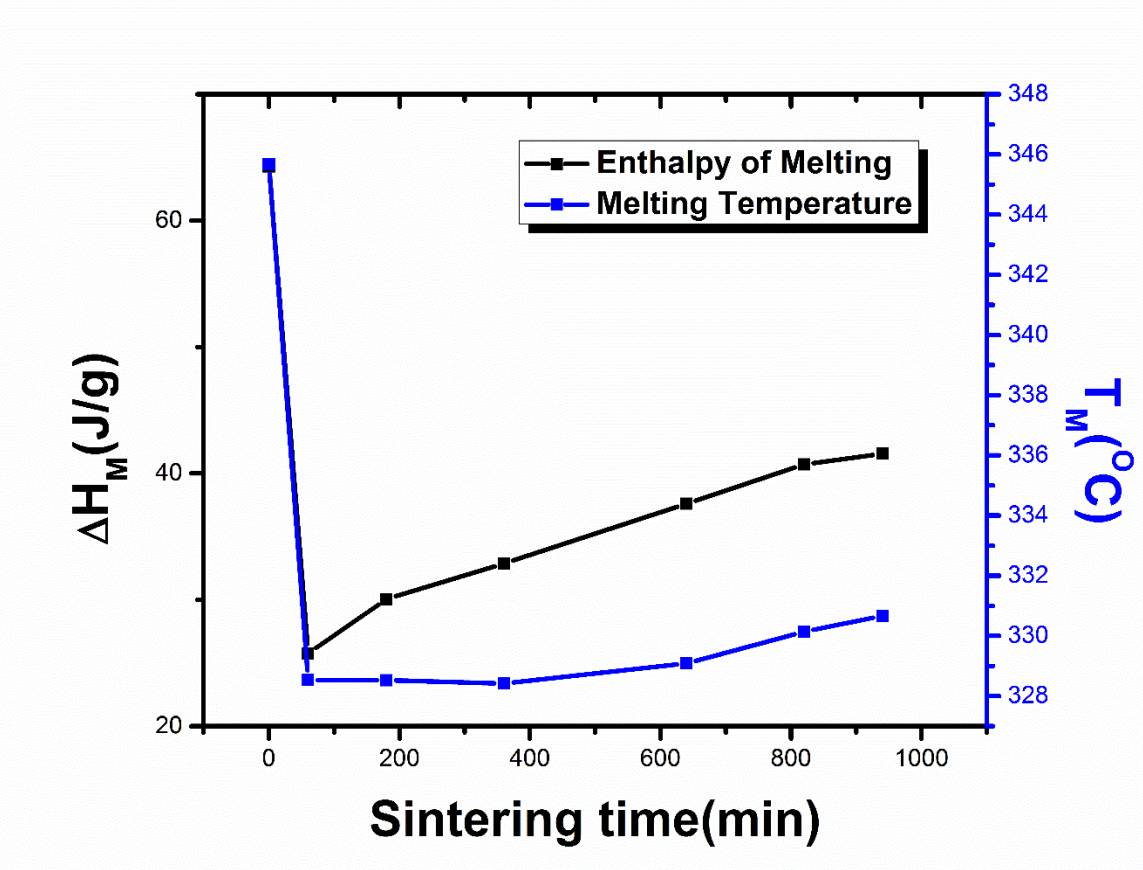

Figure 2-7: Effect of sintering time on enthalpy of melting and melting temperature

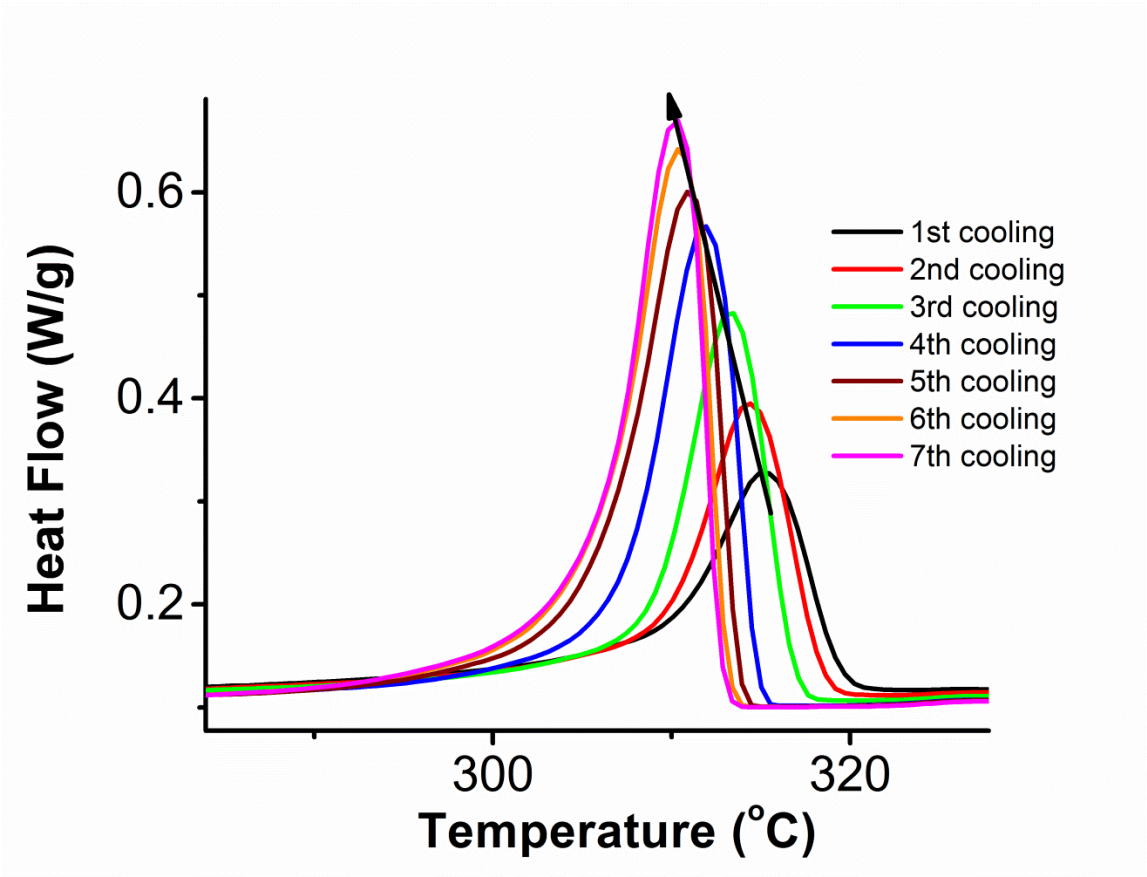

Figure 2-8: Effect of successive sintering steps on crystallization behavior of UHMWPTFE

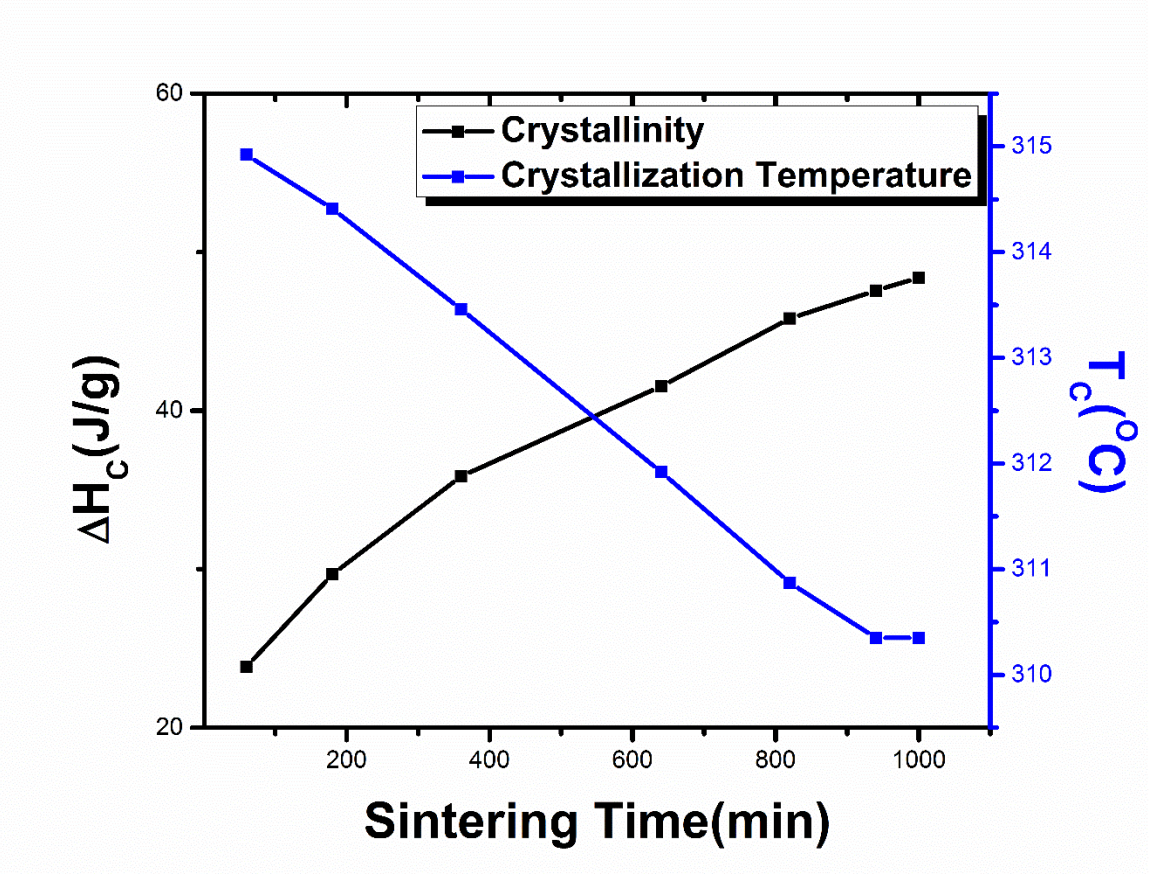

Figure 2-9: Effect of sintering time on the enthalpy of crystallization and crystallization temperature

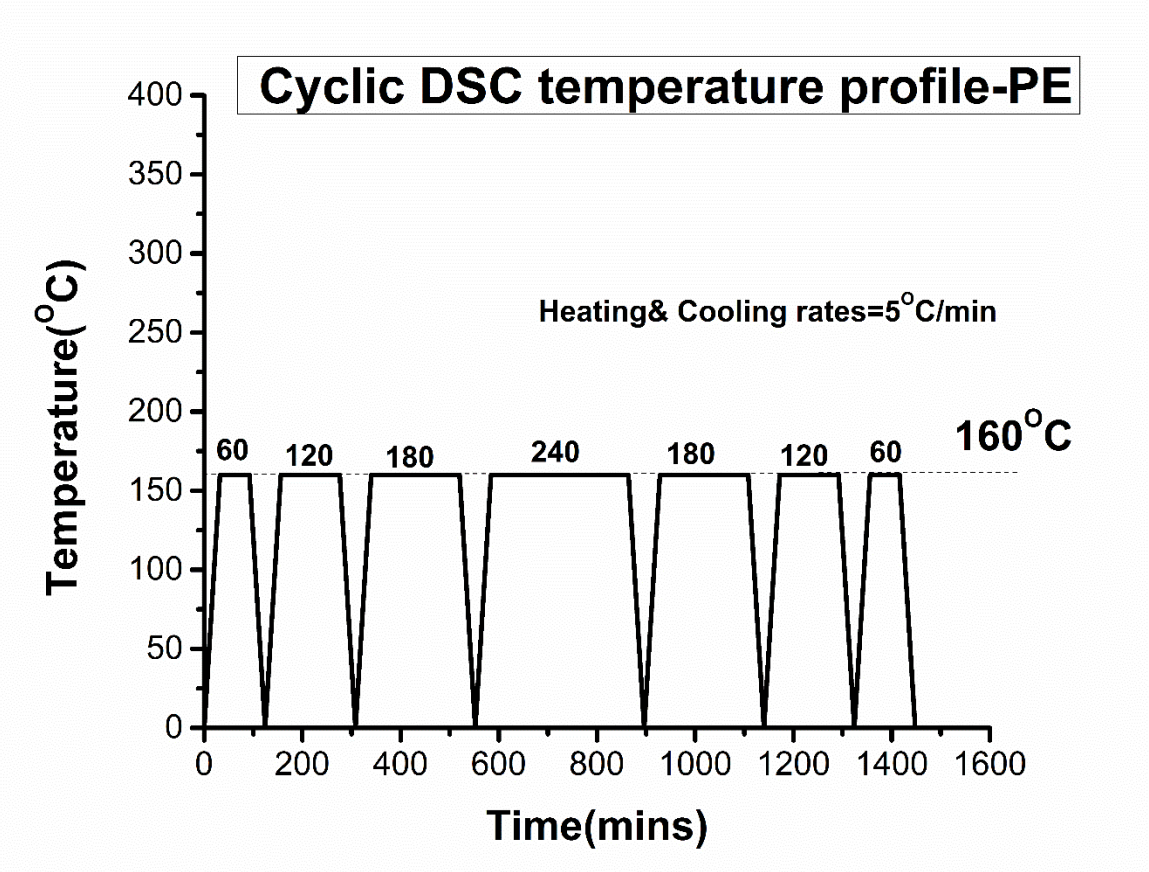

Figure 2-10: Cyclic thermal loading profile for UHMWPE

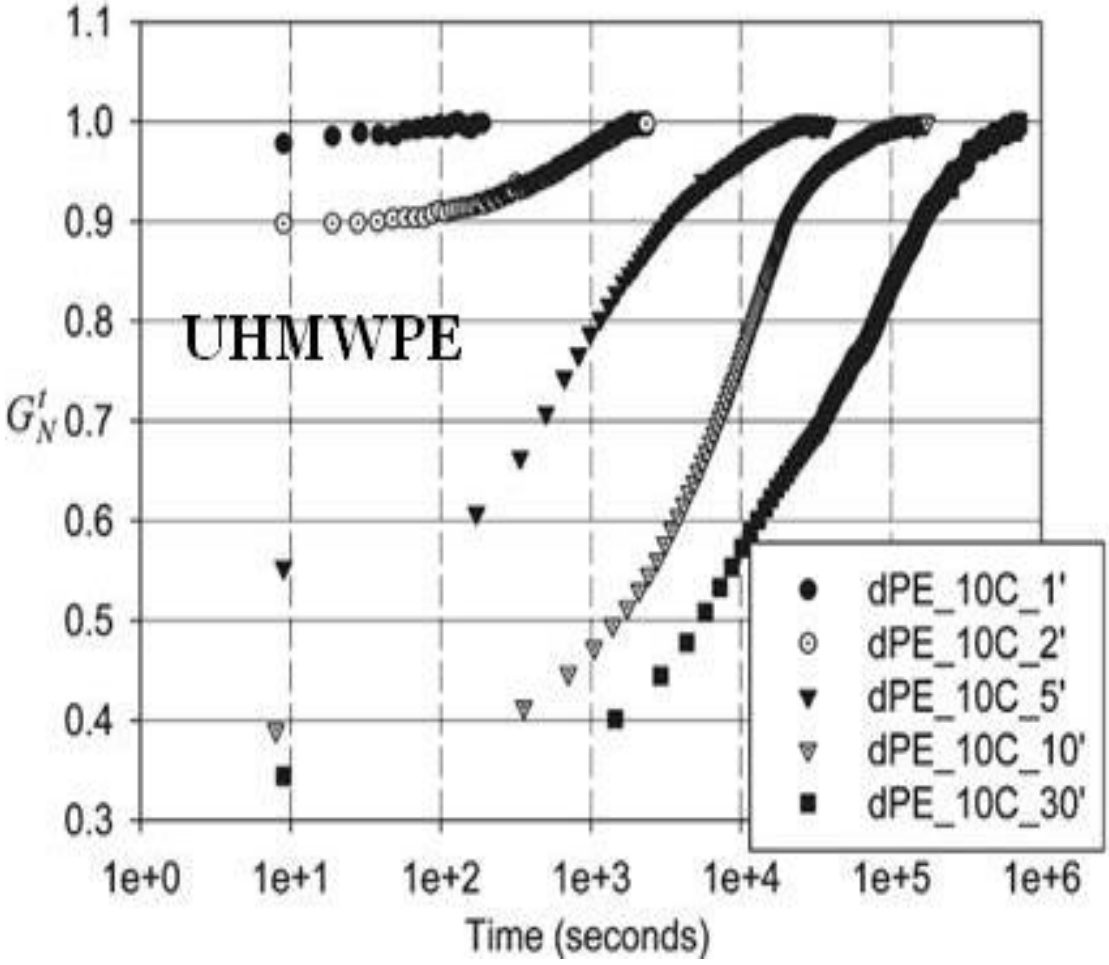

Figure 2-11: Evolution of storage modulus as a function of annealing time for different molecular weights of UHMWPE[56]

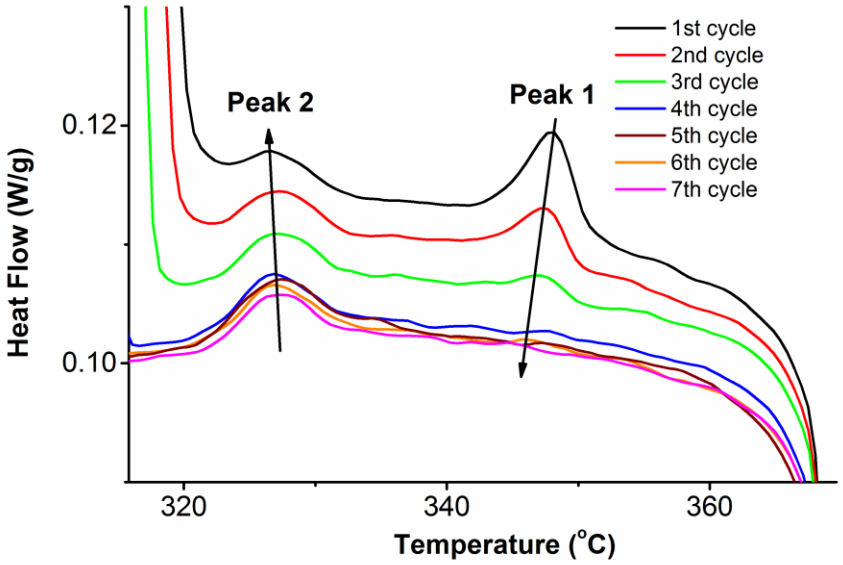

Figure 2-12: Exothermic peak 2 grows at the expense of Peak 1

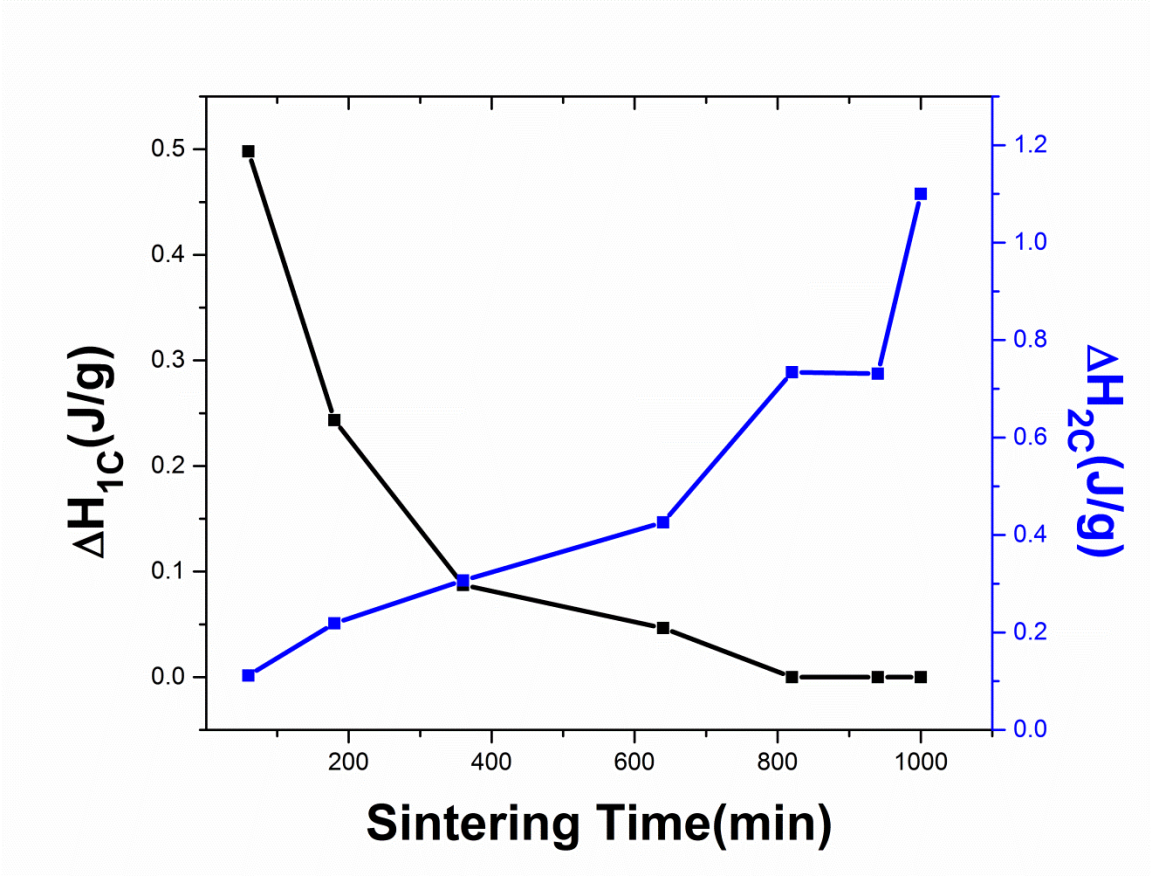

Figure 2-13: The enthalpy associated with Peak 1 decreases while that associated with peak 2 increases as a function of sintering time

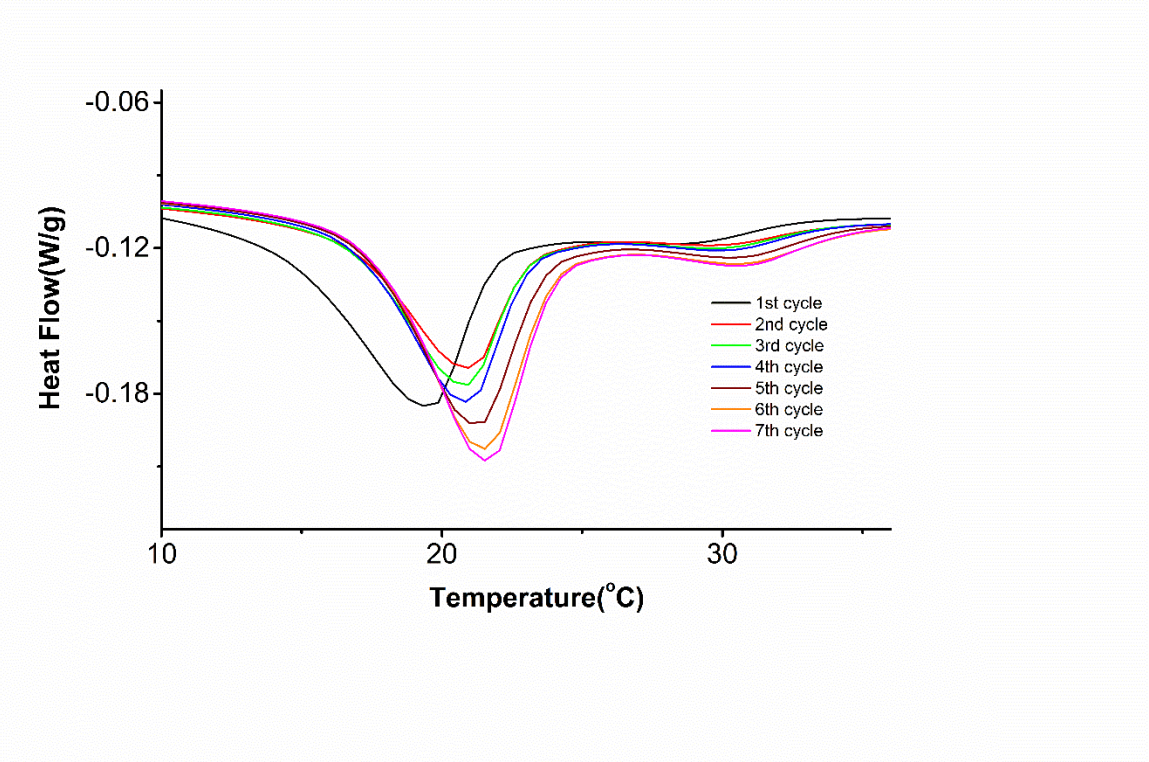

Figure 2-14: Enthalpy associated with endothermic peaks corresponding to 19 and 30°C transitions increases with successive cycling steps

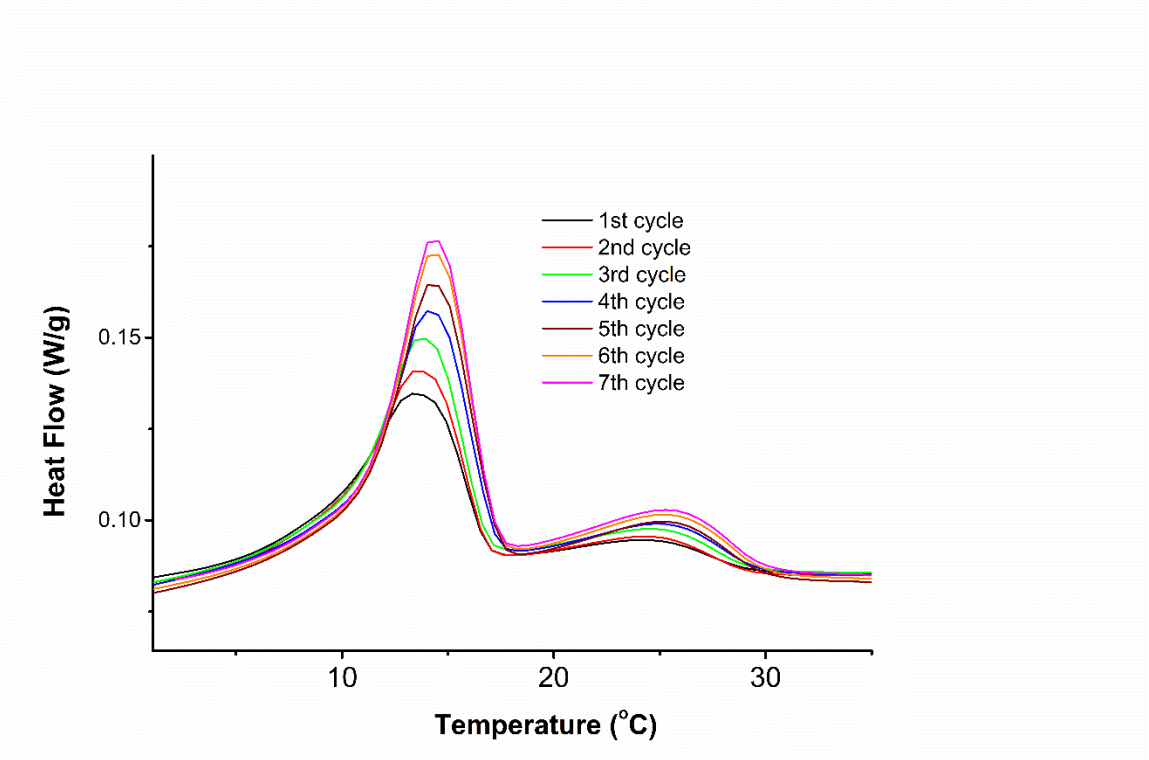

Figure 2-15: Enthalpy associated with exothermic peaks corresponding to 19 and 30°C transitions increases with successive cycling steps

2.4.2 Thermo-mechanical Analyzer

Another technique to characterize such a melt may be the TMA. Although TMA is not a conventional technique for monitoring crystallization and melting transitions, their results can complement the information received from a DSC (Figure 2.16, Figure 2.17, Figure 2.18 and Figure 2.19). In order to do this the following cyclic TMA (Figure 2.20) was conducted and contrasted with the cyclic DSC. In these studies, the cycling was done between 150^{o} and 370^{o}C owing to the lack of controlled cooling below 150^{o}C in the air-cooled TMA. Nevertheless, such a variation was not expected to significantly alter the melting/crystallization behavior.

Figure 2.21 shows dimensional changes associated with the seven melting transitions. Again, the first melting is very different from the rest due to change in crystal structure from extended to folded chain. As can be seen, such a crystalline transition is very well captured even in the macroscopic dimension changes. Differentiation of the dimension changes yields Figure 2.22. Here the area under each melting peak corresponds to the dimension change associated with that melting transition. It shows that from second through seventh melting, both the melting temperature and the dimension change associated with the melting transitions increase. This is in agreement with our DSC results.

Figure 2.23 and Figure 2.24 shows the dimension changes associated with the crystallization transitions. Here, the dimension change associated with crystallization increases whereas the crystallization temperature decreases with successive sintering steps. Again, these results are in agreement with our DSC results.

Thus, TMA which measures macroscopic dimension changes, an extensive property of the system, is sensitive enough to capture subtle variations in thermal transitions originating from micro structural rearrangement.

Figure 2.25 shows a correlation between the TMA and DSC crystallization data. The enthalpy of crystallization (ΔH_c) obtained from DSC correlates well with the dimension change associated with crystallization (Δh_c) obtained from TMA.

Therefore, TMA can be used not only independently but also in correlation with DSC to study melting/crystallization transitions and crystal structure. Further, both the cyclic DSC and TMA results indicate that sintering is associated with molecular ordering.

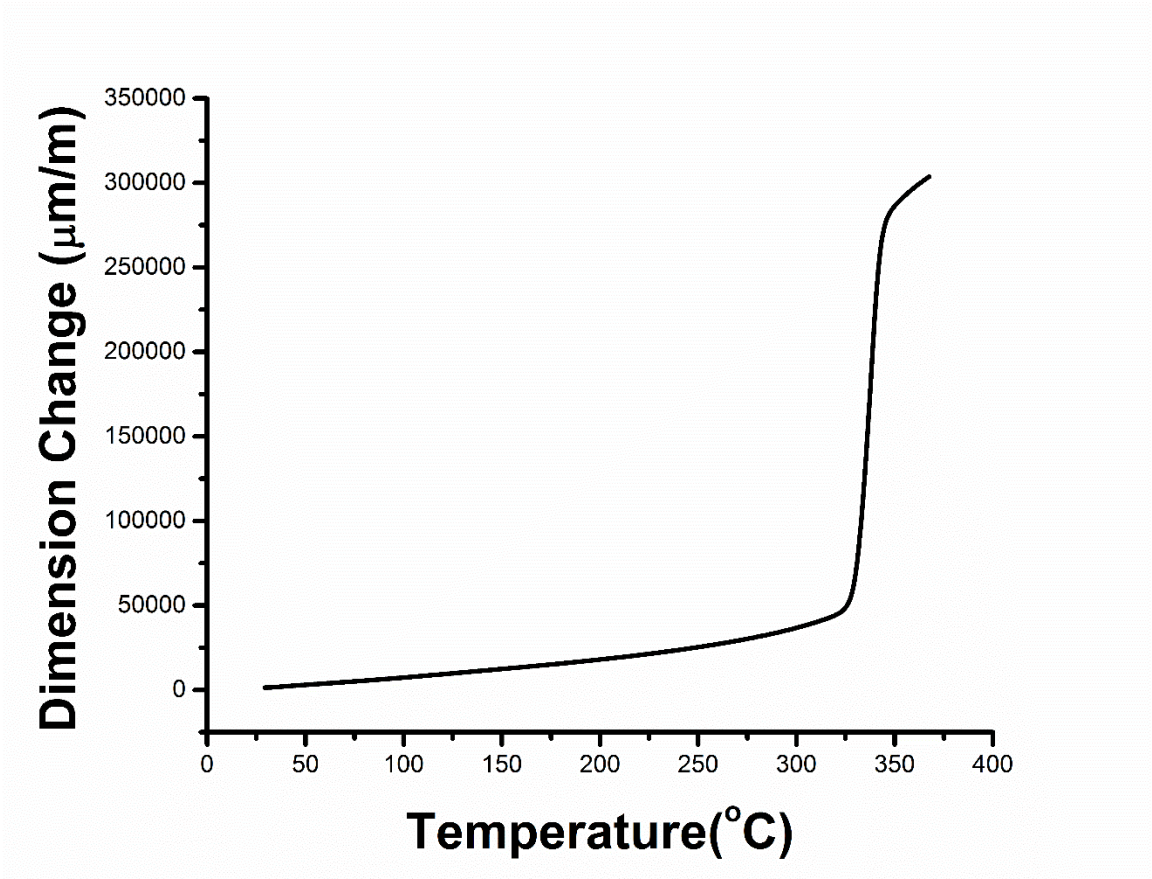

Figure 2-16: Dimension change associated with the melting transition in UHMWPTFE

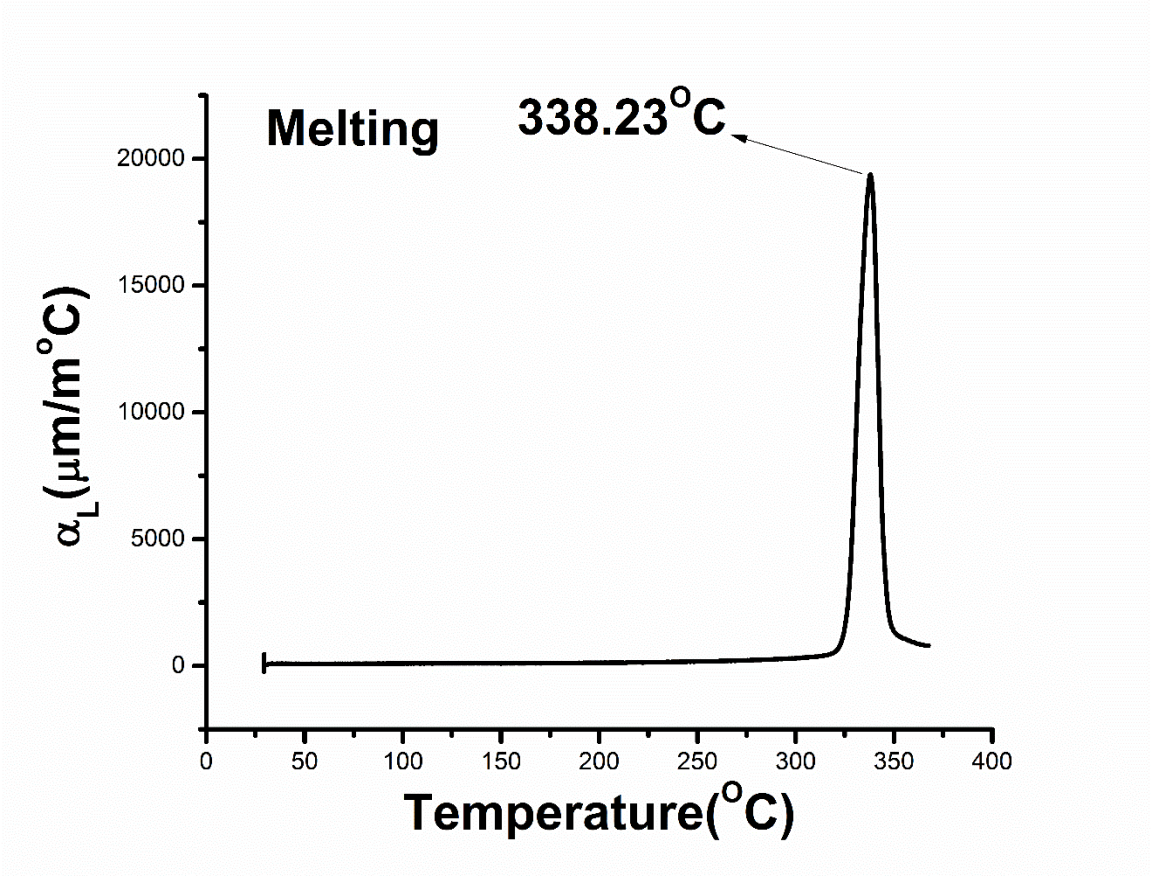

Figure 2-17: Derivative of dimension change associated with the melting transition.

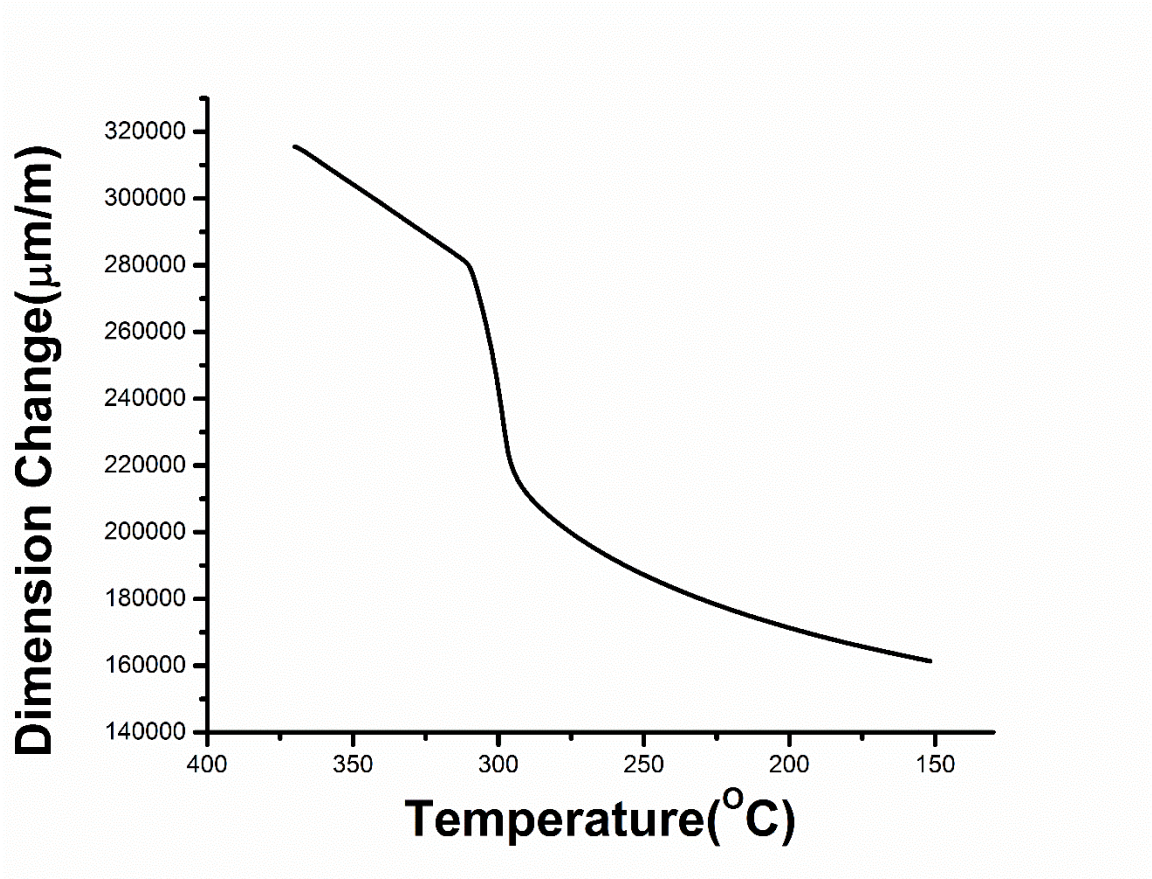

Figure 2-18: Dimension change associated with the crystallization transition in UHMWPTFE

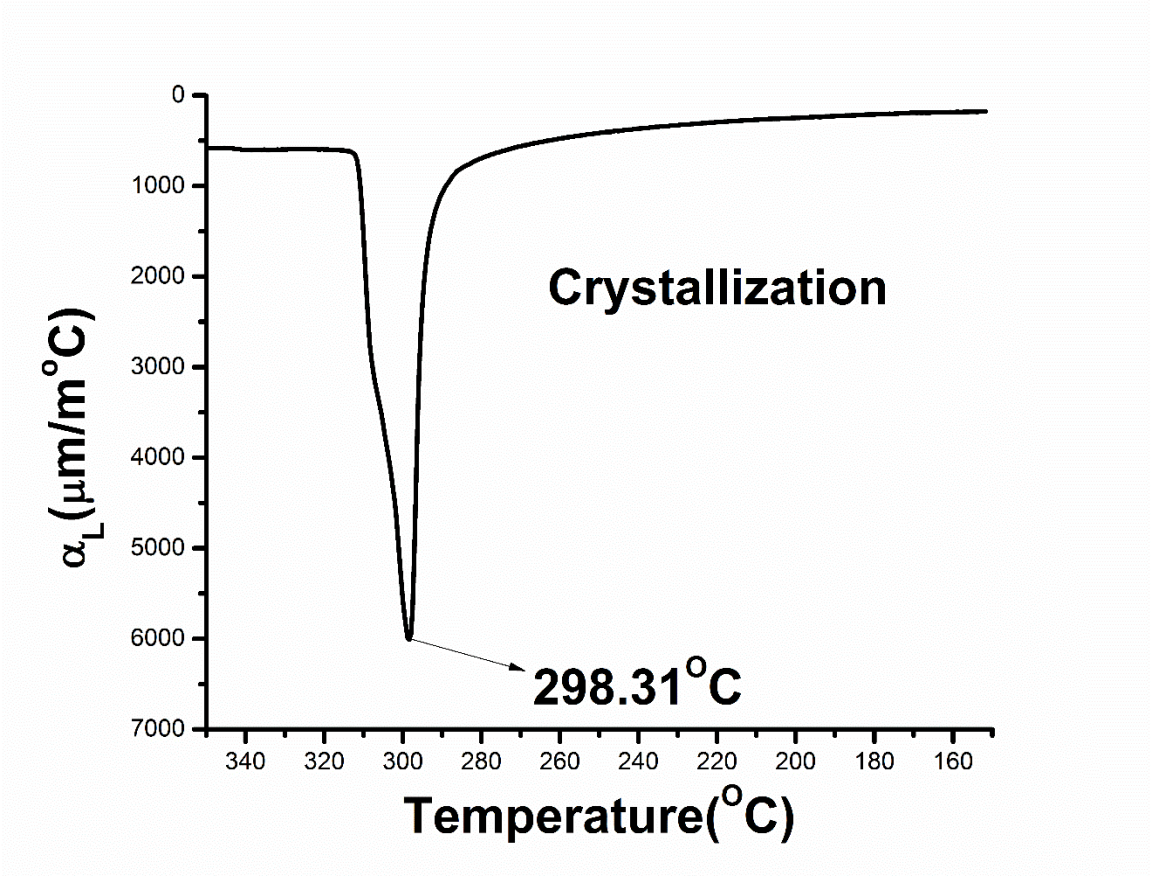

Figure 2-19: Derivative of dimension change associated with the crystallization transition

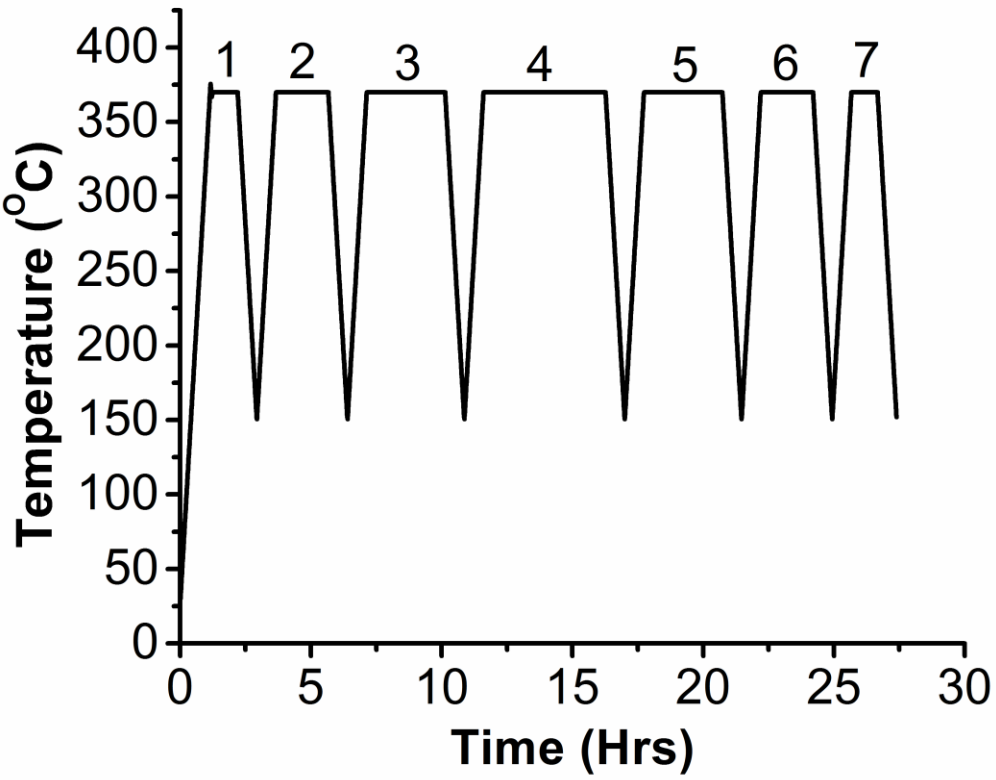

Figure 2-20: Cyclic TMA thermal loading profile

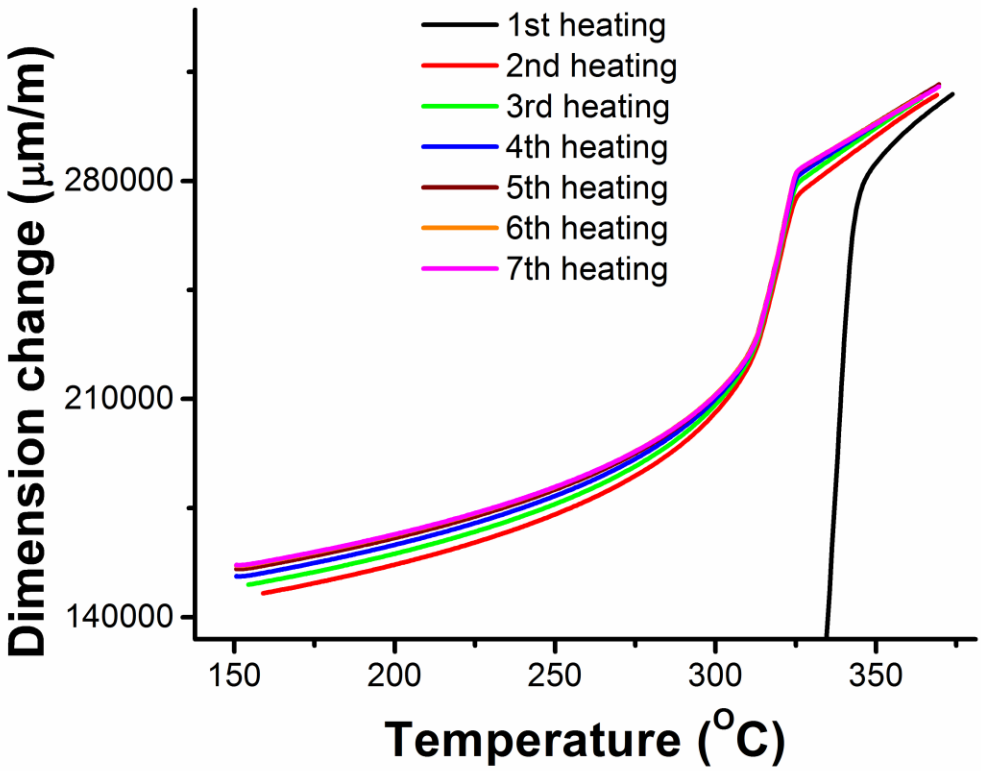

Figure 2-21: Dimension changes (μm/m) associated with seven melting transitions

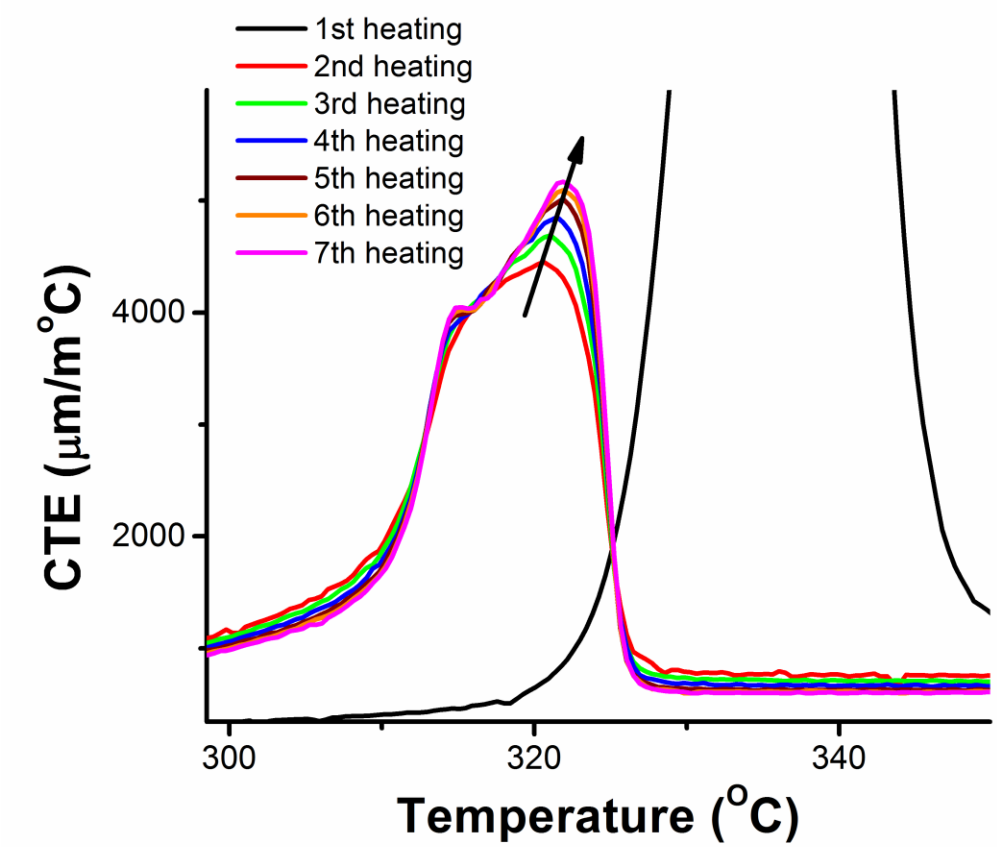

Figure 2-22: Derivative of the dimension changes associated with the seven melting transitions

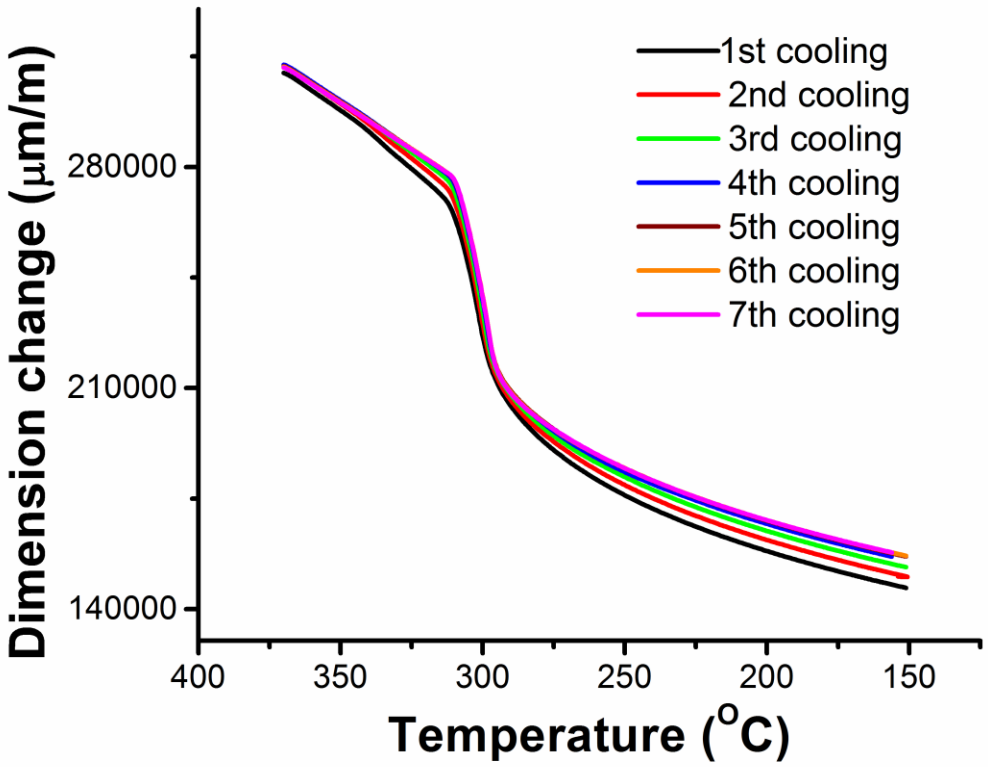

Figure 2-23: Dimension changes associated with seven crystallization transitions

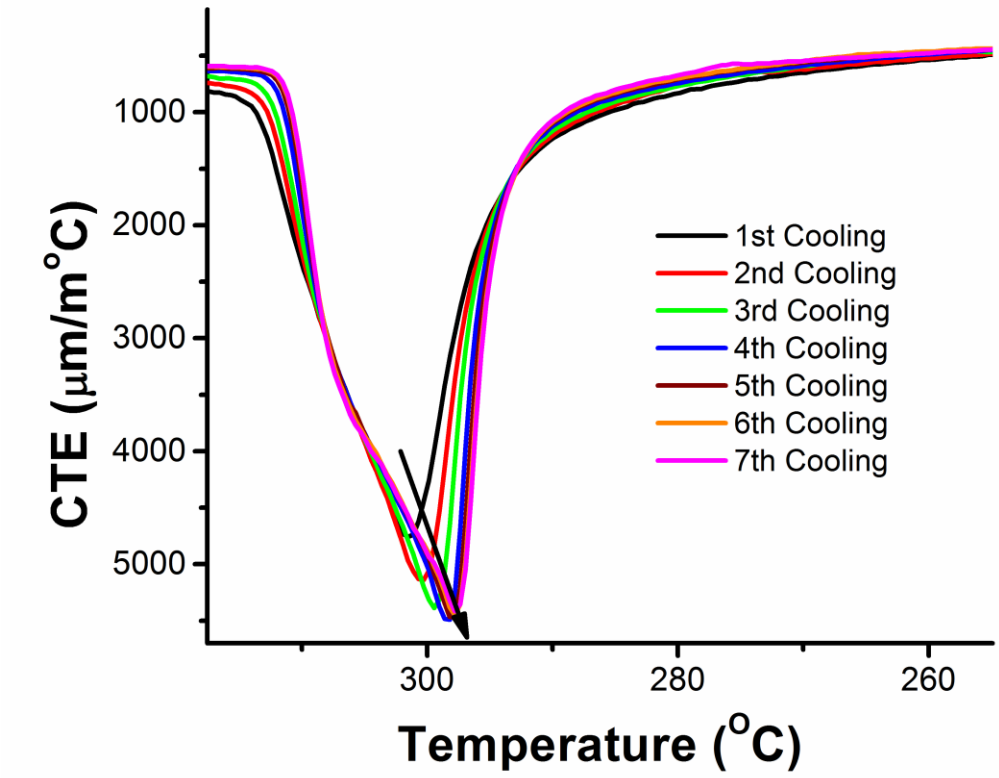

Figure 2-24: Derivative of the dimension changes associated with the seven crystallization

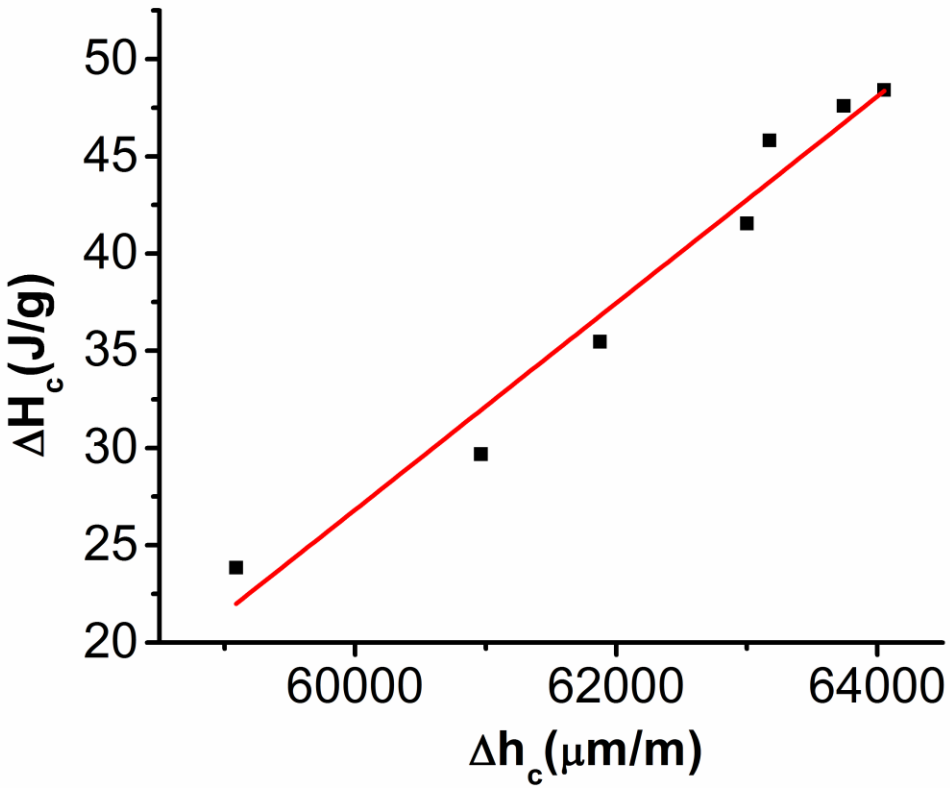

Figure 2-25: TMA-DSC correlation (Crystallization data)

2.4.3 Closer look at Cyclic DSC crystallizations

Since GPC cannot be performed on PTFE, an empirical way to determine its molecular weight was from its heat of crystallization measurements using the relation (1) based on data from Suwa[57].

$$M_n = 2.1 \times 10^{10}\ \Delta H_C^{-5.16} \qquad (1)$$

This might suggest that the ΔH_c increase (Figure 2.8) is a mere consequence of chain scission at 370°C and not a result of the cyclic thermal loading profile (Figure 2.5). Further, it has been shown that sintering (360° -382°C) leads to slow thermal breakdown [58]. To interrogate this, two independent continuous DSC experiments were conducted in which the sintering times were 1000mins (equal to the sum of the isothermal times of the cyclic DSC) and 2060min (equal to the total time of the cyclic DSC). If chain scission was leading to the ΔH_c growth then ΔH_c corresponding to the seventh cooling in the discontinuous sintering should approximately equal that obtained after 1000mins continuous sintering. Further, the ΔH_c obtained after 2060mins continuous sintering should be significantly higher. A comparison of the experimental results is shown in Figure 2.26.

Isothermal sintering for 1000min and 2060 min (approximately equal to the total time for discontinuous sintering exp.) leads to much lower crystallization enthalpy than the 7th cooling cycle in discontinuous experiment. Thus, dramatic crystallinity growth was not a function of chain scission.

Figure 2.27 shows a different thermal history that leads to the same final enthalpy of crystallization 43J/g, as that obtained from the seventh cooling step in cyclic DSC. In designing this thermal profile, it was assumed that the dramatic increase in crystallinity in

the cyclic DSC experiment was a result of two independent processes-Isothermal annealing at 370^{o}C and Lamellar thickening in the solid state. For comparison sake, the isothermal annealing time at 370^{o}C was kept equal to the sum total of the isothermal times in the cyclic DSC. Further, the solid state thickening time was chosen to be nearly equal to the total heating/cooling time in cyclic DSC. Previous work by Wunderlich has shown nearly 40% thickening of PTFE lamellae in 40 minutes on annealing at 316^{o}C[59].

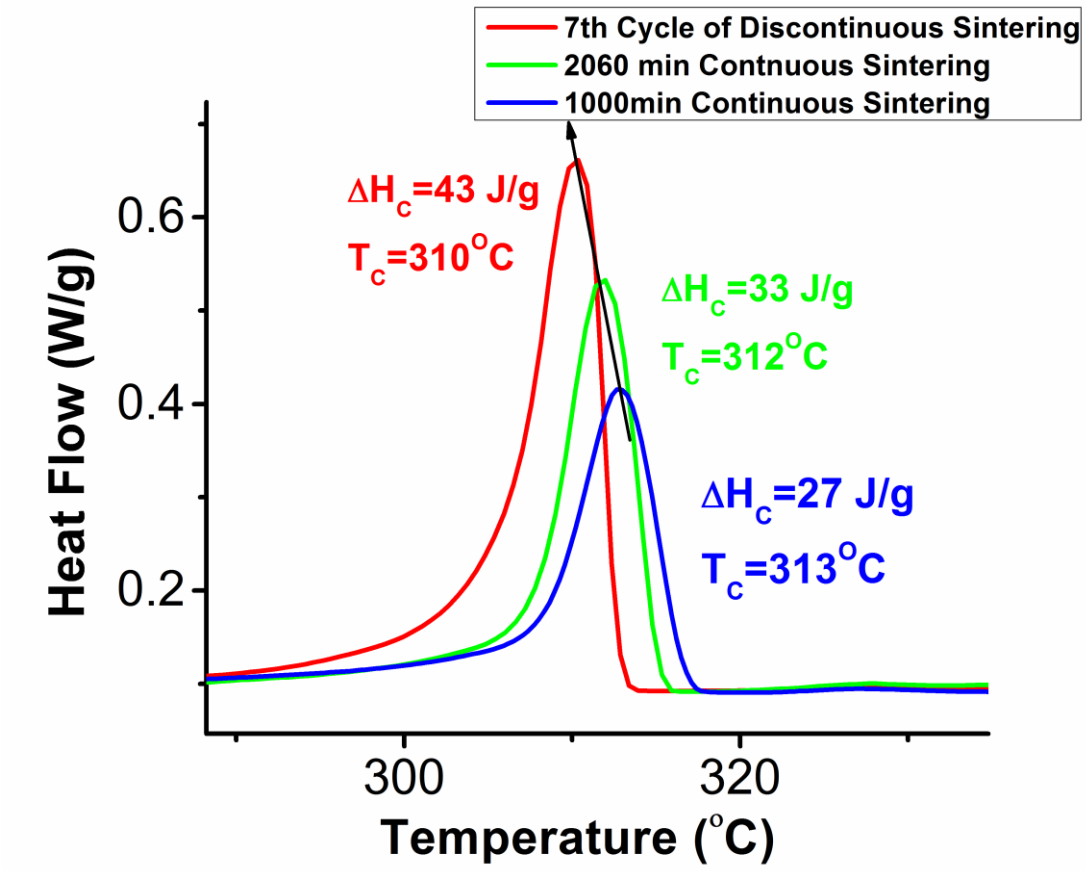

Figure 2-26: Comparison of final crystallinities resulting from different thermal treatments

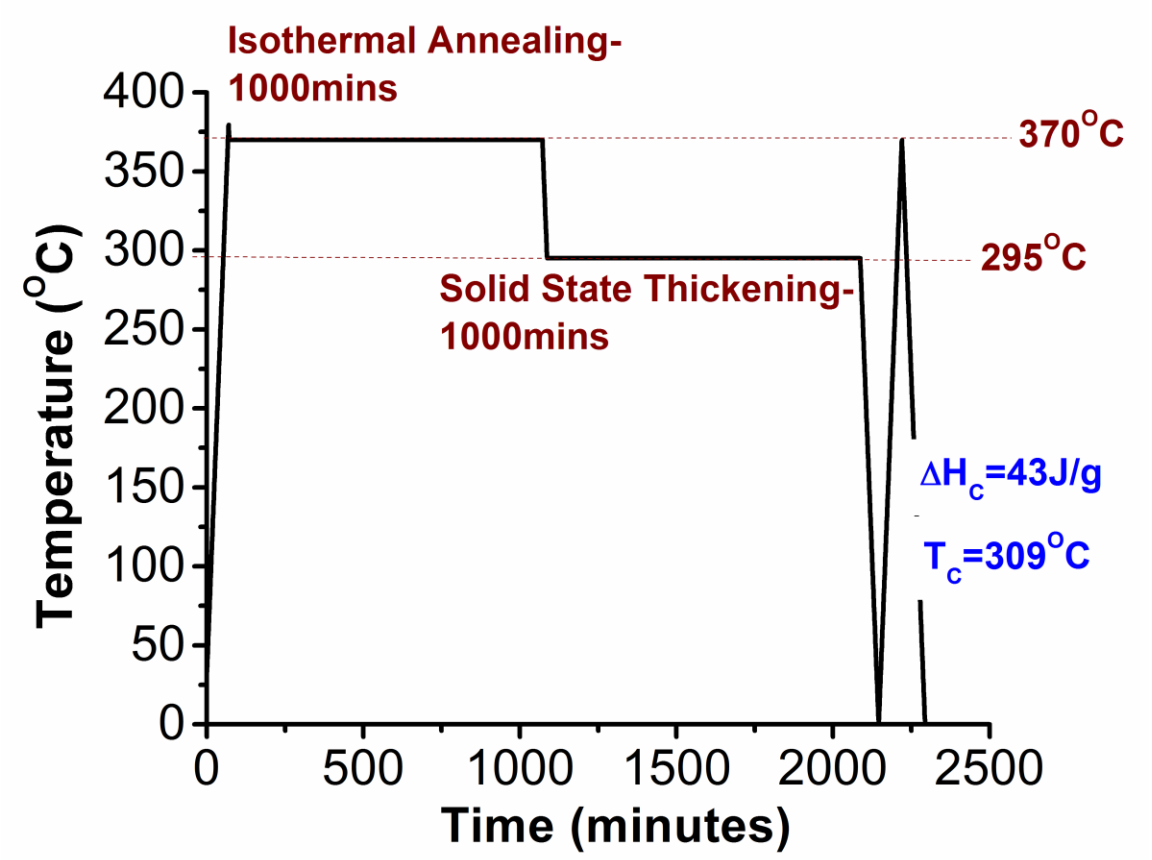

Figure 2-27: DSC temperature profile showing the independent effects of annealing and solid state thickening

2.4.4 Wide Angle X-Ray scattering:

In our quest to understand the molecular mechanism of PTFE sintering, the system was studied by a variety of experimental techniques. However, the results obtained were indicative of two distinct processes-Melt state molecular ordering as evidenced by an increase in crystallization/melting enthalpy with sintering time and entanglement formation as evidenced by increase in storage modulus with sintering time. A point to note here is that an increase in storage modulus can also come from molecular ordering. Further, there is evidence in literature of such molecular ordering in the melt state where P. Geil, based on microscopy studies showed that increasing sintering times lead to the formation of striated bands on the cryogenically fractured surface of PTFE and it is well known in PTFE literature that such striated bands are a characteristic of PTFE crystalline structure[45]. However, this was not an in-situ study as the samples were water quenched from the melt state and it was assumed that resulting structure will be identical to that prevailing in the melt. However, this might not be a good assumption for a material like PTFE which shows very fast crystallization kinetics. Therefore, in order to make any conclusive remark on this problem, one would need an in-situ technique for monitoring the state of order or disorder in the melt.

One such technique might be X-ray scattering on molten PTFE. Although, it is highly unlikely for a material to show crystalline order in its melt state, WAXS studies on molten PTFE has revealed the existence of a distinct Bragg's peak well above its melting point, which is an in-situ evidence of melt state order. This peak only disappears at 400^{o}C but is present at conventional sintering temperatures[60]. This is not surprising when one considers the extraordinary stiffness of the PTFE chains[55].

However, we are interested in the time evolution of this peak. Therefore, in our high temperature X-Ray scattering study, virgin PTFE was subjected to a temperature profile as indicated by Figure 2.28 and scattering studies were performed at locations indicated by the red dots.

Figure 2.29 shows the evolution of 100 peak as a function of temperature during heating and cooling and as a function of time at the sintering temperature of 370^{o}C.In figure 17, the broad amorphous scattering background has been subtracted. As can be clearly seen, increase in temperature from 24^{o}C (Room temperature) to 370^{o}C led to a significant decrease in scattering angle which is indicative of looser packing at higher temperatures. Further, following the 10 hour sintering step, subsequent cooling led to an increase in scattering angle which is indicative of better packing of the chains with decrease in temperature. There is existing literature on the comparison and contrasting of PTFE crystalline structure before and after sintering[60]. The focus here, however is the evolution of melt state order at the sintering temperature. Figure 2.30 presents a closer look at the evolution of 100 peak at 370^{o}C as a function of sintering time after subtraction of amorphous scattering background. As can be seen, increase in sintering time leads to a corresponding increase in scattering angle which is indicative of better packing or more perfect crystals. This result shows that the residual order present in PTFE melt increases in perfection with sintering time. Moreover, the intensity of the 100 peak also increases with sintering time. Further, the associated amorphous hump which was subtracted from Figure 2.29 and Figure 2.30, itself deceases with sintering time (Figure 2.31).A simultaneous increase in the intensity of the crystalline peak (Figure 2.30) and a decrease

in the associated amorphous hump (Figure 2.31) further shows that the crystalline content of PTFE melt increases with sintering.

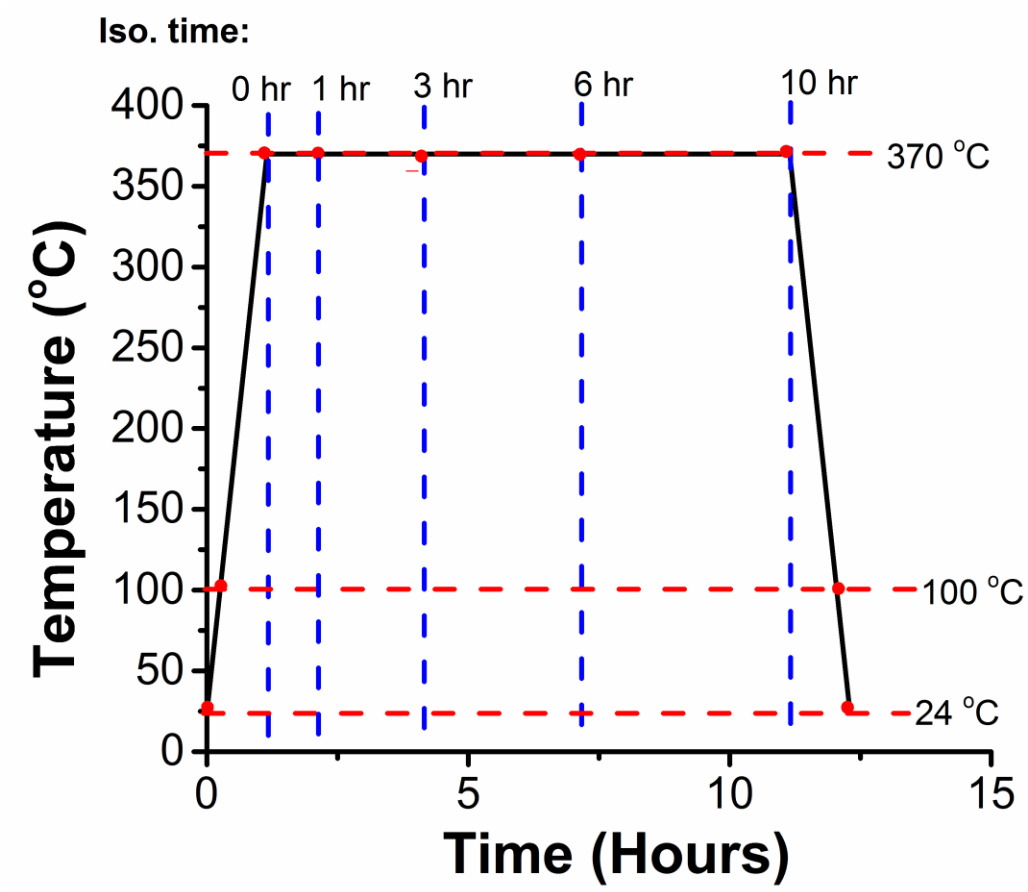

Figure 2-28: Time-Temperature profile for high temperature WAXS studies. Scattering studies were performed at locations indicated by the red dots.

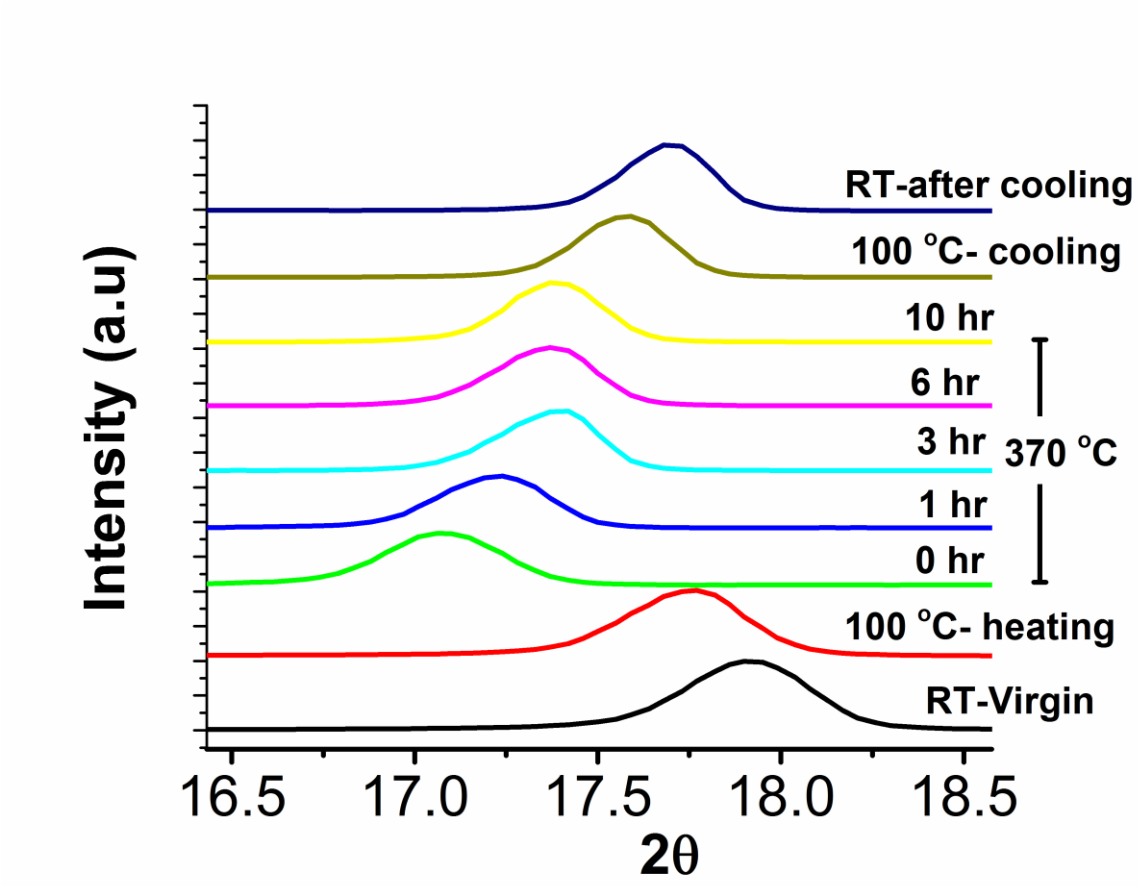

Figure 2-29: Evolution of 100 WAXS peak as a function of temperature and time (amorphous hump subtracted)

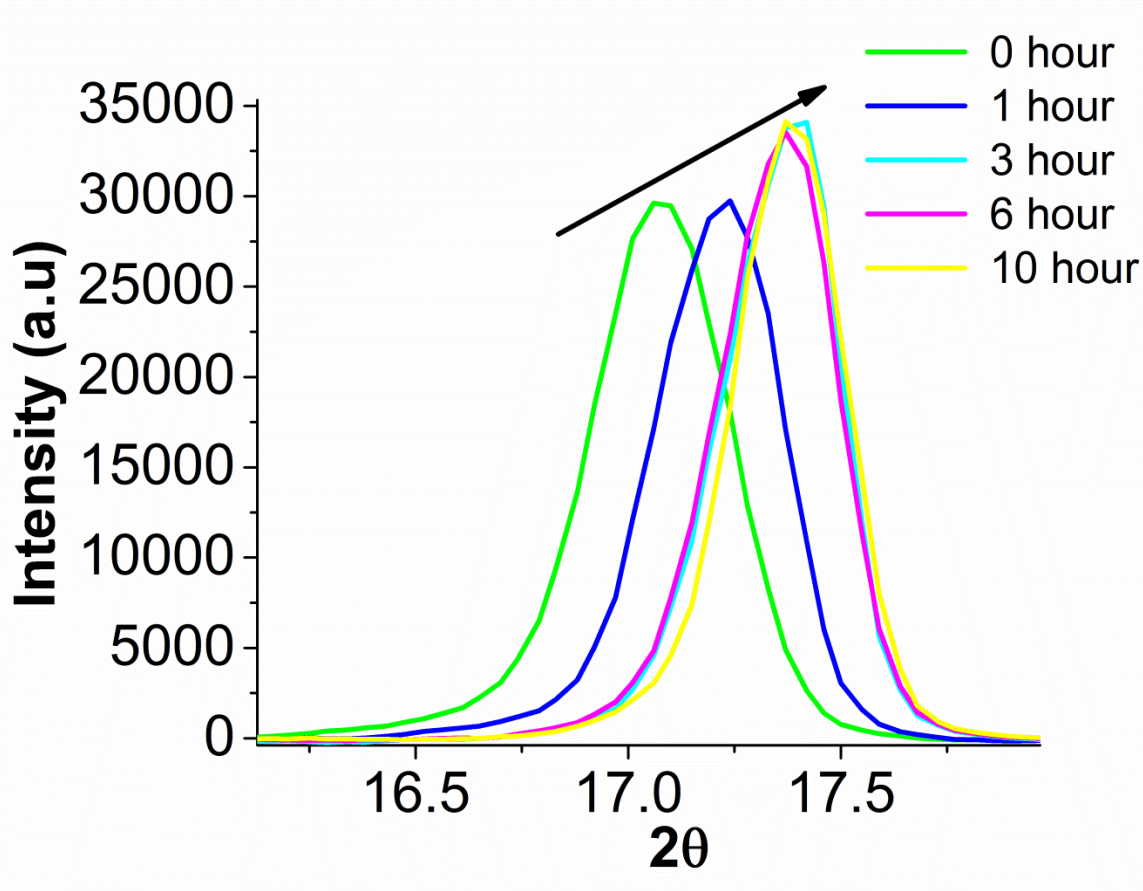

Figure 2-30: Evolution of 100 peak at 370ºC as a function of sintering time (amorphous hump subtracted)

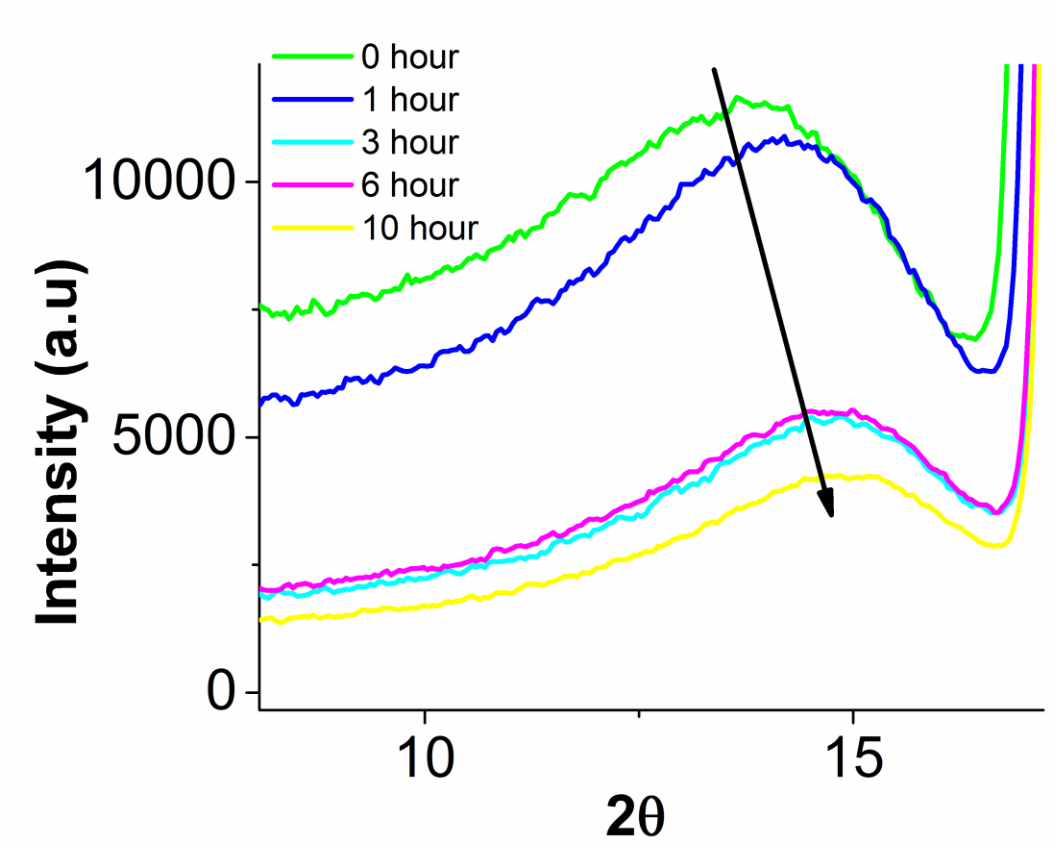

Figure 2-31: Evolution of amorphous hump at 370ºC as a function of sintering time

2.4.5 Small Angle Light Scattering (SALS):

The SALS experiment was again performed to study the structure evolution of UHMWPTFE melt. UHMWPTFE is a white solid below its melting point of 345^{o}C. However, above the melting point the material becomes transparent or semi-transparent due to loss or partial loss of the crystalline fraction, thus allowing for the passage of light. In the SALS experiment an UHMWPTFE film of thickness 0.15 mm was preformed using the standard preforming procedure described in this chapter and its light transmission was measured at 370^{o}C for 18 hours. Linkam TMS93 heating stage was used for temperature control and nitrogen was circulated to avoid any high temperature degradation of the film. Figure 2.32 shows the variation of transmitted light intensity as a function of time. As can be seen, the light transmission decreases as a function of sintering time and reaches a plateau after 2 hours. This decrease in light transmission can be due molecular ordering in the melt state as already evidenced by cyclic DSC, cyclic TMA and high temperature WAXS experiments.

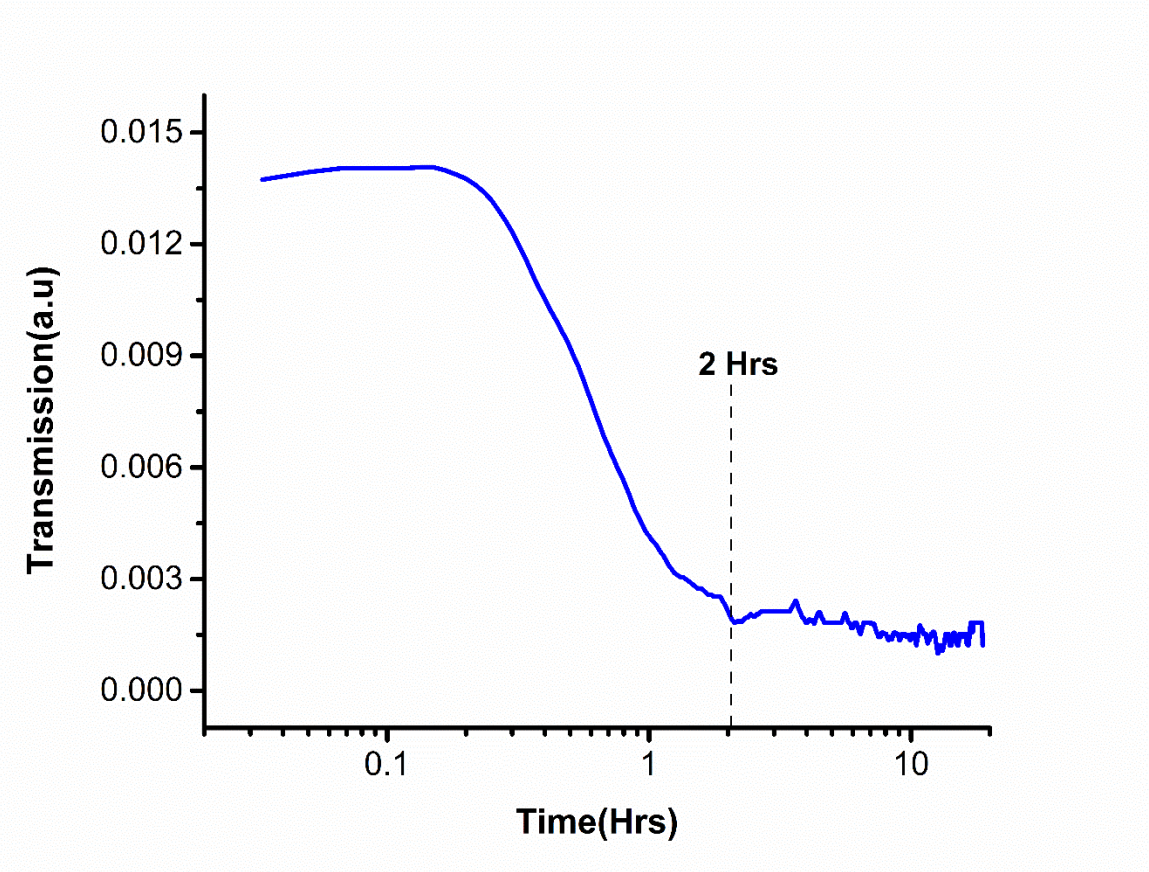

Figure 2-32: Change in light transmission of a 0.15 mm UHMWPTFE film as a function of sintering time at 370°C for 18 hours

2.4.6 Non-standard compression testing:

Compression test is considered a better measure of intrinsic material properties than tension test, since geometric instabilities such as necking and crazingare suppressed[61]. In the case of semi-crystalline polymers, the yield stress is related to morphological transition from a spherulitic to a fibrillar structure while the strainhardening modulus is related to network connectivity[62,63], and depends strongly on entanglement in thermoplastics and chemical crosslink in thermosets[34,38,61]. So far, we have evidence of two molecular processes that are associated with sintering. The increase in storage modulus as a function of sintering time might be suggestive of entanglement formation in the melt state while the high temperature WAXS and SALS experiments are indicative of molecular ordering in the melt state. Therefore, in this situation non-standard compression testing would prove to be a very powerful technique to study both these molecular processes simultaneously. If sintering is associated with molecular ordering in the melt state then increasing the sintering time will lead to increase in the yield stress while if it is associated with interparticle entanglement formation then increasing the sintering time will lead to increase in the strain hardening modulus. Figure 2.33 shows the stress-strain curves for UHMWPTFE billets that have been sintering for different times in compression. As can be seen, increasing the sintering time leads to a simultaneous increase in both the yield stress and the strain hardening modulus. This result indicates that the two processes of molecular ordering and molecular entanglement formation occur simultaneously during the sintering of UHMWPTFE.

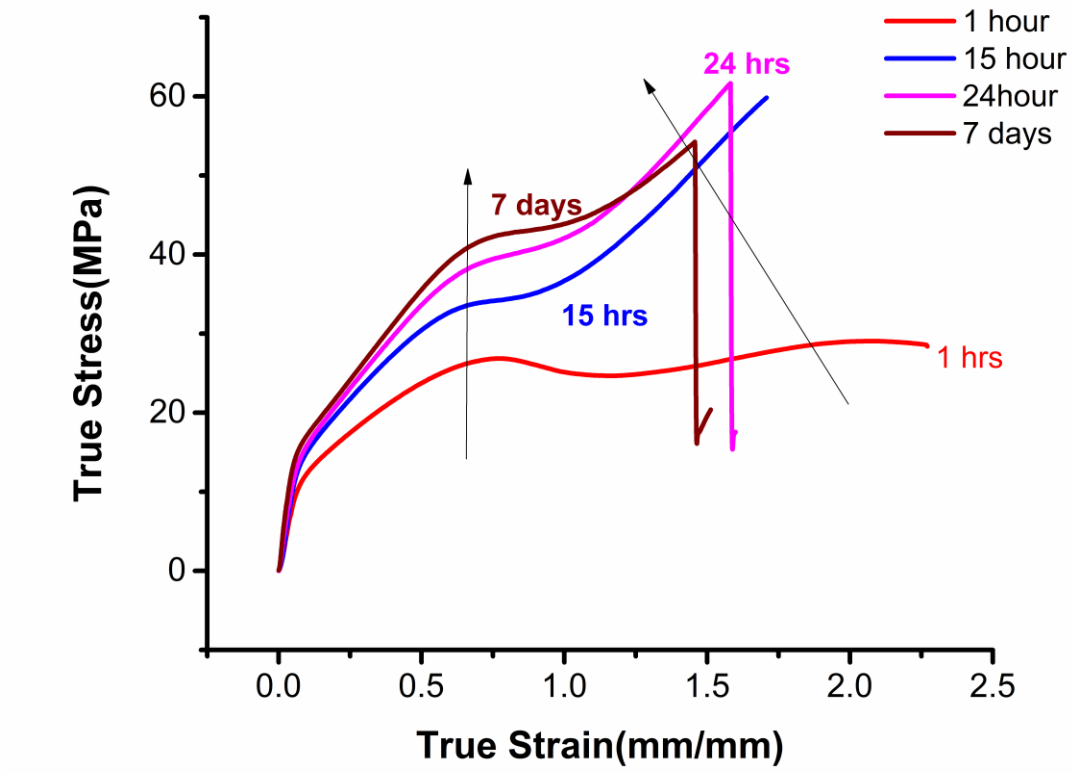

Figure 2-33: Compressive stress-strain curves for UHMWPTFE billets sintered for different times

2.5 Conclusion

This chapter elucidates the molecular mechanisms associated with UHMWPTFE sintering.Two potential molecular processes seem to be playing a role: entanglement formation and melt state ordering. The increase of storage modulus of the melt as a function of sintering time and higher strain hardening modulus for billets sintered for longer times are indicative of entanglement formations. On the other hand, results from cyclic DSC, cyclic TMA, high temperature WAXS and high temperature SALS are suggestive of melt state ordering.

Further, TMA was established as a complimentary technique for monitoring melting/crystallization transitions. Both DSC and TMA exhibited a non-equilibrium evolution of PTFE melt. The enthalpy of crystallization and melting was found to increase with successive sintering steps. Further, the crystallization temperature decreased whereas the melting temperature increased with successive sintering. These results were endorsed by in-situ high temperature X-Ray scattering studies on molten PTFE. Results obtained from the cyclic TMA experiment correlated well with the corresponding cyclic DSC. It was established that the dramatic growth in enthalpy of crystallization and melting was not due to chain scissions at 370^{o}C. Further, it was shown to be possibly resulting from two independent processes-Isothermal annealing at 370^{o}C and lamellar thickening in the solid state.

It was shown that UHMWPTFE exhibits a double yield phenomenon at room temperature under compression.

CHAPTER 3

KINETICS OF ULTRA HIGH MOLECULAR WEIGHT PTFE SINTERING

3.1 Introduction

This chapter focuses on understanding the effect of different fluoropolymer additives, particle size distribution and processing conditions on the sintering kinetics of UHMWPTFE. Further, a secondary objective of this work is to identify strategies that might enhance the recyclability of UHMWPTFE.

Firstly, the effect of sintering temperature, different thermal loading profiles and particle size on the sintering kinetics of UHMWPTFE will be studied. Two types of fluoropolymer additives will be studied. A lower molecular weight PTFE fraction will be homogeneously mixed with UHMWPTFE over a composition range and the effect of the lower molecular weight fraction on the sintering kinetics of UHMWPTFE will be investigated. Further, UHMWPTFE regrind powder will be homogeneously mixed with UHMWPTFE virgin powder and the effect of regrind fraction on the sintering kinetics will be studied. Moreover, the effect of reducing the particle size of regrind fraction on the sintering kinetics will be investigated.

The kinetics of sintering will be studied in-situ by monitoring the storage modulus evolution as a function of sintering time and the kinetics will be quantified by the absolute value of the storage modulus and its rate of growth. Further, the dimension change of the billet in the machine direction will be monitored in-situ.

3.2 Experimental

3.2.1 Materials and sample preparation

Virgin UHMWPTFE molding powders having three different particle sizes M15X, 2-2 and 2-6 were used. Further, a low molecular weight PTFE and two UHMWPTFE regrind powders R500 (~500 µm) and R50 (~50 µm) were used in the current study.

Samples were made by following the controlled two stage pre-forming strategy described in chapter 2.

3.2.2 Method

Thermo-mechanical analyzer TMA Q400 (TA Instruments, USA) both in standard and volumetric mode were used for in-situ sintering studies. Dimension change and storage modulus evolution were monitored in the standard mode while density evolution was monitored in the volumetric mode. For all TMA studies a preload force of 0.01N was applied to sustain contact between the probe and the specimen surface. Heating and cooling rates were 5^{o}C/min for all studies unless otherwise stated.

3.3 Results and Discussion

3.3.1 Anisotropy

It is a well-known fact that uniaxially compressed PTFE billets are anisotropic in nature and exhibits different expansion behavior in the axial and transverse directions. To quantify this phenomenon we introduce an Anisotropy factor (AF) defined by equation 3.1.

$$A_F = \frac{H(t)/H(0)}{D(t)/D(0)} \ldots\ldots\ldots\ldots (3.1)$$

Where, H(0)and D(0)are the initial height and diameter of the PTFE billet, whereas H(t) and D(t) are the instantaneous height and diameter at any time 't' during the sintering process. The axial and volumetric expansion ratios can be measured using the standard and volumetric TMA respectively while the transverse expansion ratio is calculated. Figure 3.1 depicts results of a 380^{o}C sintering for 1000 minutes from both standard and volumetric TMAs. Since the geometry of the sample is known to be cylindrical, the associated changes in diameter i.e. the transverse expansion ratio can be calculated from the axial and bulk extension ratio. As can be seen, the axial expansion ratio is higher than the transverse expansion ratio, making the expansion behavior anisotropic. Finally, Figure 3.2 shows the evolution of Anisotropy factor. The anisotropy decreases with the progress of sintering.

It is because of this anisotropic expansion of PTFE that the dimension change in the axial direction cannot be satisfactorily used to quantify sintering kinetics. Nevertheless, the dimension changes associated with the sintering experiments will be reported but the storage modulus evolution and in some instances density evolution will be used to quantify sintering kinetics.

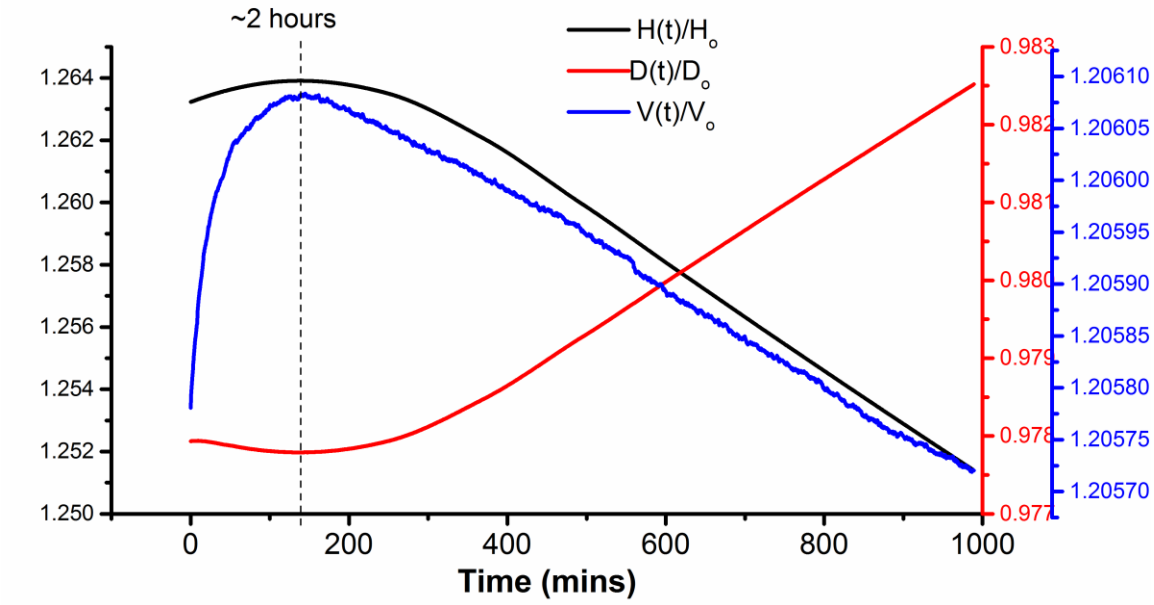

Figure 3-1: Axial, transverse and bulk extension ratio as a function of sintering time for 380^{o}C sintering of M15X

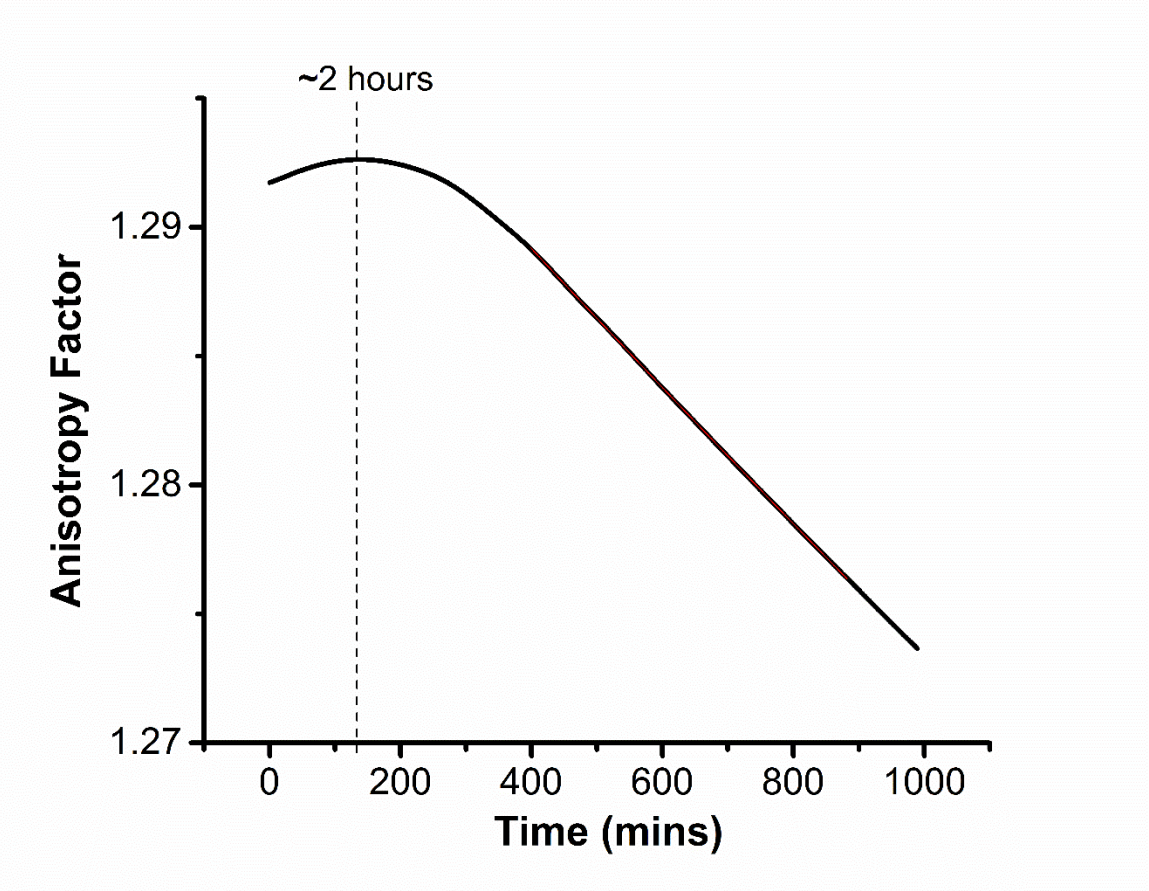

Figure 3-2: Evolution of anisotropy factor for 380°C sintering for 1000mins of M15X

3.3.2 Effect of sintering temperature

Sintering temperature is a very important process parameter that affects the final properties of the sintered part. This section investigates the effect of sintering temperature on the kinetics of the sintering process. Figure 3.3 shows the evolution of storage modulus as a function of sintering time for different sintering temperatures. As can be seen, higher sintering temperatures lead to higher rate of growth of storage modulus indicating faster sintering kinetics (Figure 3.4). As discussed in the previous section, dimension change cannot be satisfactorily used for quantifying the sintering process due to anisotropic expansion of UHMWPTFE. However, as shown in Figure 3.5, higher sintering temperatures lead to greater contraction of the billets which is indicative of faster sintering kinetics. A point to note here is that in this study the starting material is the same for all sintering temperatures. Therefore, any effect coming from anisotropic expansion is not affect the expected trend in kinetics. However, when the starting materials are different either in terms of microstructure or particle sizes, dimension change cannot be used to predict the sintering kinetics possibly due to different anisotropies.

As discussed in chapter 1, the sintering process is associated with inter-particle entanglement formation and kinetics of this entanglement formation might increase with increase in temperature. Therefore, faster entanglement formation might be responsible for faster sintering kinetics at higher temperatures.

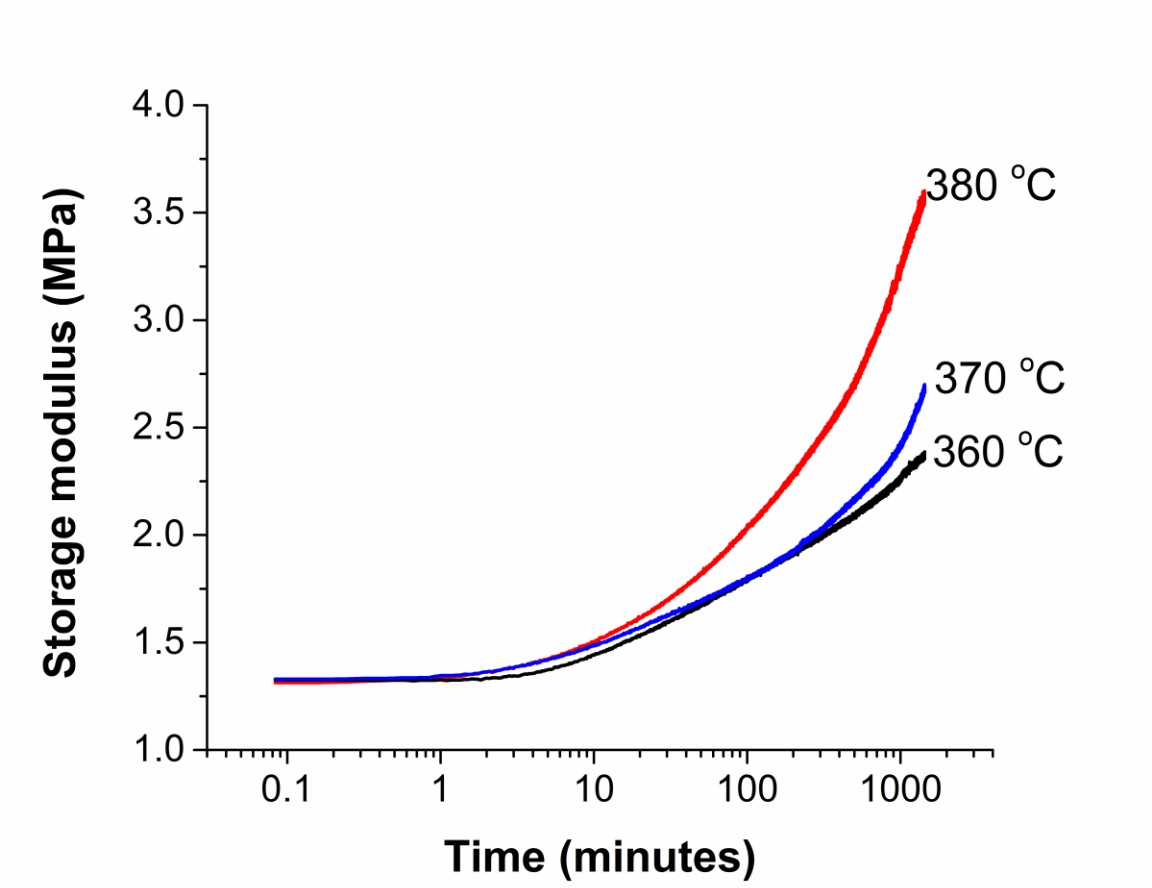

Figure 3-3: Effect of sintering temperature on storage modulus evolution of M15X

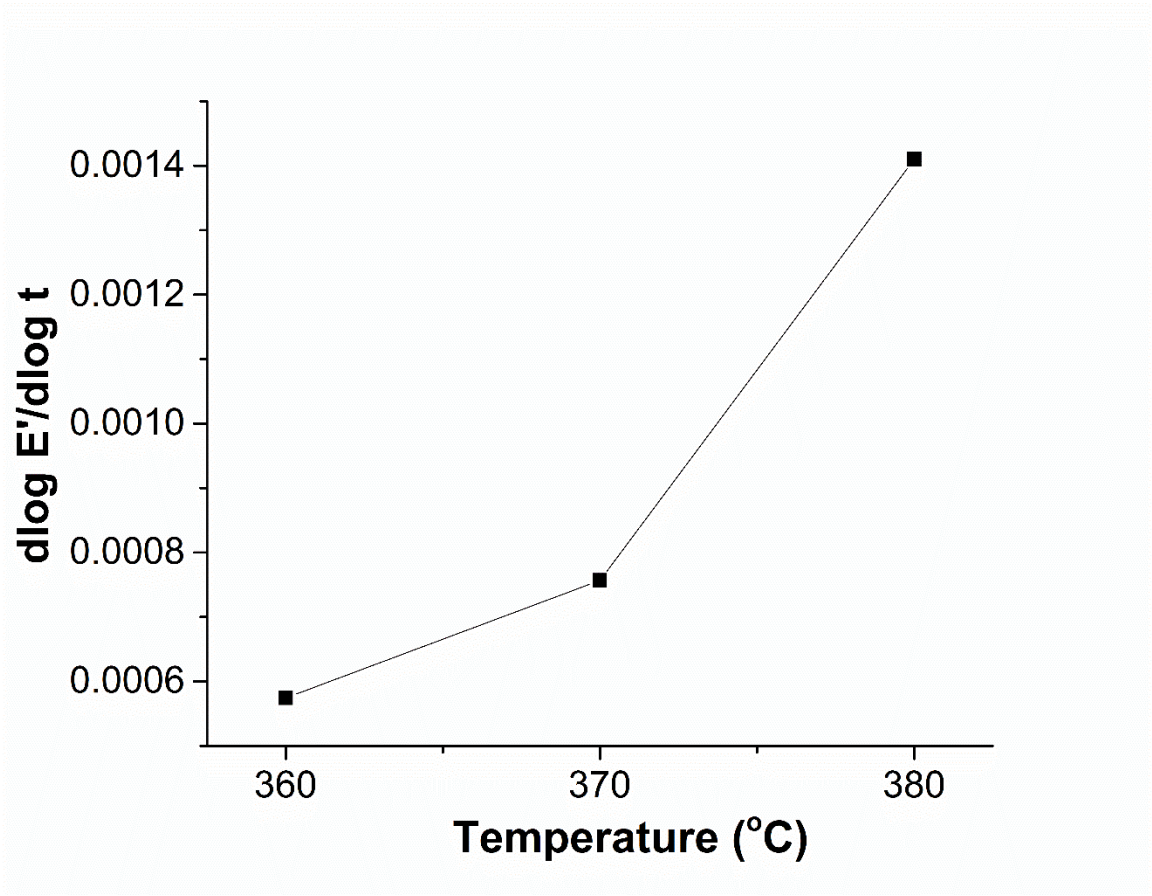

Figure 3-4: Effect of sintering temperature on the rate of growth of storage modulus of M15X

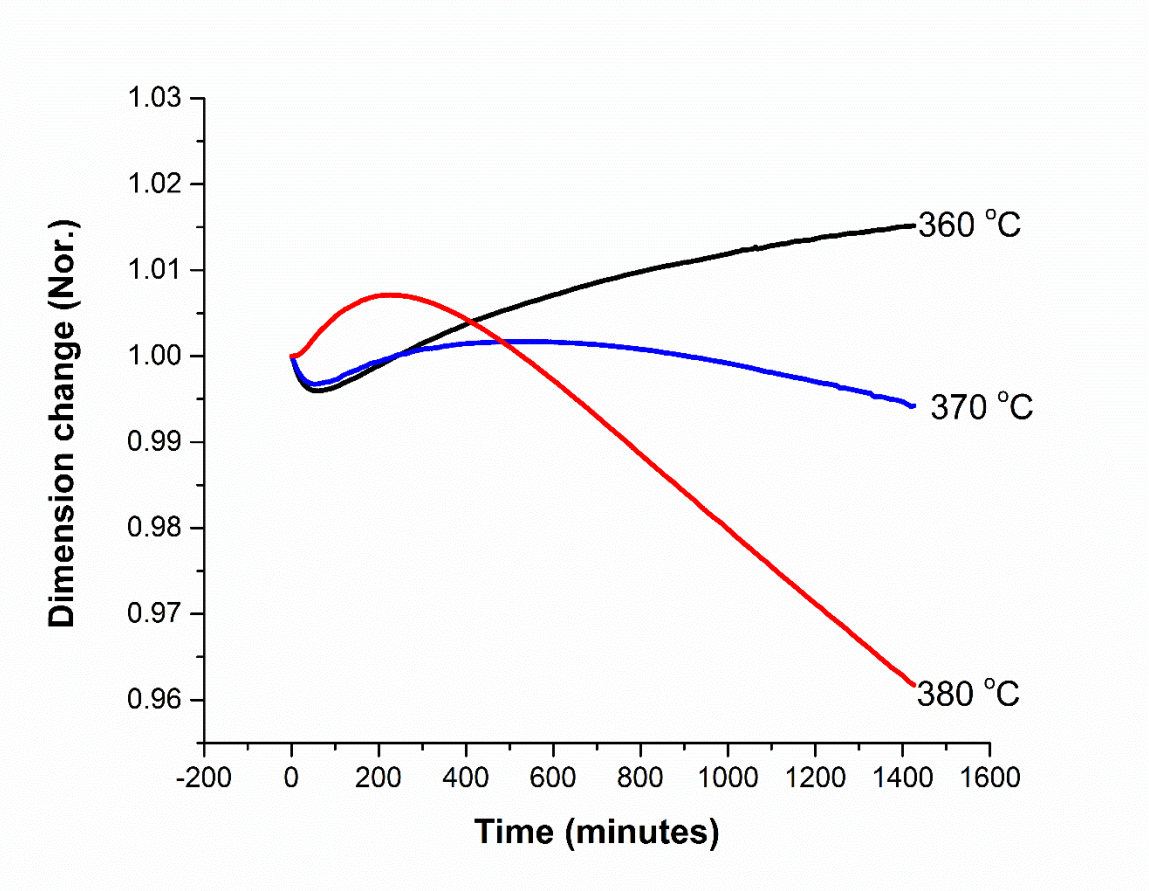

Figure 3-5: Effect of sintering temperature on dimension change in the axial/machine direction of M15X

3.3.3 Effect of thermal loading profile

Conventionally, sintering involves holding the preform at the sintering temperature for a specified period of time. However, in this section a cyclic thermal loading profile (Figure 2.20) will be applied and compared to continuous sintering. Figure 3.6 compares the storage modulus evolution for continuous and cyclic sintering at 370^{o}C. As can be seen, continuous sintering leads to higher absolute value and rate of growth of storage modulus. Initially the storage modulus closely follows one another. However, for the cyclic sintering every time the material is thermally cycled, it starts at a slightly lower value of storage modulus and this cumulative effect leads to lower absolute storage modulus.

A rationale for this behavior might come from our fundamental understanding of the sintering process developed in chapter 2. In cyclic sintering, intermittently cooling the material below its crystallization temperature will not only hinder the ongoing entanglement formation process but also might result in crystallization induced disentangling. Conversely, this result provides additional support to entanglement formation being responsible for sintering.

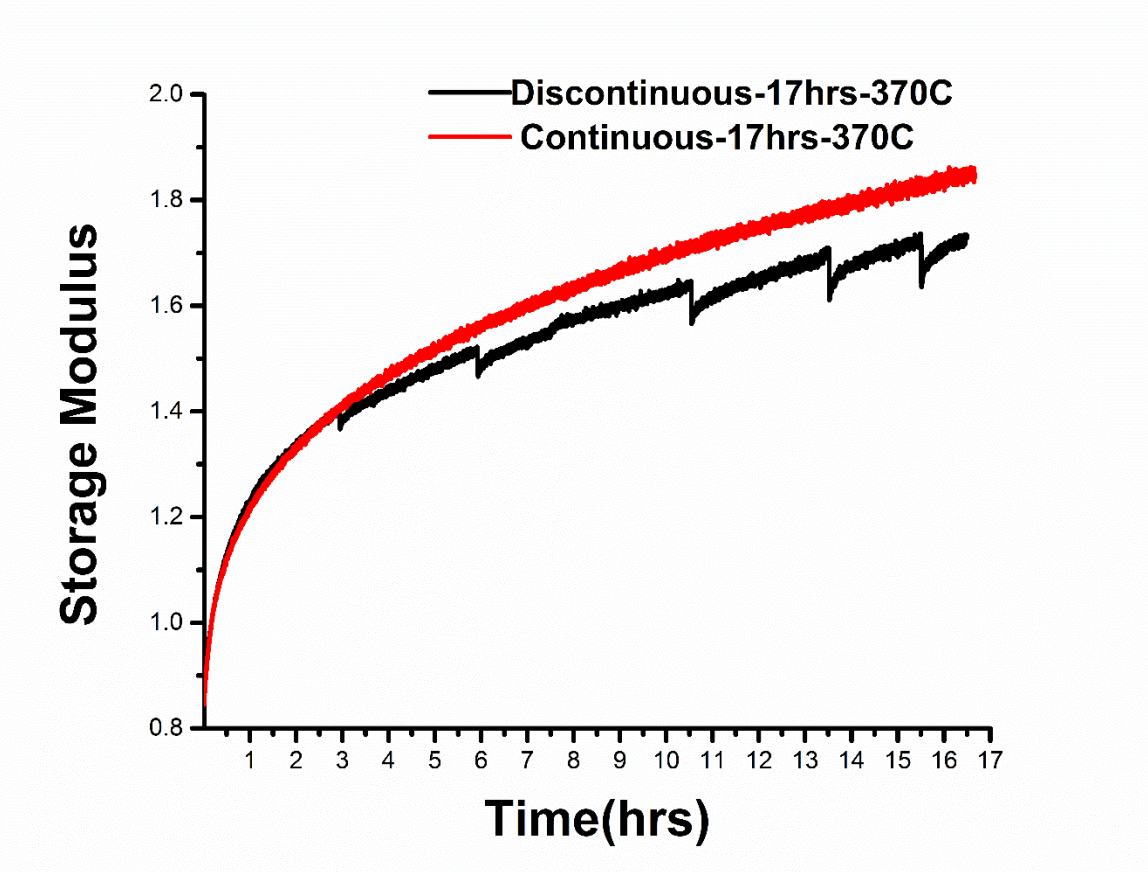

Figure 3-6: Effect of thermal loading profile on storage modulus evolution of M15X

3.3.4 Effect of particle size

Three different particle sizes (M15X>2-2>2-6) of virgin UHMWPTFE was prepared by jet milling of M15X for different durations. Figure 3.7 and figure 3.8 shows the density and storage modulus evolution at 380^{o}C for the different particle sizes. Lower the particle size, higher the densification and higher the rate of storage modulus growth. This is expected because lower the particle size higher will be the area of contact between particles and higher the interparticle entanglement formation. However, the dimension change in the axial direction cannot predict this trend as shown in figure 3.9 and figure 3.10. This might be due to different anisotropy shown by different particle sizes. However, at 380^{o}C the dimension change is more pronounced than 370^{o}C due to faster sintering kinetics.

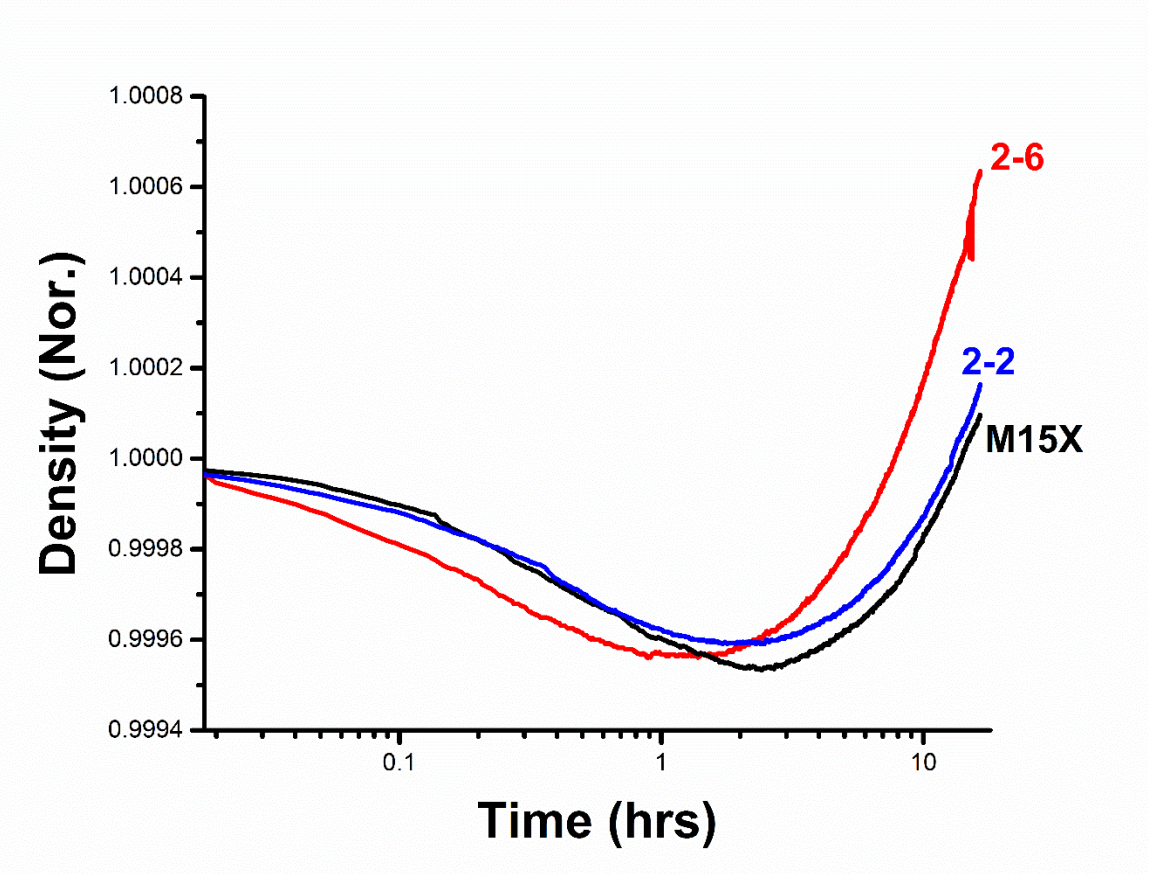

Figure 3-7: Effect of particle size on density evolution at 380ºC

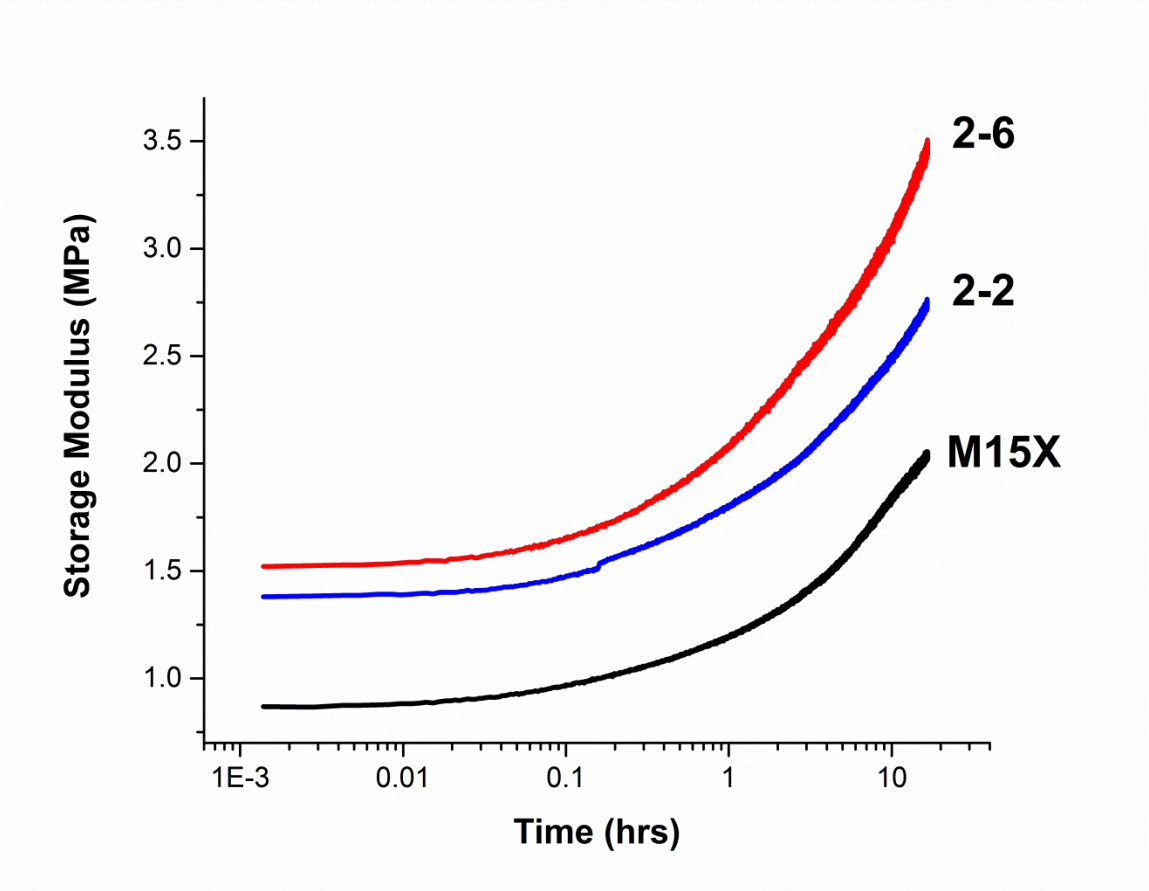

Figure 3-8: Effect of particle size on storage modulus evolution at 380°C

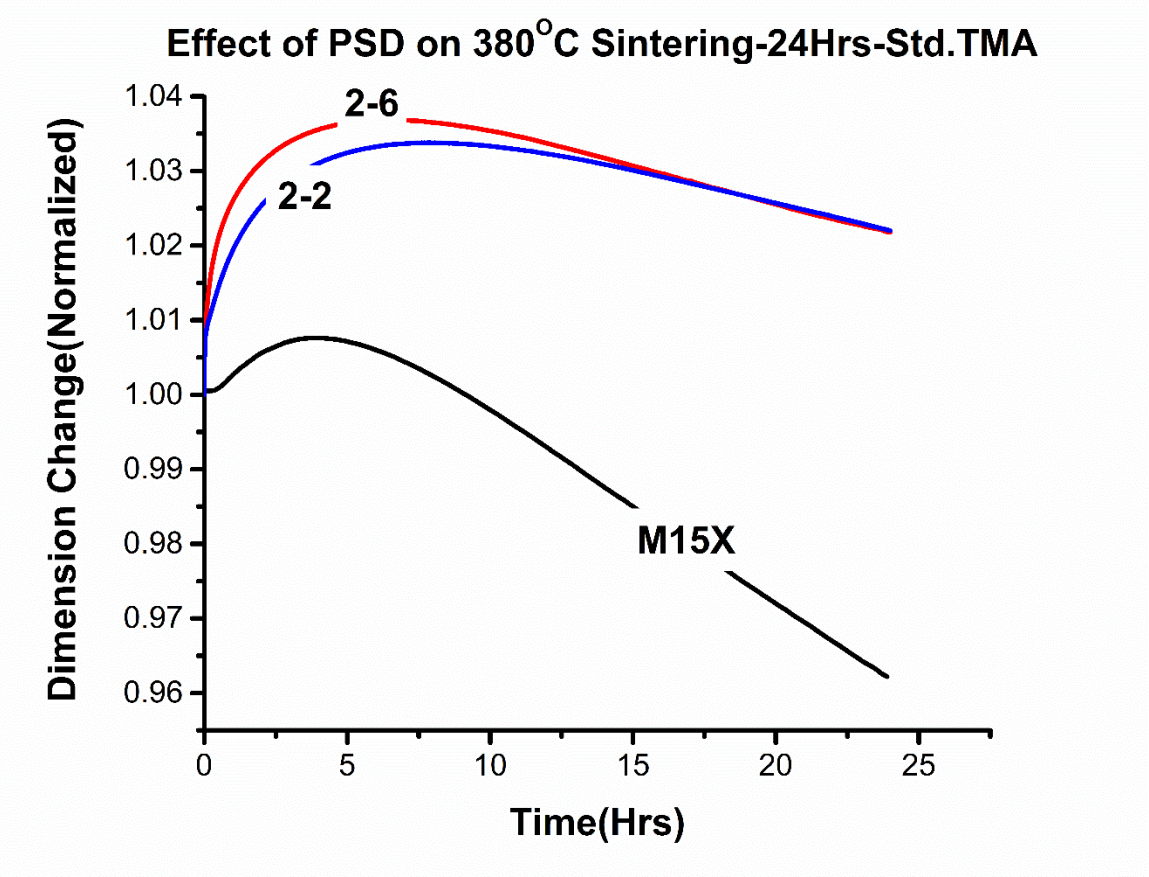

Figure 3-9: Effect of particle size on dimension change at 380ºC

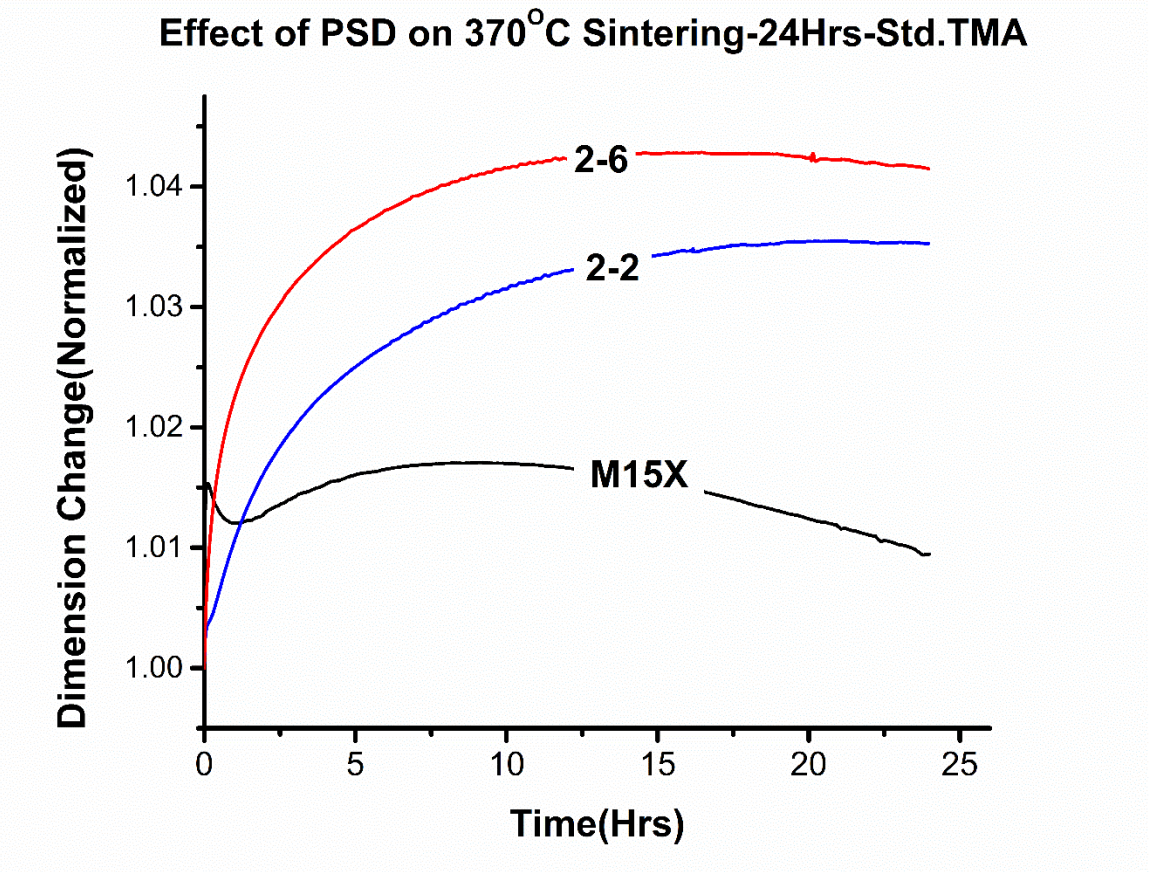

Figure 3-10: Effect of particle size on dimension change at 370°C

3.3.5 Effect of lower molecular weight PTFE fraction

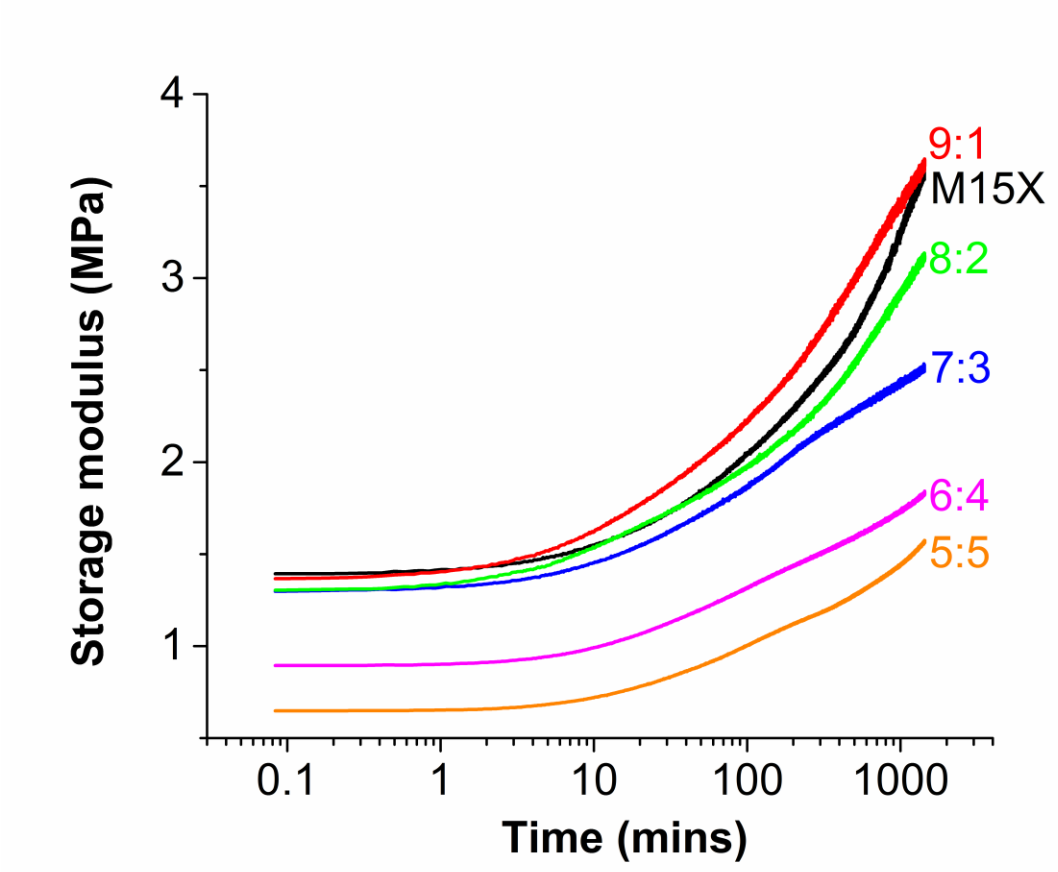

Figure 3-11: Effect of lower molecular weight PTFE fraction on storage modulus evolution of M15X at 380°C

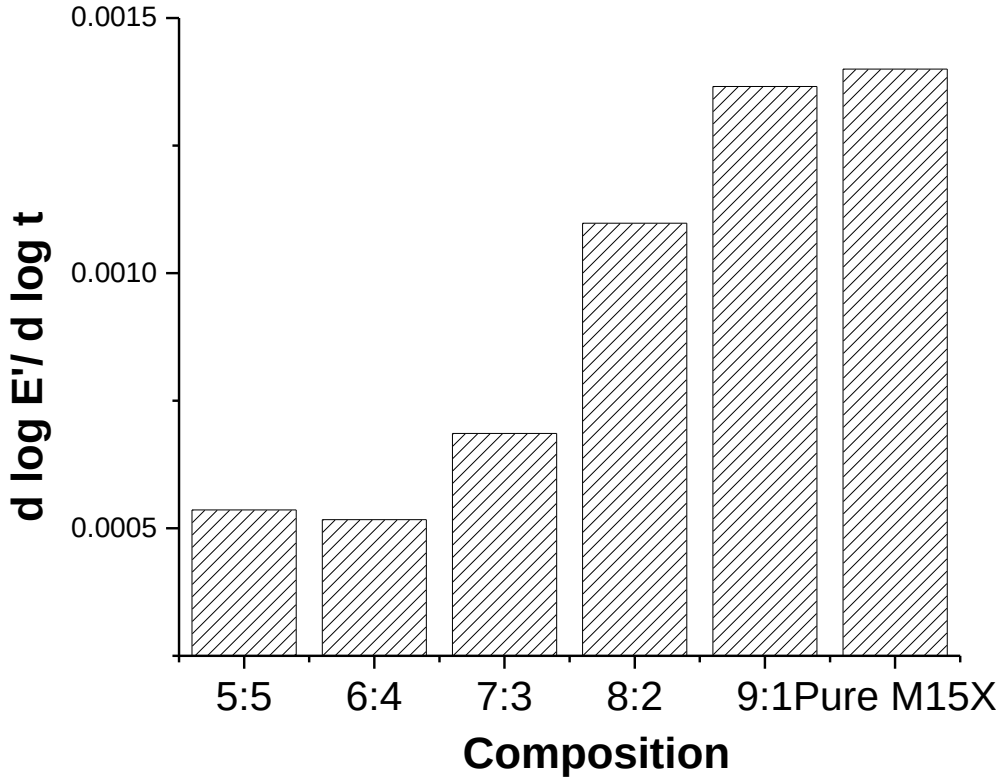

Figure 3-12: Effect of lower molecular weight PTFE fraction on rate of growth of storage modulus at 380ºC

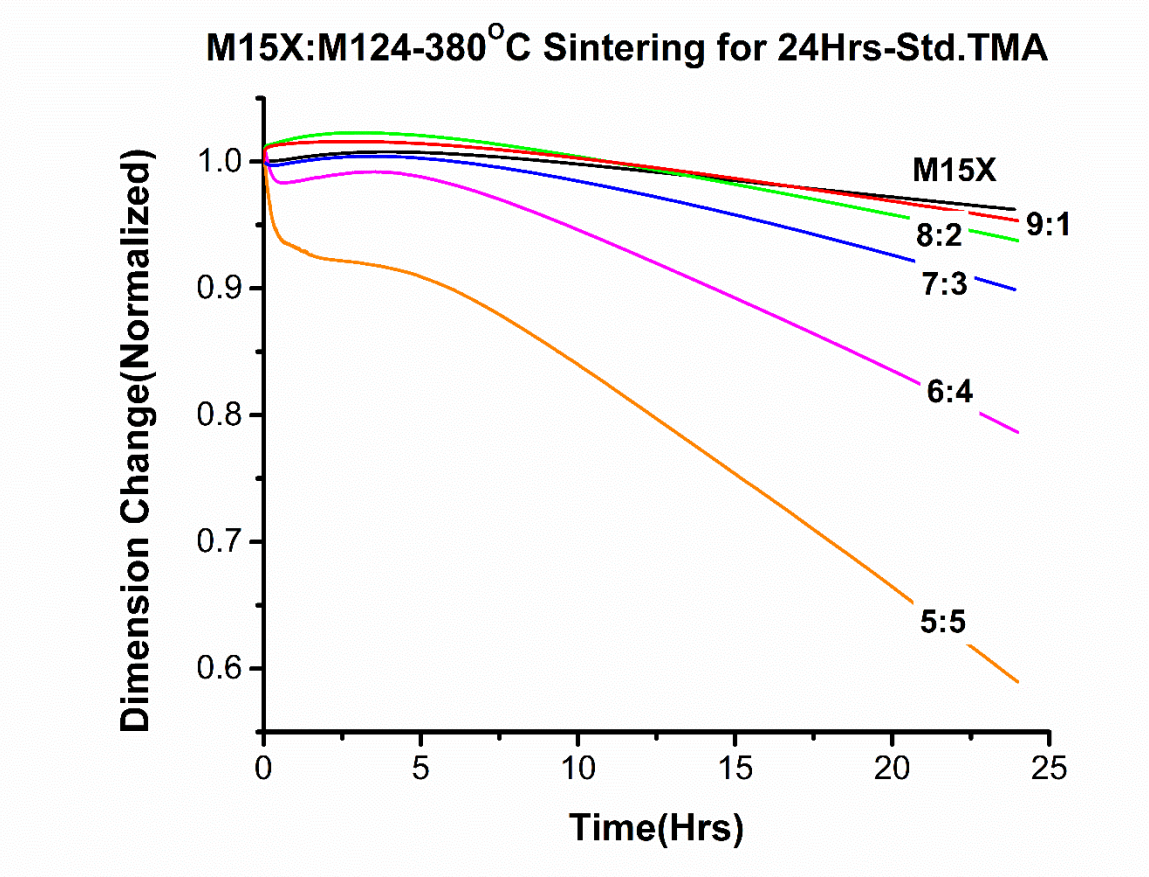

Figure 3-13: Effect of lower molecular weight PTFE fraction on dimension change at 380ºC

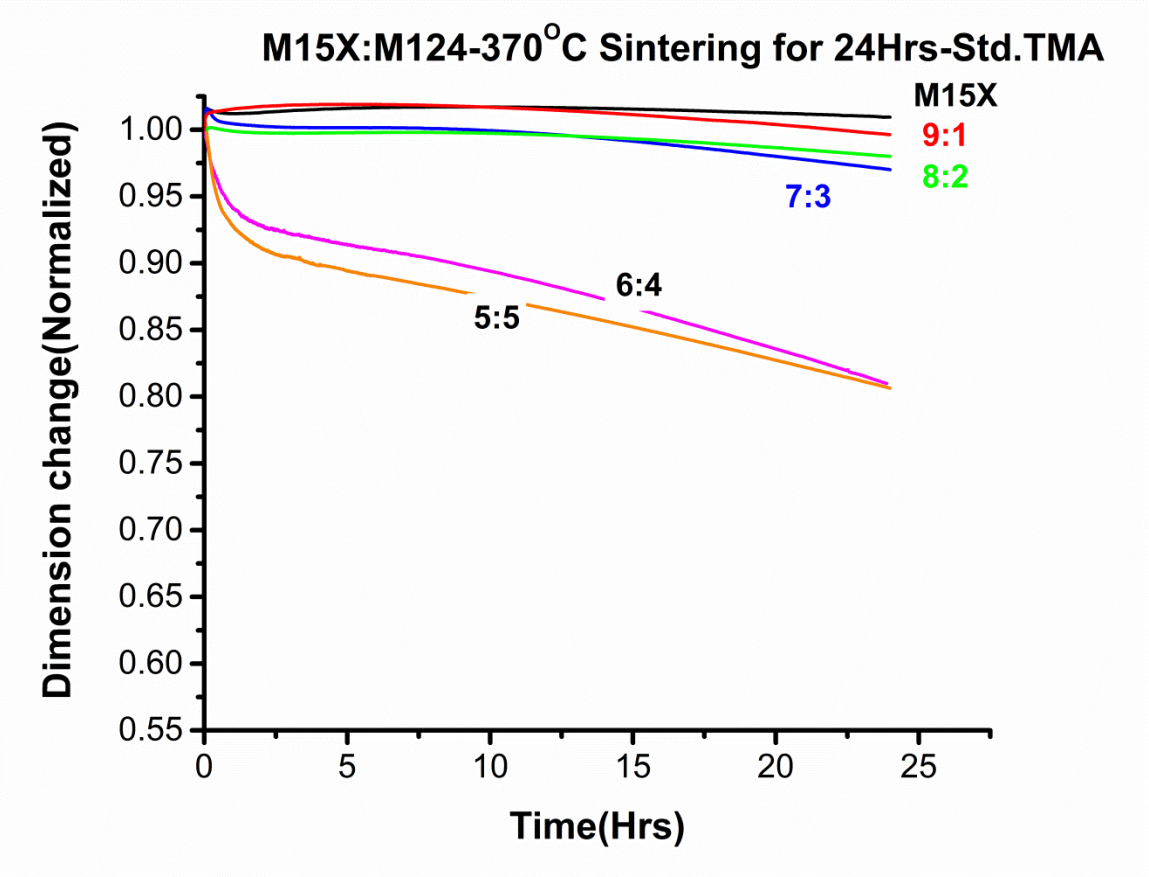

Figure 3-14: Effect of lower molecular weight PTFE fraction on dimension change at 370ºC

3.3.6 Effect of regrind fraction

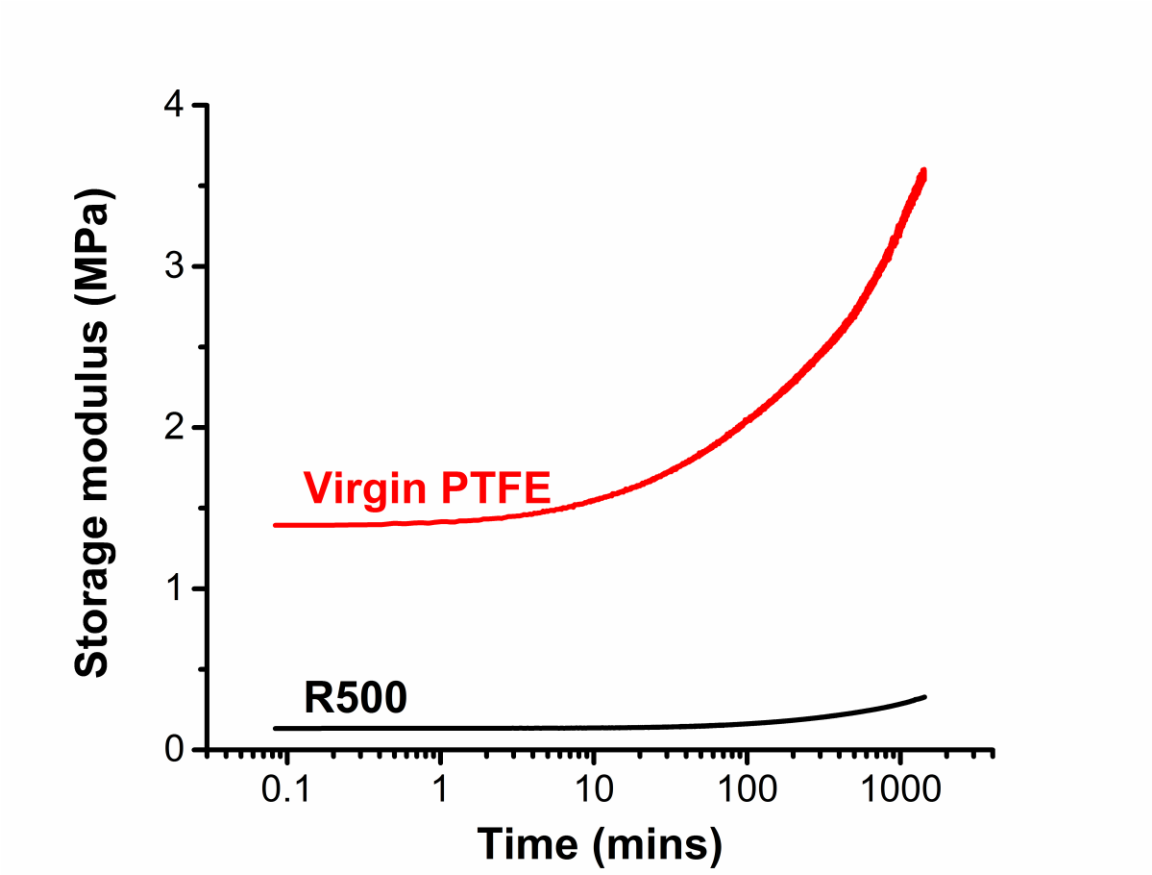

Figure 3-15: Comparison of storage modulus evolution between virgin and regrind PTFE at 380°C

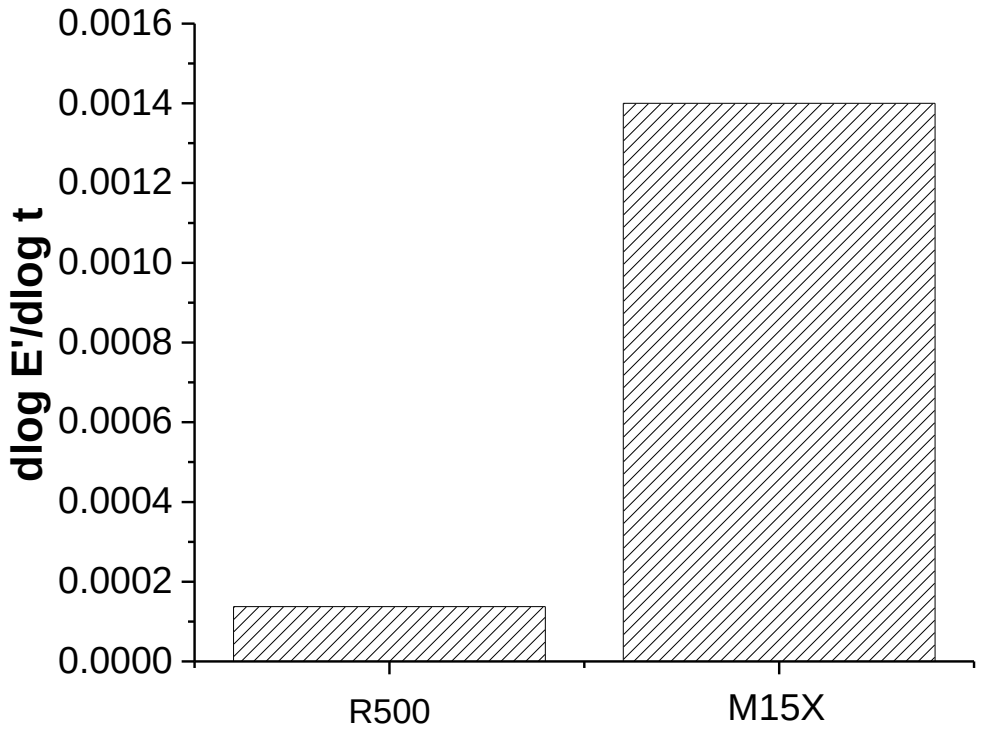

Figure 3-16: Comparison of rate of growth of storage modulus between virgin and regrind PTFE

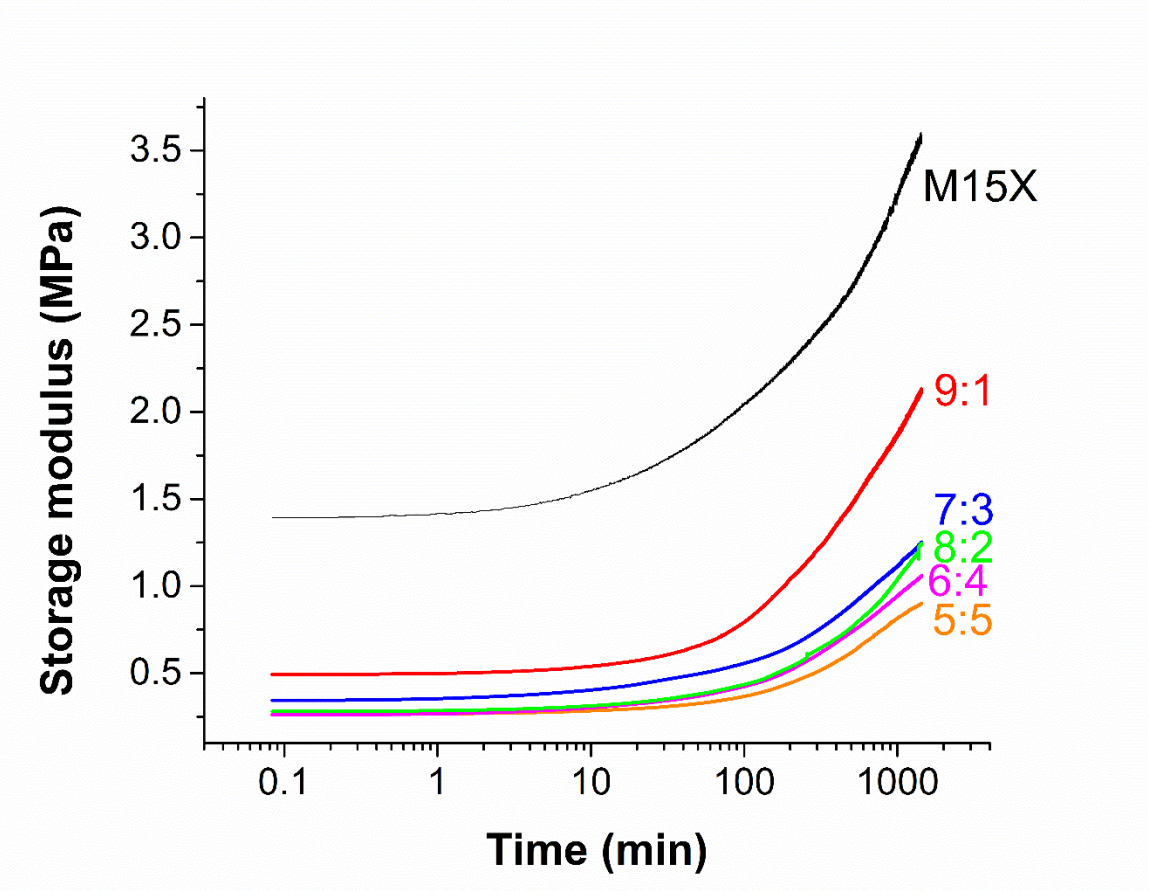

Figure 3-17: Effect of R500 fraction on storage modulus evolution at 380ºC

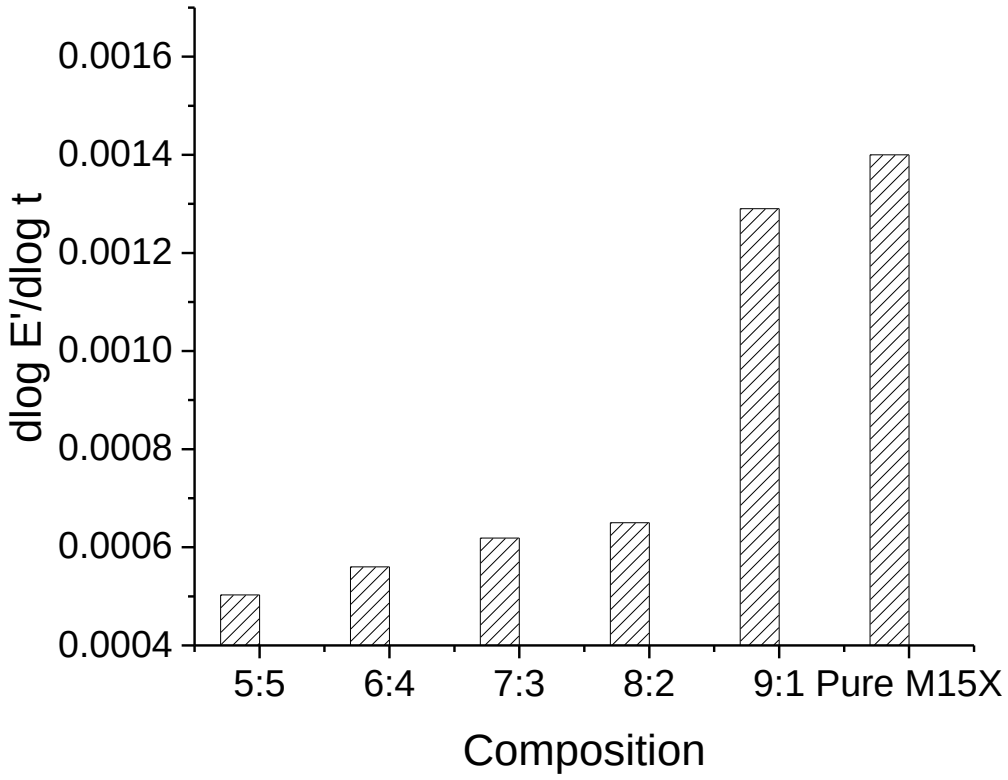

Figure 3-18: Effect of R500 fraction on rate of growth of storage modulus evolution at 380ºC

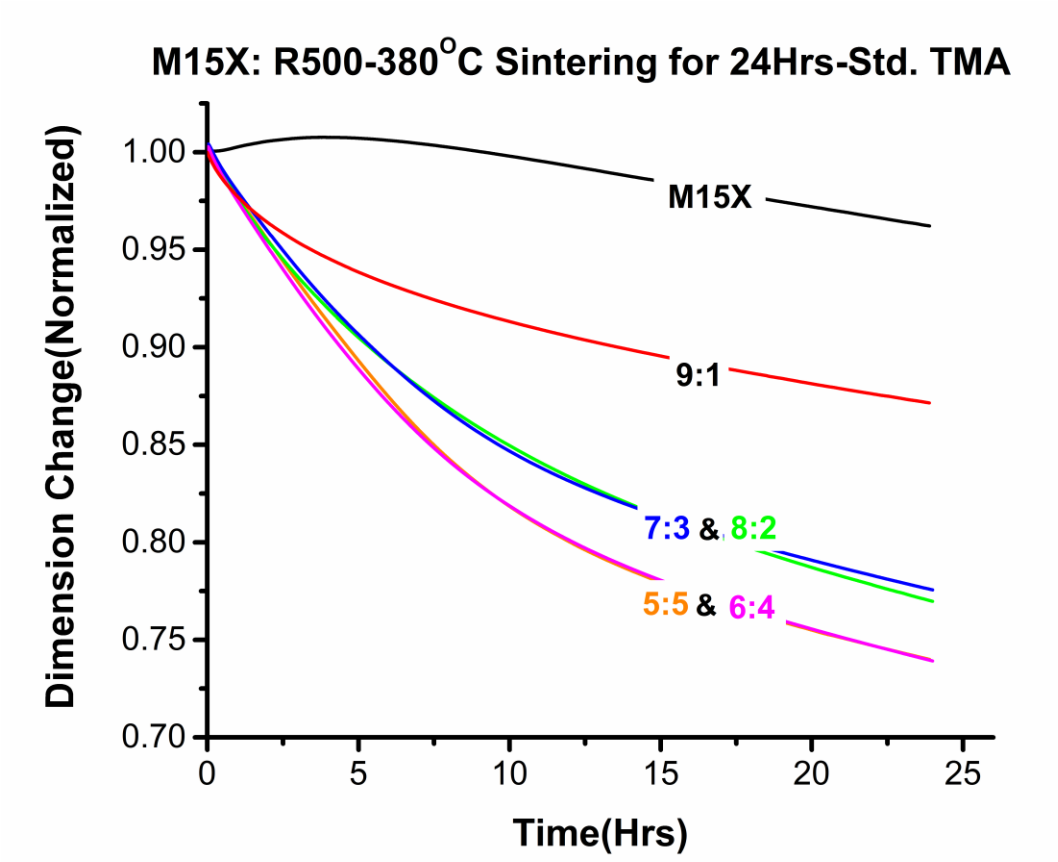

Figure 3-19: Effect of regrind fraction (R500) on dimension change of M15X at 380ºC

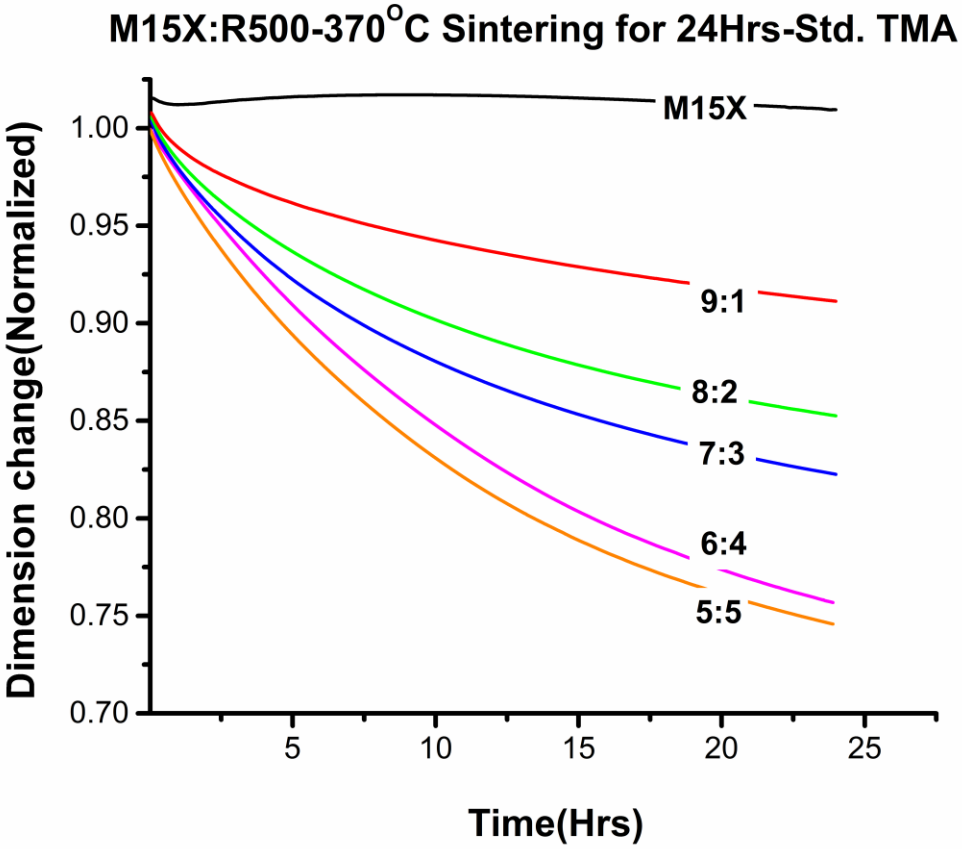

Figure 3-20: Effect of regrind fraction (R500) on dimension change of M15X at 370ºC

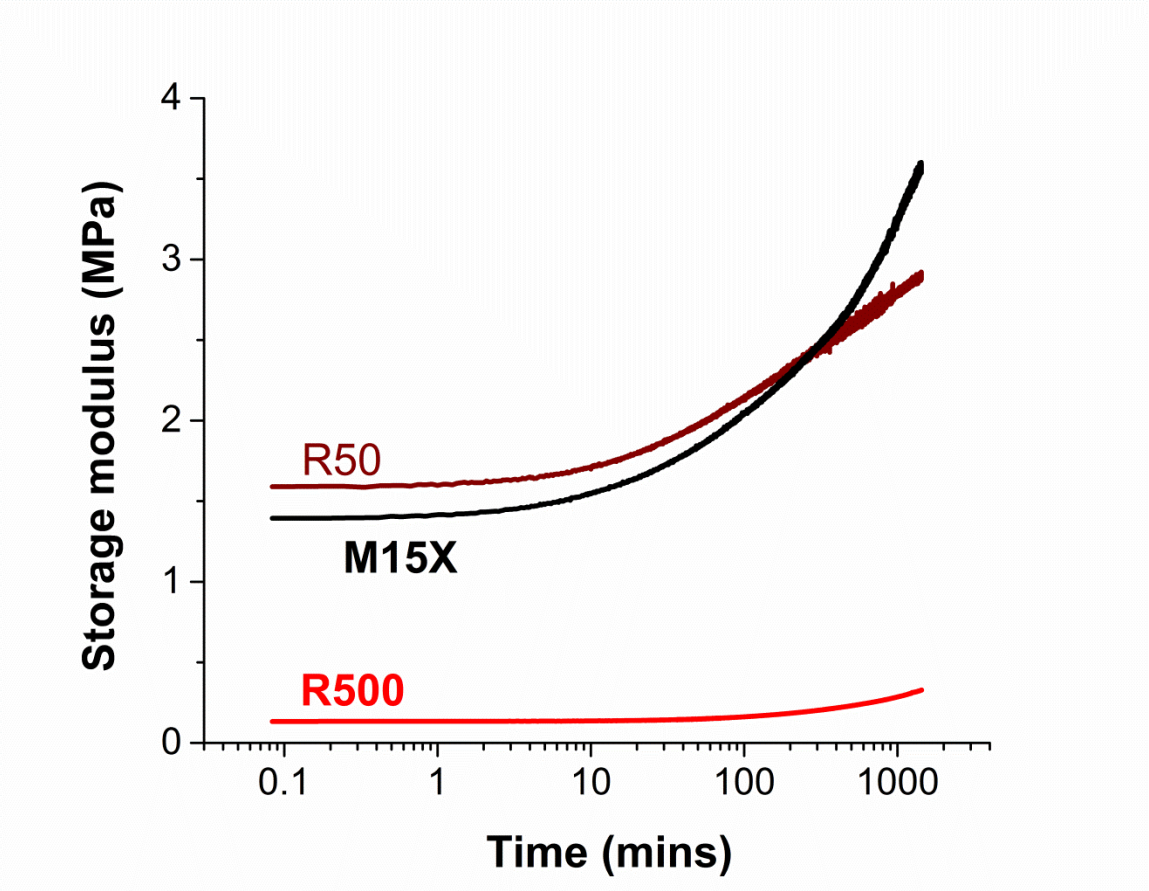

Figure 3-21: Comparison of storage modulus evolution of M15X, R500 and R50

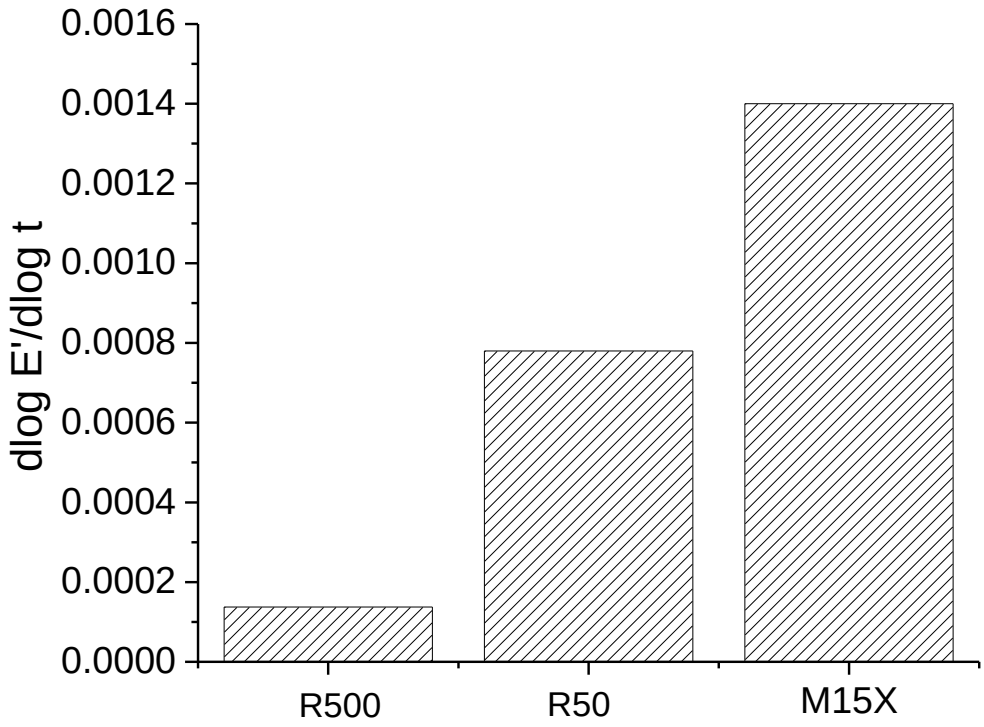

Figure 3-22: Comparison of rate of growth of storage modulus evolution of M15X, R50 and R500

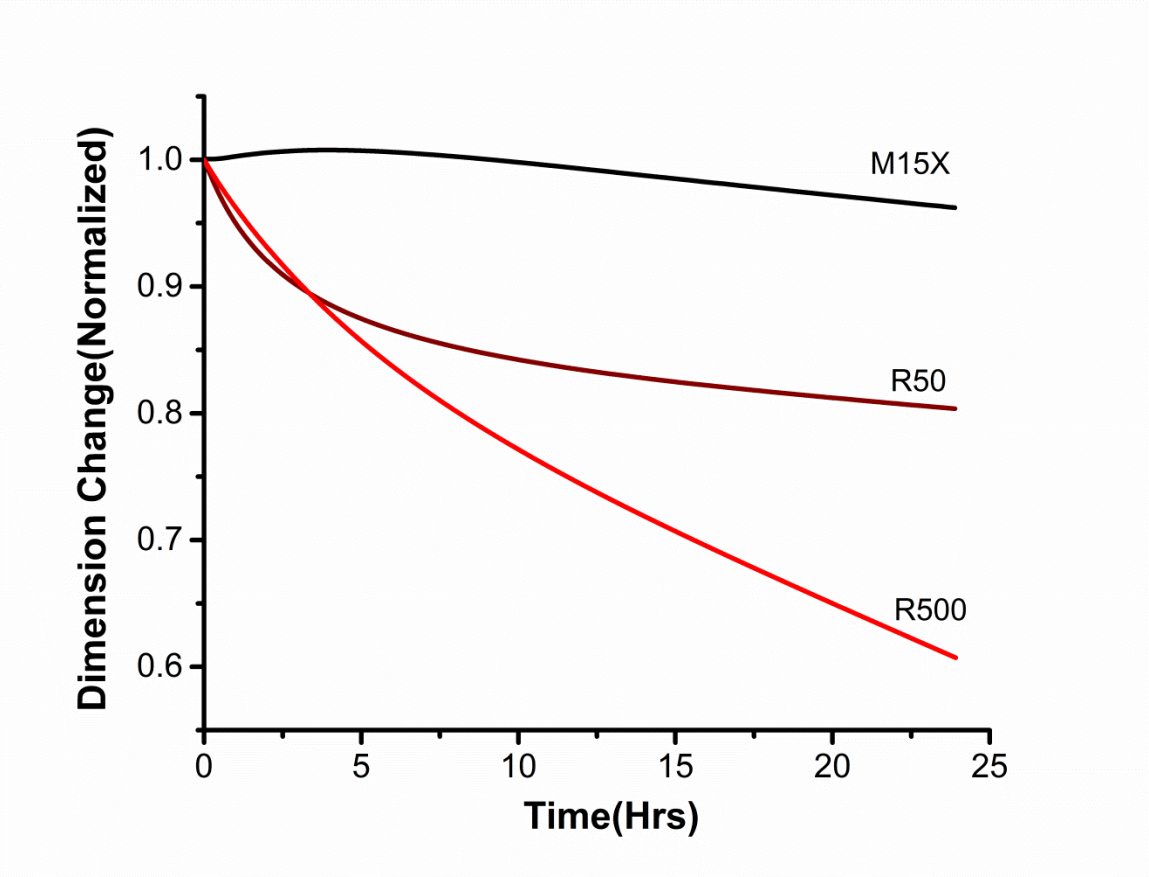

Figure 3-23: Comparison of M15X, R500 and R50 in terms of their dimension change at 380ºC

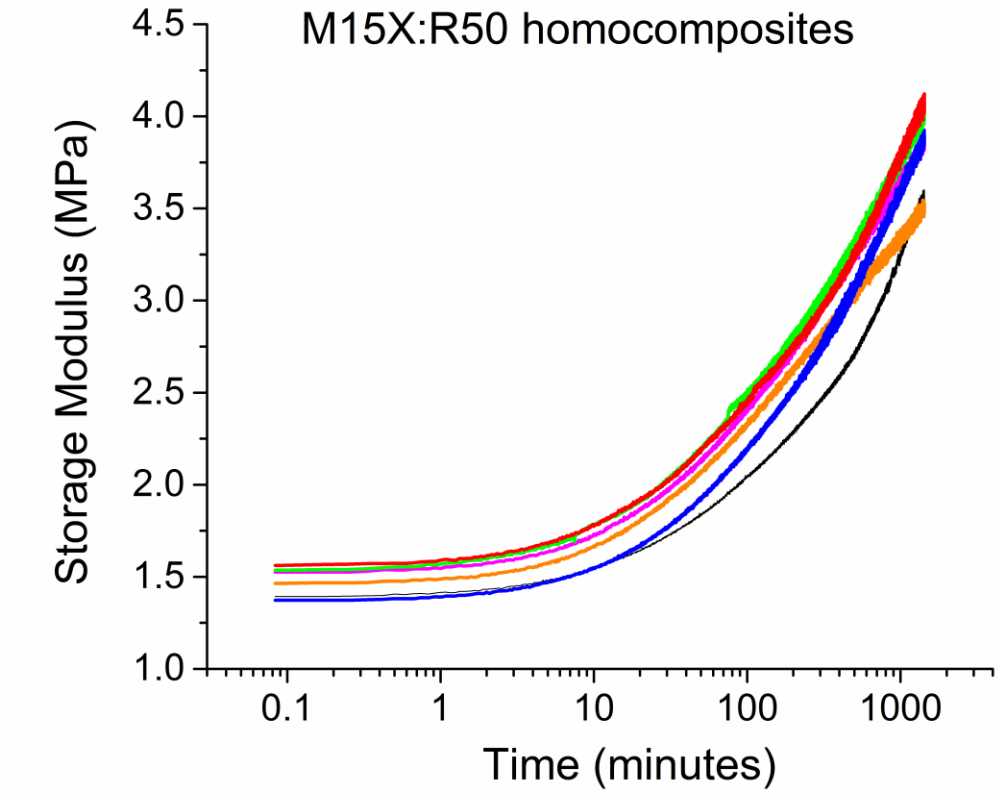

Figure 3-24: Effect of R500 fraction on storage modulus evolution at 380ºC

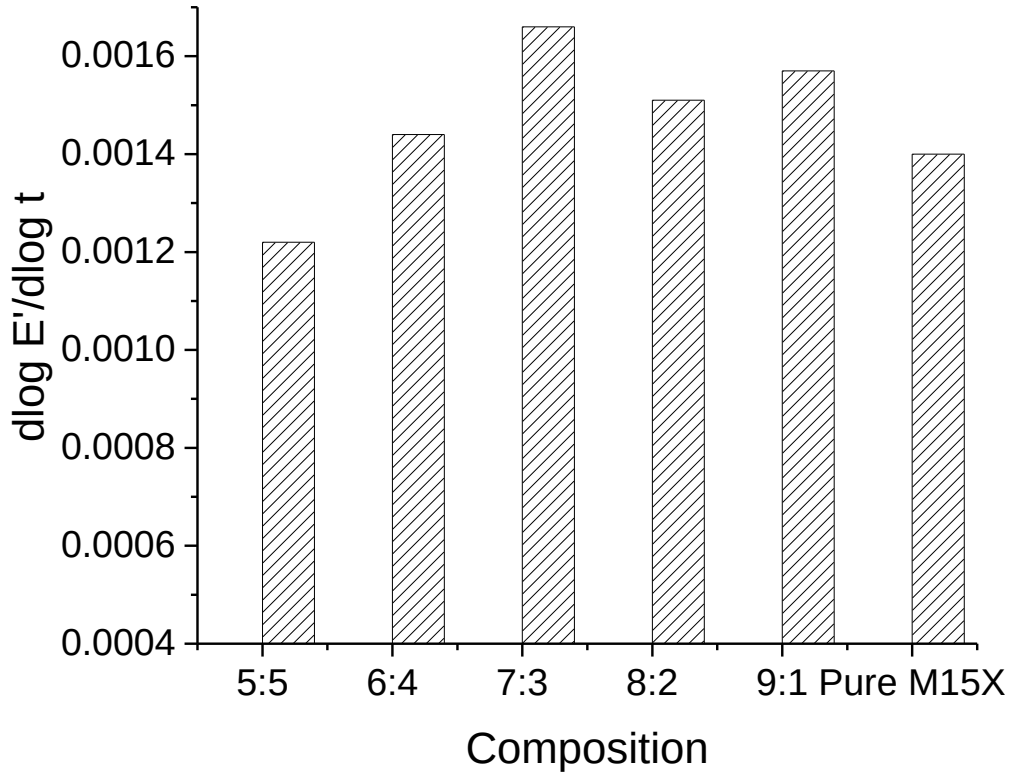

Figure 3-25: Comparison of sintering kinetics of homocomposites of M15X with R50

3.4 Conclusions

This work showed that increase in sintering temperature and decrease in particle size leads to faster sintering kinetics. Lower molecular weight PTFE fraction has an adverse effect on sintering kinetics. UHMWPTFE regrind powder (R500) by itself shows very poor sintering kinetics and its inclusion into M15X drastically affects its sintering behavior. However, lower particle size regrind powder R50 and homocomposites thereof shows superior sintering behavior. Further, this work established that the storage modulus and density evolution can be used as effective measures of the sintering process. However, dimension change in the machine direction is not only a function of the sintering process but it is strongly affected the anisotropic nature of uni-axially compressed preform expansion.

CHAPTER 4

EFFECT OF ASYMMETRIC DOUBLE NETWORK ON THE NON-LINEAR MECHANICAL PROPERTIES OF EPOXIES

4.1 Abstract

The effect of network heterogeneity on the thermal and non-linear mechanical properties of epoxy resin is investigated. Asymmetric Double Network (DN) epoxies were formulated using miscible stoichiometric blends of amines following a controlled three stage cure schedule. The widely different reactivities of the aromatic and aliphatic amines allowed sequential network formation leading to the development of Double Networks where the two networks were different both in terms of their backbone stiffness and in terms of crosslink density. The study involves correlating these complex network architectures with non-linear mechanical properties such as strain hardening modulus (G_R) and important engineering properties such as fracture toughness. Initial results demonstrate that asymmetric DN epoxies exhibit high glass transition temperature and high fracture toughness simultaneously-a synergistic enhancement that is commercially desirable but scientifically challenging. This work further shows that the strain hardening response of amorphous glassy epoxies is not only dependent of the average crosslink density but it is sensitive to the details of the network architecture.

4.2 Introduction

Epoxies are one of the thermosets commonly employed in coatings, adhesives, electronics, and aerospace applications. They are known for their small cure shrinkage,

good chemical and creep resistance, as well as broad service temperature range. However, they are susceptible to brittle failure due to highly crosslinked network structures[9]. Moreover, certain applications require high thermal stability and high fracture toughness simultaneously but conventionally it has been difficult to achieve high fracture toughness in high T_g systems[10-12].

Most epoxy formulations found in the open literature have glass transition temperatures above room temperature. The resins are typically prepared by curing adifunctional epoxide diglycidyl ether of bisphenol A (DGEBA) with a single aliphatic or aromatic diamine[9,13-16]. Few studies have investigated the use of miscible blends of amines with different molecular weights and functionalities[17-27]. For example, symmetric double network epoxies with highly tunable thermal and mechanical properties have been prepared by sequentially reacting stoichiometric blends of an aliphatic and aromatic curing agent[26]. Further, pre-stressed double network epoxies with improved fracture toughness have been developed and characterized[28]. There are even fewer reports on homogenous mixtures of epoxide monomers[29,30]. However, there is no previous work that investigates the effect of asymmetric Double Network (DN) on the thermal and mechanical properties of epoxy resins. An asymmetric DN system is one which consists of two networks having different crosslink densities.

Asymmetric DN hydrogels are developed by Gong and coworkers as a potential candidate for artificial soft tissues[31]. Formed via radical chemistry, they exhibit excellent strength and toughness even at 90 wt% water content. During their synthesis, a highly crosslinked polyelectrolyte network is swollen with an aqueous solution of monomer and

crosslinker for a lightly crosslinked neutral polymer network. Due to isotropic expansion, the polyelectrolyte chains are merely extended and have no preferred orientation.

Gong and coworkers observed that a high molar ratio of second component to the first is needed to obtain the unusual synergistic effect from the two fragile polymer networks[31]. Chain entanglement has been related to load transfer within the matrix[32]. The toughening mechanism is associated with microscale fragmentation of highly crosslinked polyelectrolyte, which improves energy dissipation during deformation[32]. The breakdown of the more brittle component has also been related to large strain hysteresis[33] and necking[34]. The approach has recently been utilized to toughen elastomers[35]. However, similar investigation using thermosets or systems with glass transition temperatures above room temperature has not been reported. The objective of the current study is to formulate asymmetric DN epoxies and correlate network architecture with non-linear mechanical properties i.e. fracture toughness and post yield response in uniaxial compression testing.

The linear, yield, and fracture behaviors of epoxies have been investigated in the past decades[10,36,37]. Shown in Figure 4.1 is a typical stress-strain curve of glassy epoxy tested in compression. The elastic modulus is a statistically averaged linear property associated with molecular packing[37]. The modulus is influenced by thermal treatment or physical aging[36]. Yielding is considered the onset of plastic deformation. The process is described as thermally activated[36]. A generalized yield criteria is proposed based on Eyring flow model and von Mises criterion to predict the effects of stress states, strain rate, test temperature, crosslinker functionalities, and crosslink densities[19]. The activation volume stays the same for all the controlled epoxy networks studied except for the most

densely crosslinked. In contrast, the internal friction coefficient is insensitive to molecular structure and strain rate. The yield strength of aliphatic and aromatic epoxies with various crosslink densities collapse together when normalized by the cohesive energy density (E_c), and plotted against test temperature normalized by T_g[22,23]. The correlation suggests that E_c and T_g are molecular parameters that govern yielding.

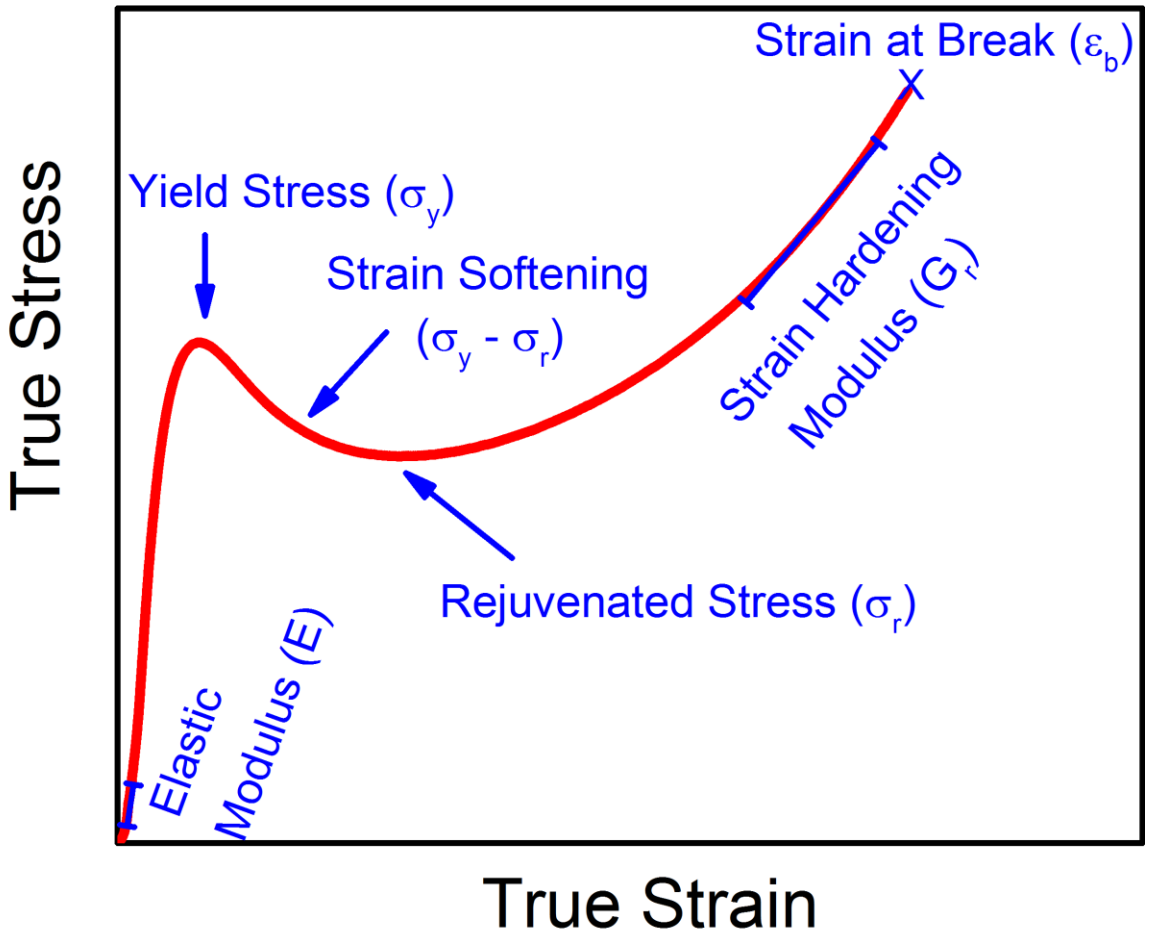

Figure 4-1: Typical stress-strain curve of glassy polymer tested in compression

Fracture toughness is an important engineering property used to evaluate materials for structural applications[10,11]. The testing measures the energy needed to propagate a sharp precrack by unit area. A highly crosslinked epoxy tends to have high T_g and yield stress but low toughness. The diminished energy dissipation is due to small process zone or damage-accumulation region in front of the crack tip[10-12].

The evolution of yield stress, strain softening, rejuvenated stress, and strain hardening modulus during network formation has recently been reported for epoxies cured with ethylene diamine[38]. Systematic changes are also observed for epoxies cured with two miscible amines in different molar ratios[26] . However, it is unclear how these non-linear mechanical behaviors are affected by more complex network architectures such as asymmetric DNs.

The objective of the current research is to engineer asymmetric DN epoxies and correlate network architecture to non-linear mechanical properties such as strain hardening modulus and fracture toughness.

4.3 Experimental

4.3.1 Materials

Diglycidyl ether of bisphenol A (DGEBA or D.E.R. 332, Epoxide equivalent weight: 171-175 g/eq) was purchased from Dow Chemical. Ethylene diamine (EDA, MW: 60.1 g/mol) was purchased from Sigma Aldrich. Aniline (MW: 93 g/mol) and 4,4'-diaminodiphenyl sulfone (DDS, MW: 248 g/mol) was purchased from Acros Organic. The structures of the chemicals are given in Table 4.1.

Table 4-1: List of chemicals used in this study

Diglycidyl ether of bisphenol A (DGEBA, n ~ 0.03)	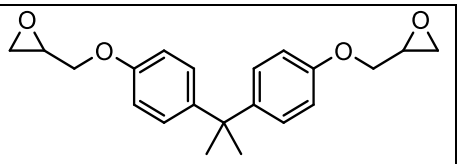
Aniline	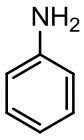
4,4'-diaminodiphenyl sulfone (DDS)	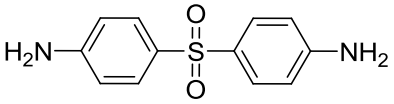

4.3.2 Network formation

The amines were chosen based on their inherently dissimilar reaction kinetics with the aliphatic amine (EDA) being the fastest, the aromatic amine (DDS) the slowest and aniline having an intermediate reactivity, thereby facilitating sequential network formation. Figure 4.2 shows the reaction exotherms corresponding to reactions between DGEBA and the three amines. As can be seen, the slow reactivity of the aromatic amine will permit selective reaction of the aliphatic amine to form the tightly cross-linked first network at low temperature followed by chain extension of the residual DGEBA molecules with aniline at a higher temperature and finally crosslinking of these extended chains with the aromatic curing agent at an even higher temperature. Therefore, by following a controlled three-stage cure schedule it would possible to form an asymmetric DN in which the aliphatic network is tightly cross-linked while the aromatic network is loosely cross-linked.

Firstly, the DDS component is stirred into DGEBA at 125^{o}C until it dissolves. The solution is cooled to 50^{o}C before the aniline and ethylene diamine components are stirred in. The mixture is degassed at 40^{o}C for 5 minutes under vacuum and quickly poured into cylindrical glass molds (11.5 mm internal diameter) treated with release agent (Surfasil, Pierce Chemicals). Further, 3 mm thick rectangular plaques are cast by using release coated glass plates separated by 3 mm teflon spacers. The molds were placed in nitrogen purged oven and fully cured following a three staged cure schedule (1st stage: 50^{o}C for 3 hours, 2nd stage: 125^{o}C for 3 hours, 3rd stage: 200^{o}C for 3 hours).

In order to do a systematic study on the effect of degree of asymmetry a series of asymmetric DNs were formulated as indicated in Table 4.2. EDA-Aniline-DDS-5-0-5

would indicate a network in which 50% of the amine hydrogens that react with the epoxide functionality come from ethylene diamine, while 0% of amine hydrogens come from aniline i.e. there is no chain extension in this particular formulation and the remaining 50% of the amine hydrogens come from DDS. A series of asymmetric networks were formulated by varying the degree of asymmetry and three single networks having the same molecular weight between crosslinks as three of the asymmetric networks were prepared for the sake of comparison. The single networks were DDS based and calculated quantities of chain extender aniline was used for tailoring the molecular weight between crosslinks to match that of asymmetric networks.

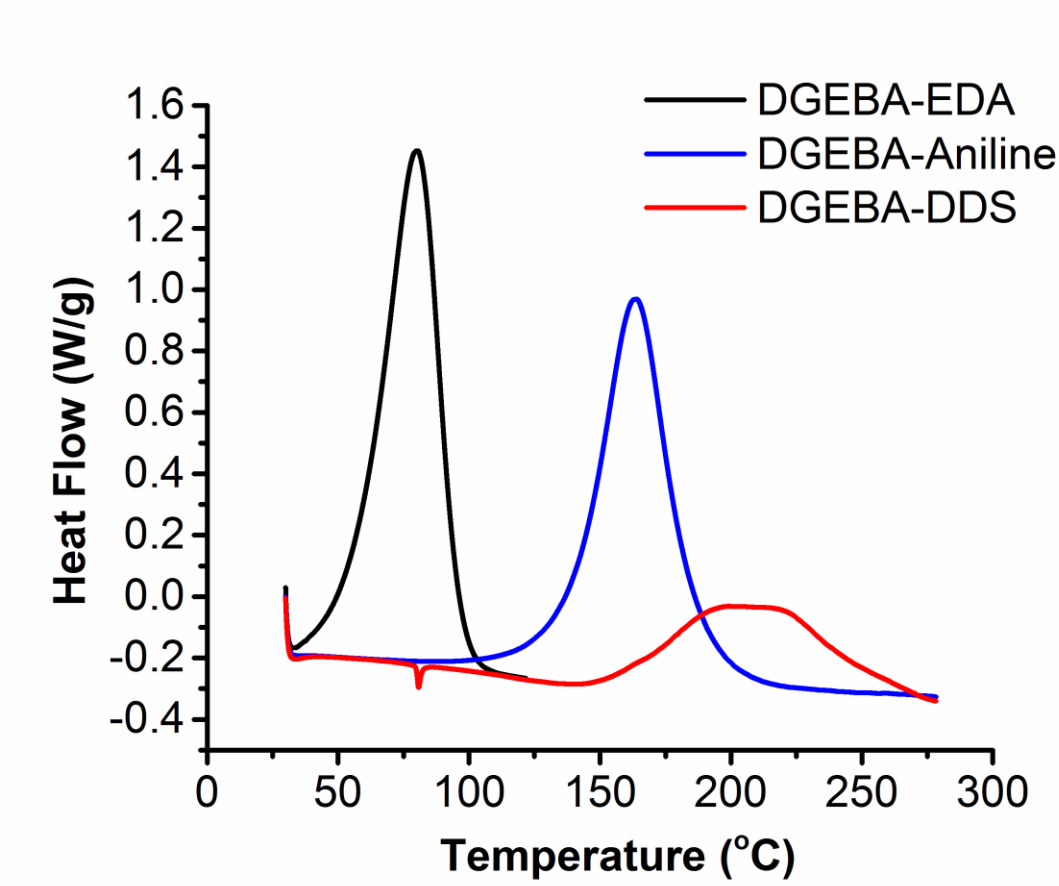

Figure 4-2: DSC reaction exotherms for reaction between DGEBA and different amines

Table 4-2: Asymmetric DN formulations

EDA-Aniline-DDS	$1/M_c$ (mol/kg)	T_g (^oC)	E (MPa)	σ_y (MPa)	σ_r (MPa)	$\sigma_y - \sigma_r$ (MPa)	G_R (MPa)	ε_b
5-0-5	2.34	165	756	125	120	5	138	1.45
5-1-4	2.12	148	797	119	112	7	126	1.60
5-2-3	1.90	125	736	119	106	13	100	1.70
5-3-2	1.67	117	956	116	101	15	99	1.80
5-4-1	1.44	99	1006	115	95	20	82	1.86

4.3.3 Differential Scanning Calorimetry (DSC)

DSC Q200 (TA Instrument) was used to study reaction exotherms for reaction between DGEBA and different curing agents and chain extenders to determine their relative reactivities. Further, it was used to determine the glass transition temperatures of fully cured epoxies having different average molecular weight between crosslinks.

4.3.4 Compression testing

Uniaxial compression test was conducted on an Instron 5500 universal tester at 20°C and a constant strain rate of 1 min^{-1}. Cylindrical bullets (Diameter ~ 11.5 mm) with 1:1 height-to-diameter ratio were machined. Soapy water and thin PTFE films were used for lubricating the ends of the specimens. The strain hardening modulus (G_R) was computed at 90% of the ultimate true strain using the following equation:

$$G_R = \frac{\partial \sigma_t}{\partial(\lambda^2 - 1/\lambda)} \qquad (1)$$

where σ_t is the true stress, λ^2-$1/\lambda$ is the Neo-hookian strain, and λ is the compression ratio. High temperature compression studies were done on the same instrument using an environmental chamber that surrounds the compression plates. Specimens were equilibrated for 30 minutes at the test temperature prior to testing. High temperature silicone oil was used for lubrication in this case.

4.3.5 Fracture Toughness

Fracture toughness measurements were made with 3 mm thick miniature compact tension (mini-CT) specimens with 20 mm width following ASTM standard D5045-99. The use of mini-CT specimens for testing glassy polymers had been reported by Jones

and Lee[64], and Hinkley[65]. The thickness satisfied the requirement for achieving plane-strain condition across the crack front, namely $B \geq 2.5 (K_q/\sigma_y)^2$, where $K_q$is the measured fracture toughness and $\sigma_y$is the yield stress estimated from the compression data.The pre-notcheswere introduced with a diamond waferingblade. After conditioning the samples at -10°C for an hour, a sharp precrack was generated on each specimen by inserting a fresh razor blade into the pre-notch and tapping lightly with a hammer.Load-displacement curves were recorded by Instron5500 at a crosshead speed of 0.5 mm/min and 20 °C. Fracture toughness (K_q) was computed using the following equation:

$$K_q = \frac{P_c f(x)}{BW^{1/2}} (2)$$

whereP_c is the critical load in kilonewton (kN), B is the specimen thickness in centimeter (cm), W is specimen width in cm, and K_q is in MPa·$m^{1/2}$. The use of K_q instead of K_{IC} denotes the use of a mini-CT specimen. The geometric factor *f(x)*is a dimensionless power function in terms of *x*, which is equal to *a/W*, orthe ratio of the precrack length to specimen width.

$$f(x) = \frac{(2+x)(0.886+4.64x-13.32x^2+14.72x^3-5.6x^4)}{(1-x)^{3/2}} (3)$$

Each reported fracture toughness value was an average of 4 to 8 measurements.

4.4 Results and Discussion

4.4.1 Crosslink Density from Stoichiometry

In this study, the difunctional amine acts as chain extenders, while the tetrafunctional reagents are the crosslinkers for network formation. The average crosslink

density has been calculated based on equation 4. From stoichiometric quantities of the reagents, $M_c$for amine-cured epoxy is given by[19]

$$M_c = \frac{2(M_e + \sum_{x=2}^{\infty} \frac{M_x}{x} \Phi_x)}{\sum_{x=3}^{\infty} \Phi_x} \qquad (4)$$

whereM_e is the epoxy equivalent weight of the epoxide monomer, x is the functionality of the amine, $M_x$is the molecular weight of the amine having x functionality, and Φ_x is the molar fraction of amine hydrogens from x-functional amine. The key assumptions for Equation 4 are one-to-one stoichiometry between epoxide and amine hydrogen and full conversion of the reagents at the end of cure.

4.4.2 Asymmetric DNs: Compression testing

Compression test is considered a better measure of intrinsic material properties than tension test, since geometric instabilities such as necking and crazingare suppressed[61]. The toughness of amorphous glassy polymers has been associated with their ability to effectively de-localize strain, which is typically characterized by small strain softening and large strain hardening modulus. Strain softening is the difference between the yield stress and rejuvenated stress, which are the maximum and minimum of the stress-strain curve, respectively (Figure 4.1). The yield stress is related to network strength and stiffness[23], and influenced by the thermomechanical history[36,61]. Taking an amorphous glassy polymer beyond the rejuvenated stress is akin to heating above its glass transition temperature[66,67]. The strainhardening modulus is related to network connectivity[62,63], and depends strongly on entanglement in thermoplastics and chemical crosslink in thermosets[34,38,61].

Shown in Figure 4.3 are the stress-strain curves of the asymmetric DN epoxies. Here the true stress is with plotted against the Neo-hookean strain. As listed in Table 2, the yield stress (σ_y), rejuvenated stress (σ_r) and strain hardening modulus (G_R) generally scale with $1/M_c$. However, the Young's modulus (E) and the strain softening (σ_y-σ_r) decreases with increase in average crosslink density. The strain at break decreases with increase in average crosslink density. Further, each asymmetric DN shows a single glass transition temperature as measured by DSC indicating microscopically homogeneous material and complete miscibility of curing agents and chain extender. Figure 4.4 illustrates the dependence of strain hardening modulus on $1/M_c$ which is a measure of the average crosslink density. This result indicates that the strain hardening response is dependent on the average molecular weight between crosslinks. It is important to note here that each of the asymmetric double networks has a highly heterogeneous distribution of crosslinks, nevertheless, the strain hardening behavior is governed by the average crosslink density for asymmetric DNs.

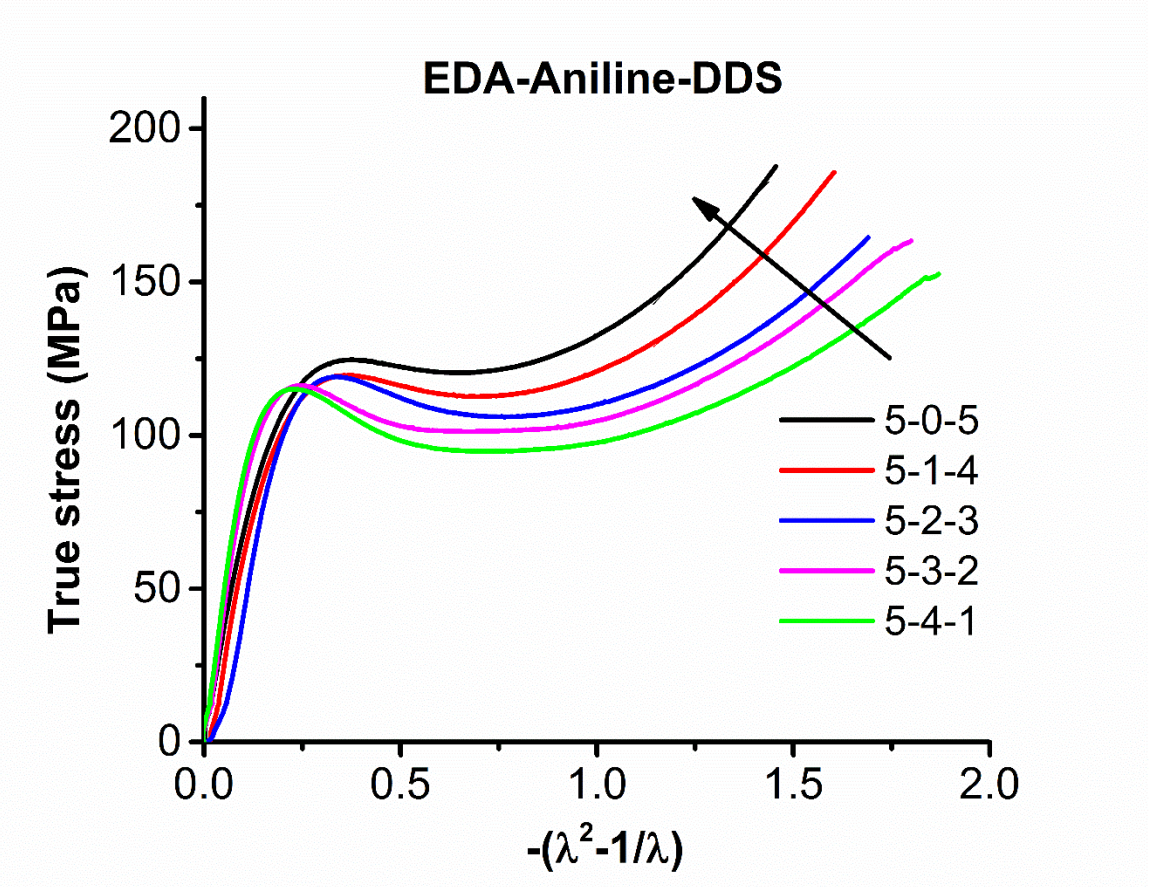

Figure 4-3: Compression data on asymmetric DNs with varying asymmetry

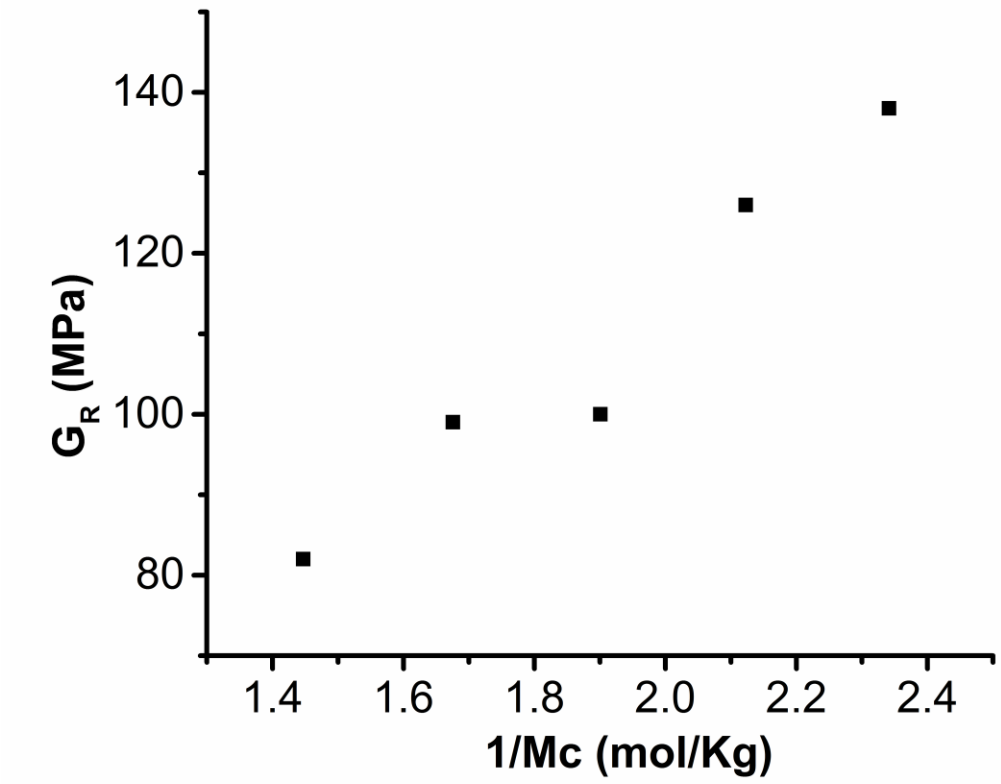

Figure 4-4: Dependence of strain hardening modulus on $1/M_c$ for asymmetric DNs

4.4.3 Comparison of asymmetric DNs with single networks having same M_c

It was demonstrated in the previous section that the strain hardening modulus increases with increase in the average crosslink density of the asymmetric DNs. The next question we wanted to answer was weather the strain hardening modulus is solely depended on the average molecular weight between crosslinks or is it sensitive to the details of the network architecture. In order to do that, three single networks were formulated that had the same molecular weight between crosslinks as three of the asymmetric formulations (Table 4.3). The single networks were based on DDS and calculated quantities of aniline was added to each in order to achieve the desired M_c. Figure 4.5 shows the compression data on all the networks tabulated in Table 4.3. The numbers next to the curves indicates the average molecular weight between crosslinks (M_c). The asymmetric DNs show slightly higher strain at break than the corresponding single networks. Figure 4.6 compares the glass transition temperatures of asymmetric DNs with the corresponding single networks. Generally, the glass transition temperature increases with increase in average crosslink density for both types of networks. But for the same average crosslink density, the single networks show much higher T_g than the corresponding asymmetric DN. This is because the single networks are completely based on DDS which is an aromatic curing agent while 50% of all asymmetric DNs are based on ethylene diamine which is an aliphatic curing agent. The higher rigidity of DDS coupled with its ability to form H-bonds with the hydroxyl groups generated from the opening of the oxirane ring on the epoxide monomer explains the higher T_g of single networks relative to corresponding asymmetric DNs. Further, the yield stresses which is a measure of network stiffness and strength, generally scales with the glass transition

temperature (Figure 4.7). The asymmetric DNs show higher strain softening than the corresponding single networks (Figure 4.8).

Table 4-3: Comparison of asymmetric DNs with Single networks have same M_c

EDA-Aniline-DDS	M_c(kg/mol)	T_g (^oC)	σ_y (MPa)	σ_r (MPa)	$\sigma_y - \sigma_r$ (MPa)	ε_b
5-2-3	526	125	119	106	13	1.70
5-3-2	596	117	116	101	15	1.80
5-4-1	691	99	115	95	20	1.86
0-1.1-8.9	526	192	138	128	10	1.56
0-2.2-7.8	596	162	133	119	14	1.71
0-3.3-6.7	691	152	130	113	17	1.84

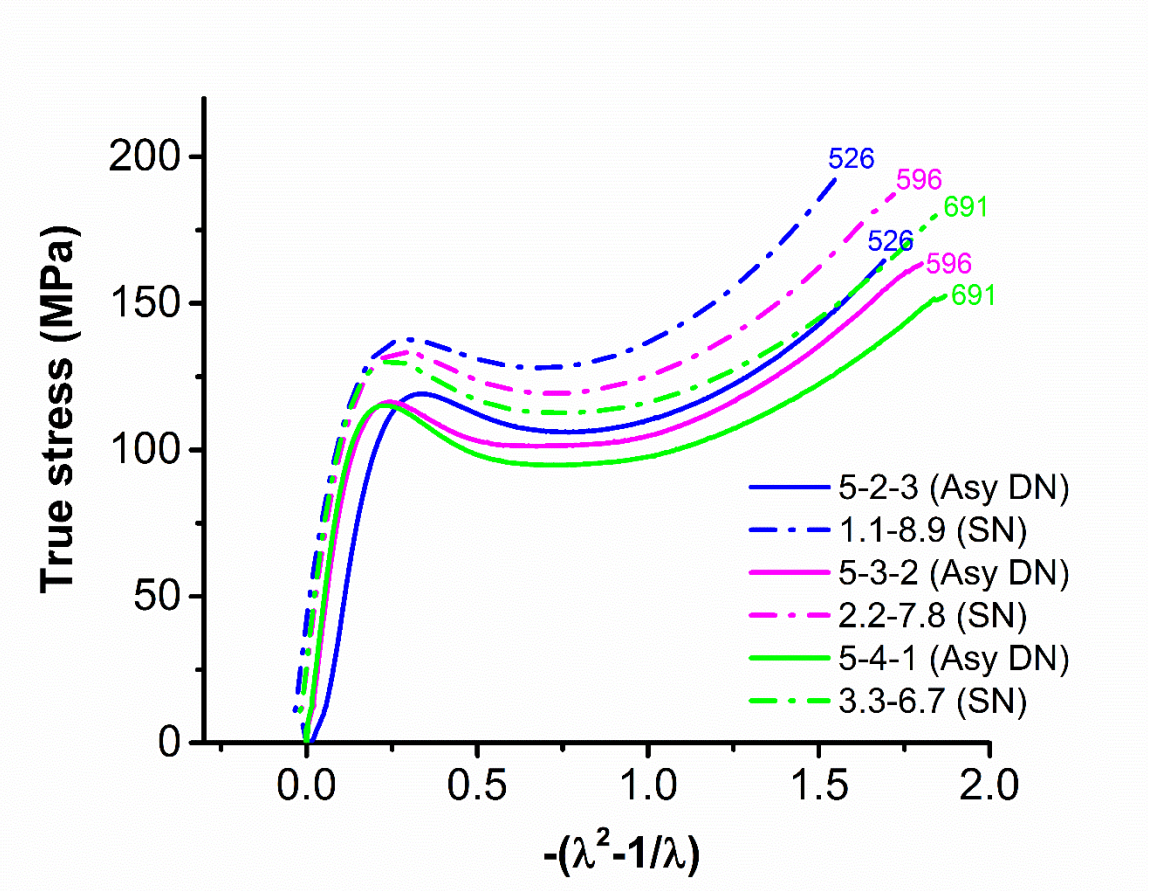

Figure 4-5: Compression data on asymmetric DNs and Single Networks having same M_c

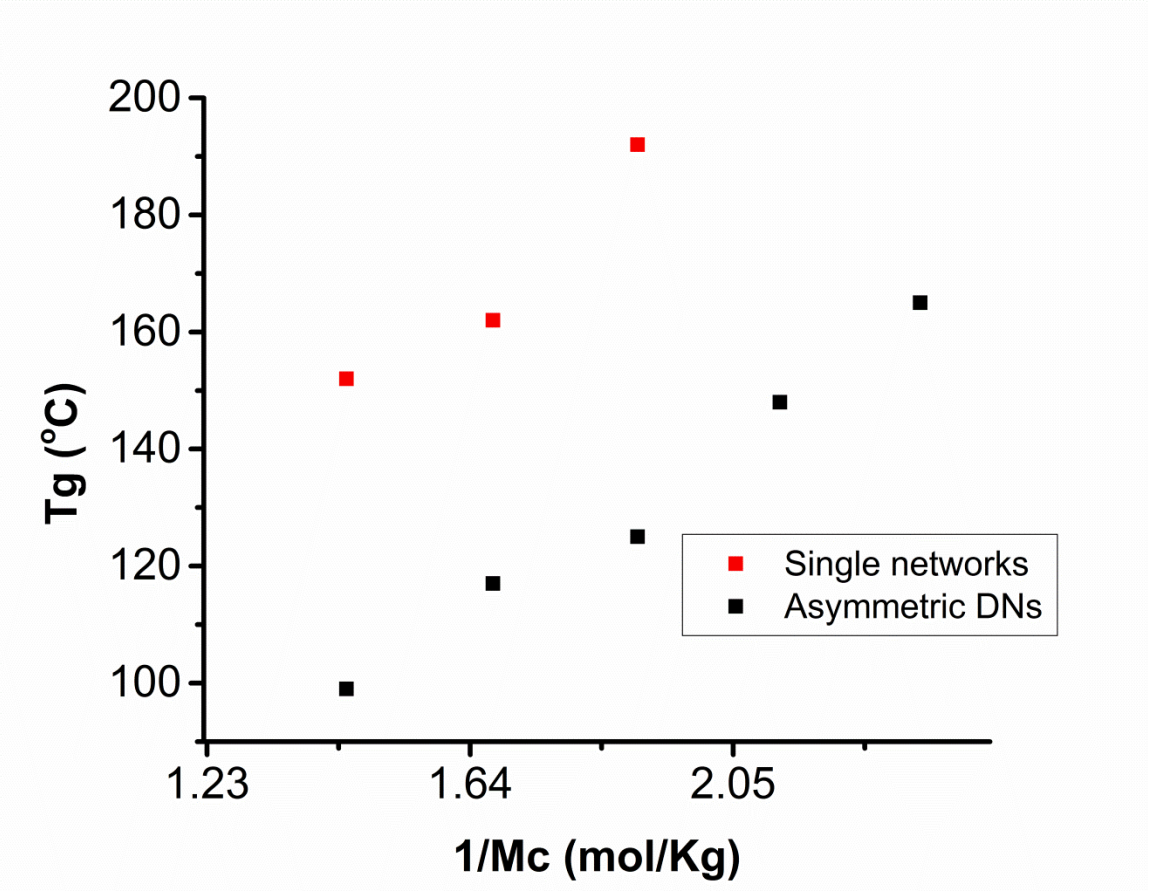

Figure 4-6: Comparison of glass transition temperatures

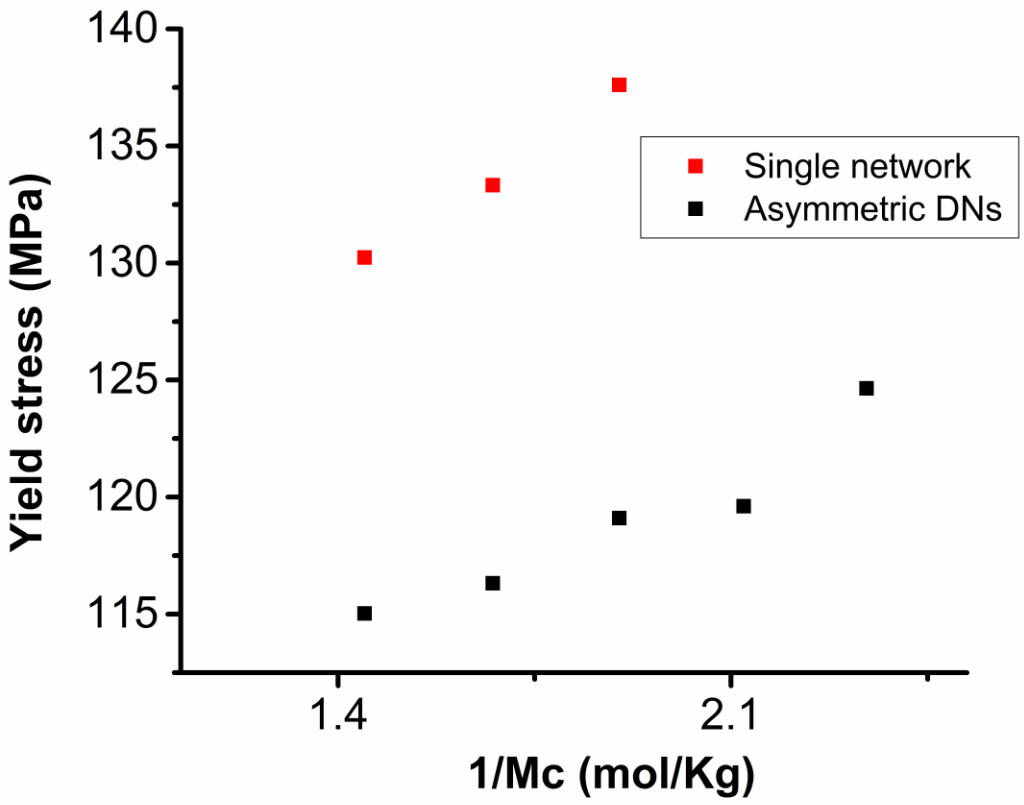

Figure 4-7: Comparison of yield stresses

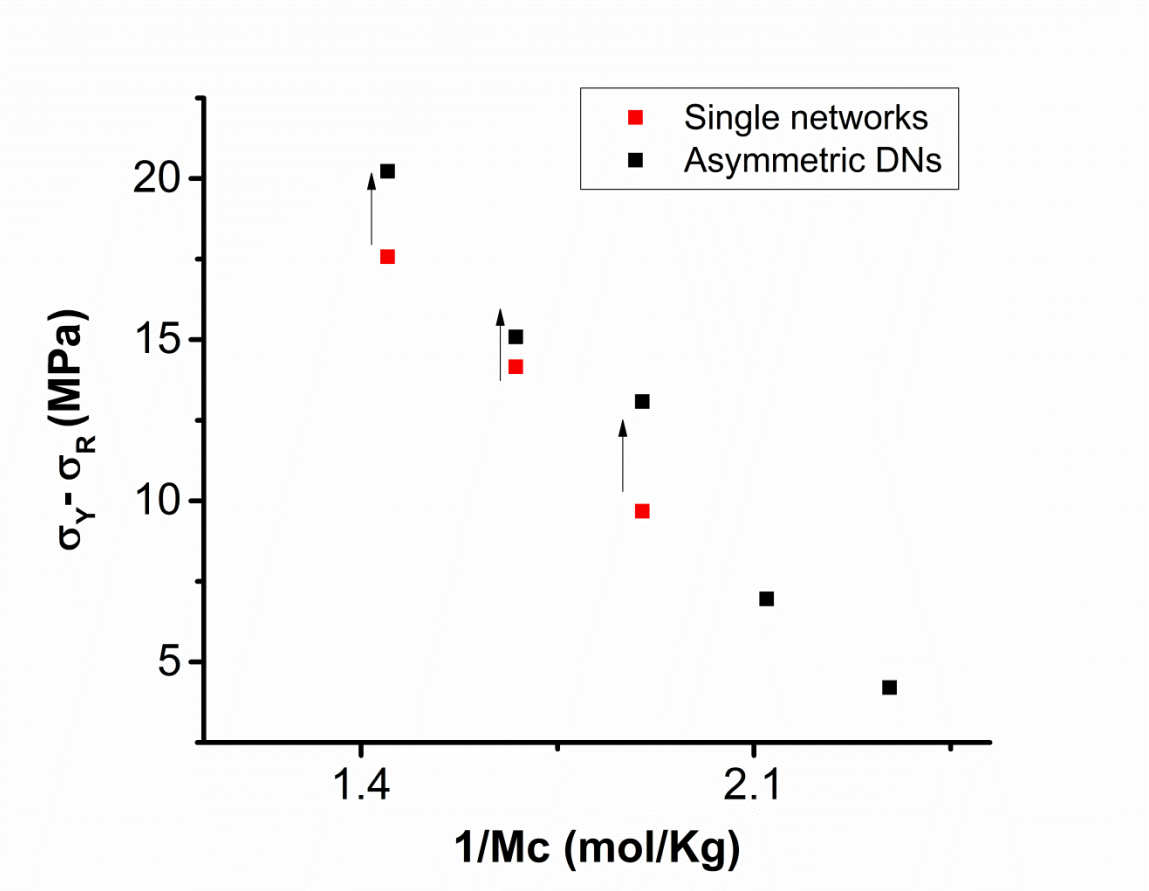

Figure 4-8: Comparison of strain softening

Figure 4.9 shows the comparison of strain hardening regime of the single networks with the asymmetric DNs. The y-axis has been normalized by the rejuvenated stresses while the x-axis has been shifted by the rejuvenated strains. Taking an amorphous glassy polymer beyond the rejuvenated stress is akin to heating above its glass transition temperature[66,67]. Therefore, normalization of the compression data by the rejuvenation point will aid in exclusively comparing the network response and disregard any effect coming from differences in chemical stiffness. Upon doing this normalization treatment, the asymmetric DNs exactly line up on the corresponding single networks having the same average molecular weight between crosslinks. This is true for all three pairs of single and asymmetric DNs. Therefore, this result indicates the strain hardening modulus in amorphous glassy epoxies is independent of the details of the network architecture and dependents only on the calculated average molecular weight between crosslinks. This is a surprising result because we expected the asymmetric DNs with their highly heterogeneous distribution of crosslink density should behave differently than the single networks with their homogenous distribution of crosslink density even though they have same molecular weight between crosslinks. Therefore, in order to probe this phenomenon more deeply we wanted to go to higher strains. This was accomplished by conducting compression tests 30^{o}C above the glass transition temperatures of these networks. Above their glass transition temperature the networks behave as rubbers and Figure 4.10 shows a plot of the true stress and Neo-Hookean strain of these rubbery networks. As can be seen, at low strains the single networks exactly line up with the corresponding asymmetric DNs but there is significant divergence in the high strain regime. Further, the asymmetric DNs are stiffer than the corresponding single networks

having the same average molecular weight between crosslinks. This might be because the asymmetric DNs have a tightly cross-linked aliphatic constituent in addition to the loosely cross-linked aromatic network. This result demonstrates that non-linear mechanical response can capture the details of network architecture.

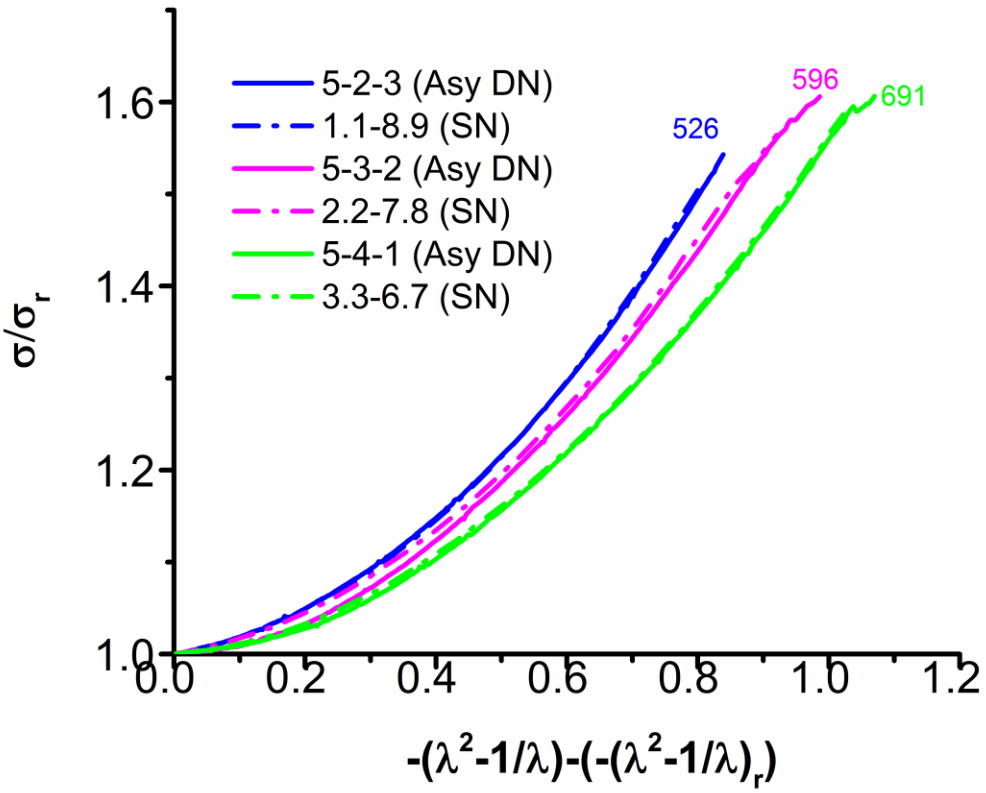

Figure 4-9: Comparison of strain hardening response

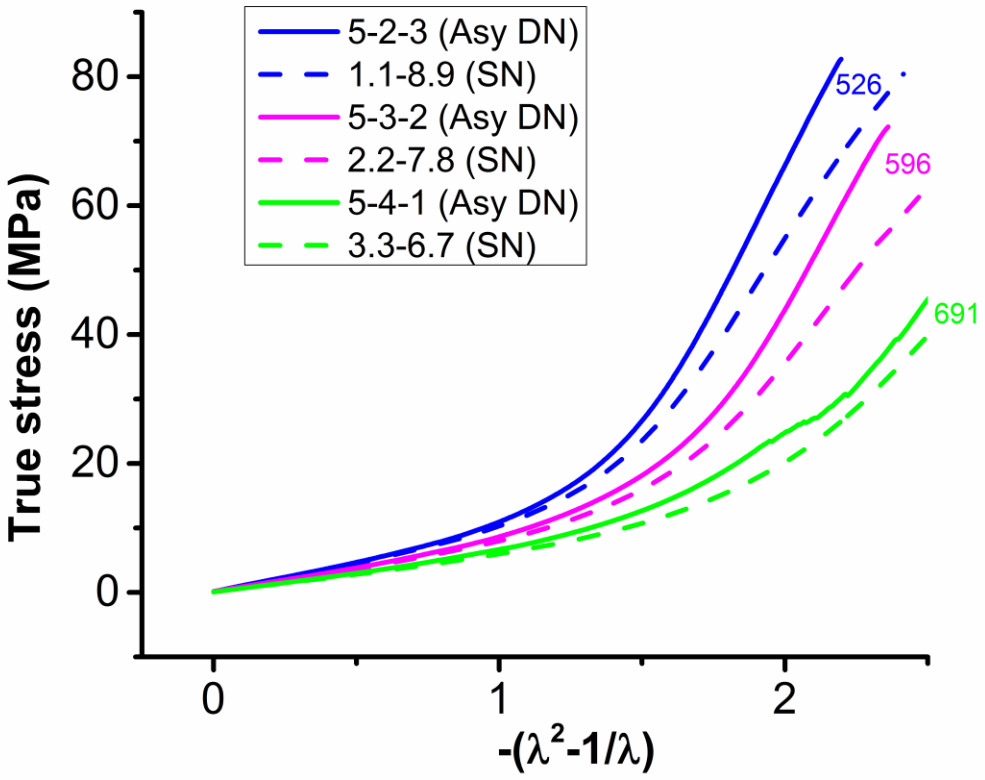

Figure 4-10: High temperature compression T_g+30°C

In order to understand how this difference in non-linear response translates into fracture behavior, fracture toughness tests were performed. Figure 4.11 shows the fracture toughness data as a function of $1/M_c$ for the asymmetric DNs corresponding single networks. The asymmetric DNs show higher fracture toughness than two of the single networks having the same M_c. Figure 4.12 shows a plot of fracture toughness as a function of T_g for the asymmetric DNs and single networks. This plot utilizes some data points from Crawfords work[31]. These are single networks based on DGEBA, etylene diamine and 3-aminomethoxypropylamine. As can be seen, for T_g close to 100 ^oC, the asymmetric DNs show superior fracture toughness than the corresponding single networks.

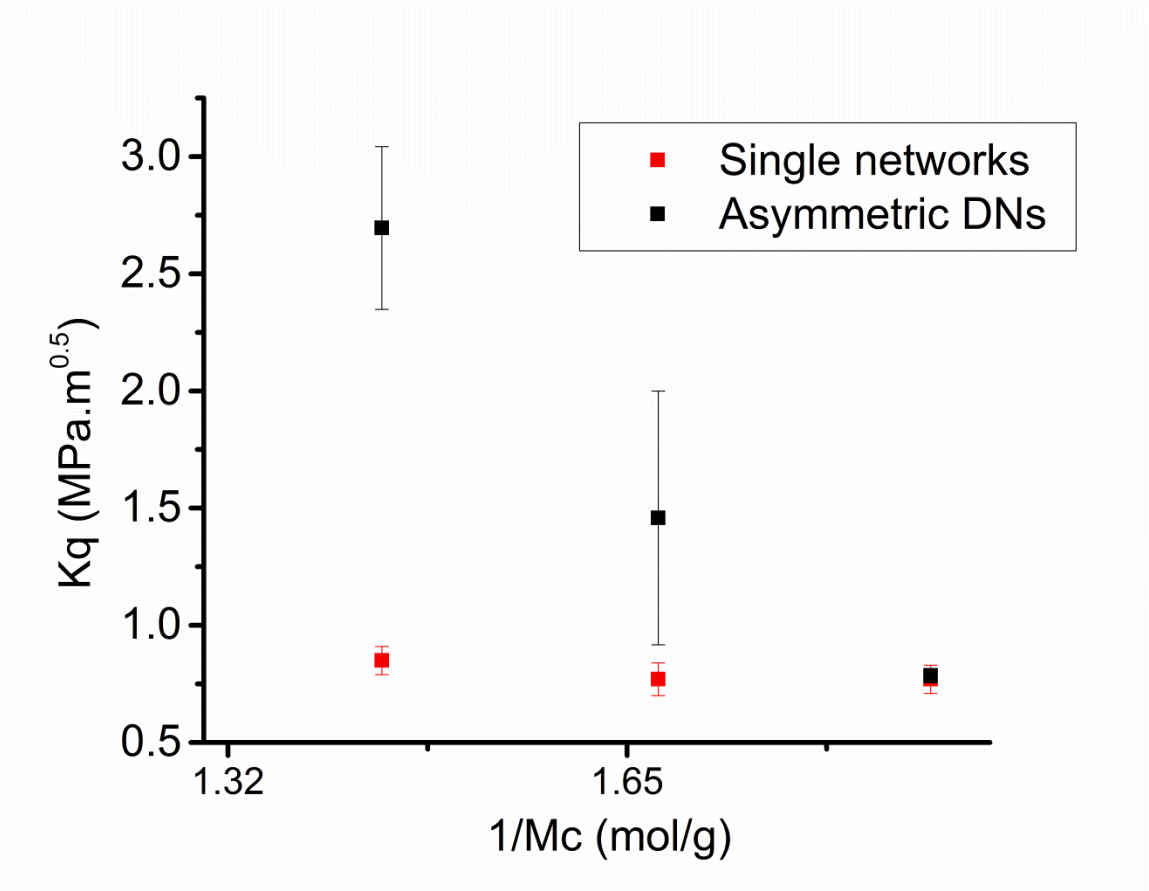

Figure 4-11: Fracture toughness of asymmetric DNs and single networks having same M_c

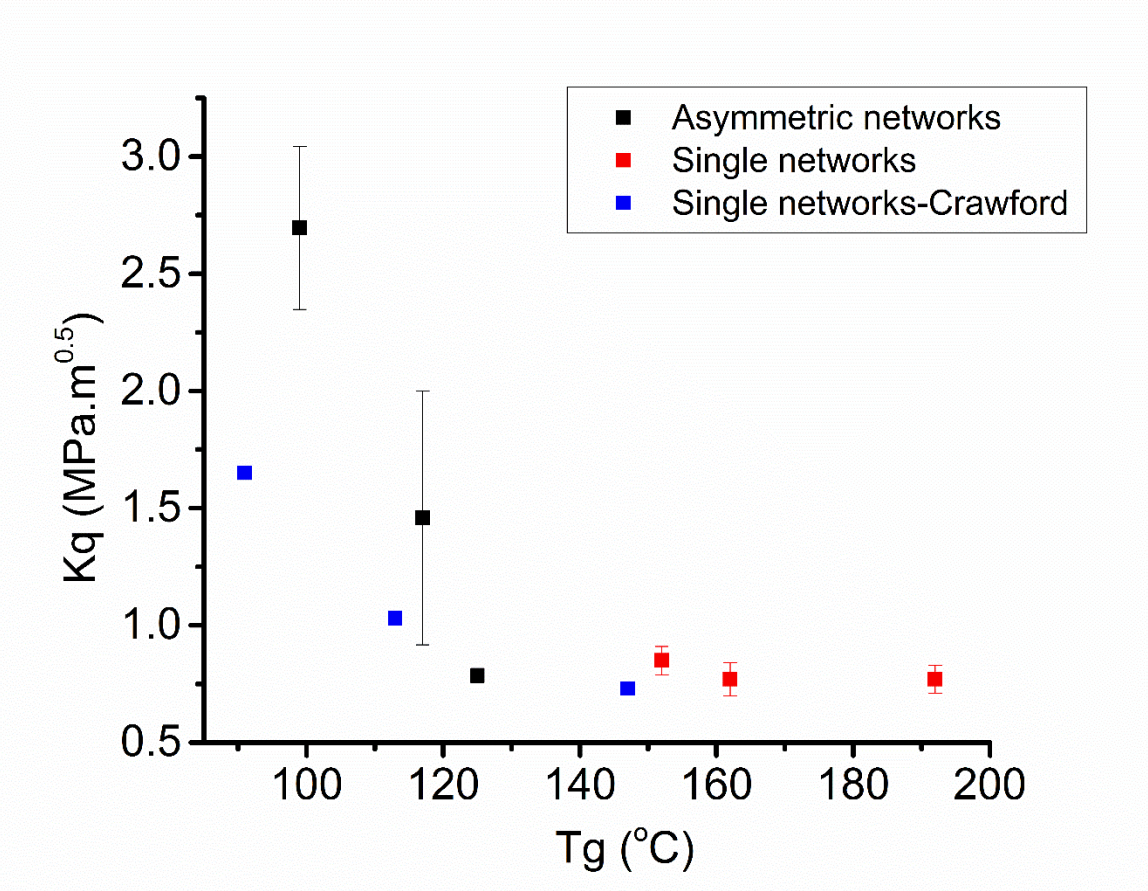

Figure 4-12: Fracture toughness of asymmetric DNs and single network epoxies as a function of T_g

4.5 Conclusion

Asymmetric DN epoxies were developed where the two networks were different both in terms of their chemical stiffness and crosslink density and their non-linear mechanical properties investigated. The asymmetric DNs were compared with single networks having the same molecular weight between crosslinks in terms of their strain hardening response and fracture behavior. Based on this study, it was inferred that network polydispersity has no effect on the strain hardening response in the glassy state. However, systematic deviations were identified in the rubbery state with the asymmetric DNs exhibiting higher stiffness than their corresponding single networks. Further, the asymmetric DNs showed superior fracture toughness compared to single networks over a range of glass transition temperatures.

CHAPTER 5

CONCLUSION AND FUTURE WORK

5.1 Dissertation summary

Chapter 2 elucidates the molecular mechanisms associated with UHMWPTFE sintering.Two potential molecular processes seem to be playing a role: entanglement formation and melt state ordering. The increase of storage modulus of the UHMWPTFE melt as a function of sintering time and higher strain hardening modulus for billets sintered for longer times are indicative of entanglement formations. On the other hand, results from cyclic DSC, cyclic TMA, high temperature WAXS and high temperature SALS are suggestive of melt state ordering. Further, TMA was established as a complimentary technique for monitoring melting/crystallization transitions. Both DSC and TMA exhibited a non-equilibrium evolution of PTFE melt. The enthalpy of crystallization and melting was found to increase with successive sintering steps. Further, the crystallization temperature decreased whereas the melting temperature increased with successive sintering. These results were endorsed by in-situ high temperature X-Ray scattering studies on molten PTFE. Results obtained from the cyclic TMA experiment correlated well with the corresponding cyclic DSC. It was established that the dramatic growth in enthalpy of crystallization and melting was not due to chain scissions at 370^{o}C. Further, it was shown to be possibly resulting from two independent processes-Isothermal annealing at 370^{o}C and lamellar thickening in the solid state. It was shown that UHMWPTFE exhibits a double yield phenomenon at room temperature under compression.

Chapter 3 focuses on understanding the effect of different fluoropolymer additives, particle size distribution and processing conditions on the sintering kinetics of UHMWPTFE. This work showed that increase in sintering temperature and decrease in particle size leads to faster sintering kinetics. Lower molecular weight PTFE fraction has an adverse effect on sintering kinetics. UHMWPTFE regrind powder (R500) by itself shows very poor sintering kinetics and its inclusion into M15X drastically affects its sintering behavior. However, lower particle size regrind powder R50 and homocomposites thereof shows superior sintering behavior. Further, this work established that the storage modulus and density evolution can be used as effective measures of the sintering process. However, dimension change in the machine direction is not only a function of the sintering process but it is strongly affected the anisotropic nature of uni-axially compressed preform expansion.

In Chapter 4 asymmetric DN epoxies were developed where the two networks were different both in terms of their chemical stiffness and crosslink density and their non-linear mechanical properties investigated. The asymmetric DNs were compared with single networks having the same molecular weight between crosslinks in terms of their strain hardening response and fracture behavior. Based on this study, it was inferred that network polydispersity has no effect on the strain hardening response in the glassy state. However, systematic deviations were identified in the rubbery state with the asymmetric DNs exhibiting higher stiffness than their corresponding single networks. Further, the asymmetric DNs showed superior fracture toughness compared to single networks over a range of glass transition temperatures.

5.2 Proposed Future work

5.2.1 Investigation of double yield phenomenon in UHMWPTFE

The focus of the last section of Chapter 2 was to correlate the mechanical response of sintered UHMWPTFE to fundamental aspects of the sintering process. However, what was not discussed in that section was the occurrence of two yield points in UHMWPTFE under compression (Figure 5.1). Herein, we report for the first time the occurrence of double yield phenomenon in UHMWPTFE in compression. Investigation of the origin of this double yield phenomenon and its rate and temperature dependence is part of the proposed future work.

Yielding in semi-crystalline polymers is related to a morphological change from a spherulitic to a fibrillar structure[68]. Double yield points in linear low density polyethylene at room temperature has been reported and attributed to broad distribution of crystalline lamellar thicknesses[69]. However, medium density polyethylene having very narrow distribution of crystalline lamellar thicknesses also exhibited a double yield phenomenon that was rate and temperature dependent[70]. Based on this result it was suggested that yielding is related to two thermally activated rate processes having different activation parameters relative to temperature[70].

Herein, we report the existence of double yield phenomenon is UHMWPTFE at room temperature under compression and some initial experiments have been performed to understand the morphological changes at different locations of the stress-strain curve. However, developing a fundamental understanding of the double yield points in UHMWPTFE can be part of future research. The crystallization enthalpy slightly

decreases after the first yield while dramatically decreases after second yield or fracture while the crystal structure remains intact (Table 5.1 and Figure 5.2)

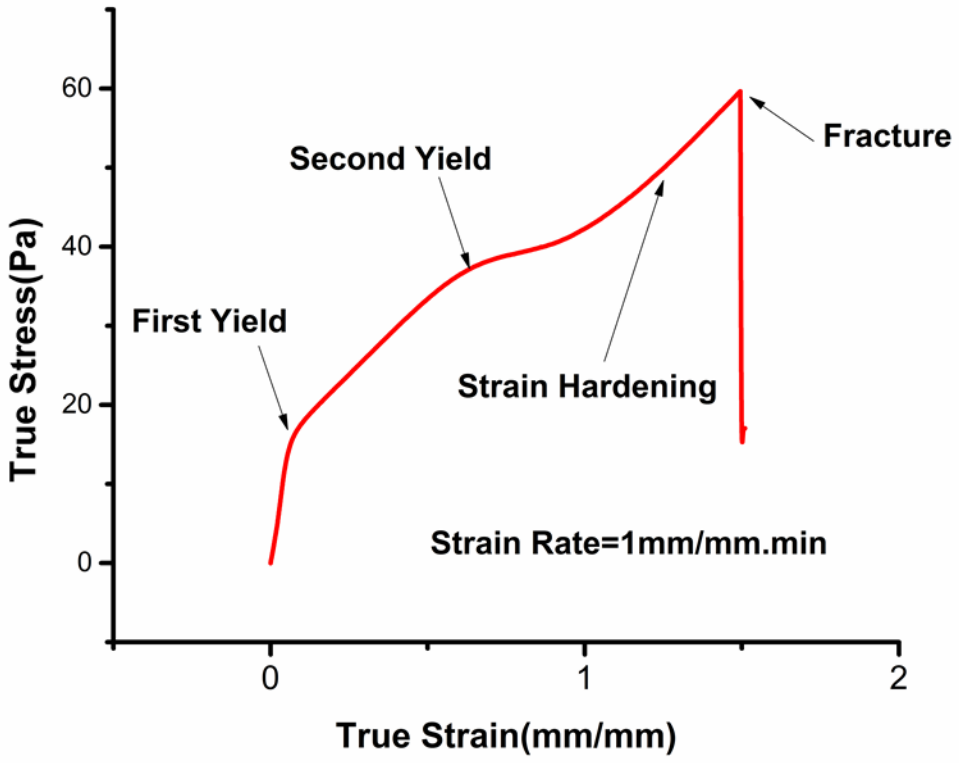

Figure 5-1: Existence of two yield points in UHMWPTFE at room temperature under compression

Table 5-1: DSC data on UHMWPTFE with different mechanical histories

	ΔH_m(J/g)	ΔT_m (^oC)	ΔH_c(J/g)	ΔT_c (^oC)
No Compression	35	331	31	312
After First Yield	32	330	30	313
Fractured	22	328	32	313

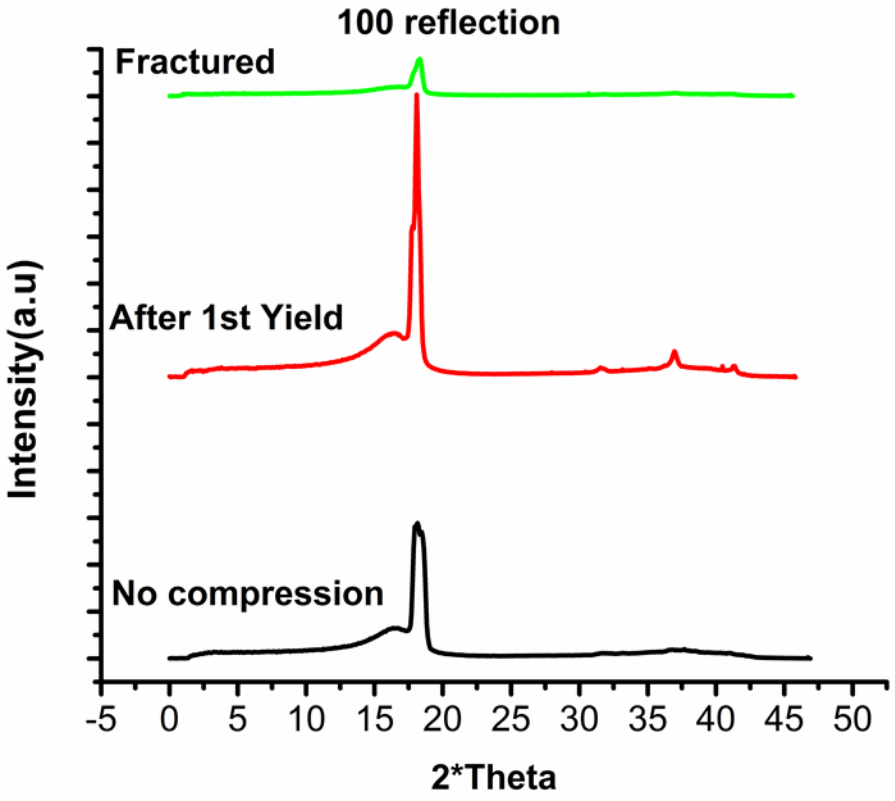

Figure 5-2: 100 WAXS peak for UHMWPTFE specimens with different mechanical histories

5.2.2 Understanding blend miscibility using P-V-T set-up

Chapter 3 involves understanding the effect of different fluoropolymer additives on the sintering kinetics of UHMWPTFE. However, the miscibility of these blends of UHMWPTFE with regrind powder or lower molecular weight PTFE powder needs to be studied as it will affect the final properties of these blends. Herein, we propose a P-V-T set-up that will enable us to do so.

5.2.2.1 Pressure-Volume-Temperature measurement techniques[71]

Piston-Die Technique

In the Piston-Die technique, a cylinder is completely filled with the sample material and the desired pressure is applied on the sample by a piston. Volume change of the sample as a function of pressure and temperature is measured by monitoring the change in position of the piston. The main disadvantage of this technique is that the material is not under hydrostatic pressure. By mathematically analyzing the state of stress and volume changes, it has been shown that the situation is fundamentally different from that of a sample under hydrostatic pressure. Further, it has been shown that the piston-die technique can be applied only when the shear modulus of the sample is significantly lower than the bulk modulus i.e. for liquids or polymer melts[72]. Therefore, this technique cannot be satisfactorily applied to investigate solid state transitions in polymers such as mesophase transition or glass transition. Further, low viscosity liquid samples may result in leakage problem around the piston which necessitates careful designing of seals which in turn is related to increased friction.

Confining Fluid Technique

In the confining fluid technique, the sample is immersed in a confining fluid (often mercury) and the volume change of the entire system (sample plus confining fluid) is monitored as a function of pressure and temperature. Finally, the volume change of the confining fluid is subtracted from this combined response. The disadvantage of this technique is the potential for interaction between the sample and the confining fluid. Further, mercury is toxic and should be avoided. But the advantages far outweigh the drawbacks because in this technique hydrostatic pressure is maintained at all times, there is no leakage problem or friction related issues. Different P-V-T machines based on the confining fluid technique has been developed[73].

5.2.2.2 Solubility Parameter from Pressure-Volume-Temperature data[74]

Hilderbrand solubility parameter[75] is the square root of cohesive energy density expressed as,

$$\delta = \sqrt{{(\Delta H_v - RT)}/{V}}$$

where $\Delta H_v$is the heat of vaporization, R gas constant, T absolute temperature and V molar volume. The heat of vaporization can be obtained from the slope of Clausius-Clapeyron equation:

$$\ln P = -{\Delta H_v}/{RT} + Constant$$

However, this approach cannot be applied for calculating the solubility parameter of polymers as polymer decompose below their vaporization temperature. Allen[76,77]proposed an alternative method for determining cohesive energy density from pressure-volume-temperature data according to which,

$$\delta = \sqrt{T(^{\alpha}/_{\beta})}$$

Where α is the thermal expansion coefficient and β is the compressibility.

Therefore, solubility parameter which can be used for estimating the miscibility for polymer blends can be calculated by measuring the coefficient of thermal expansion from isobars and the compressibility from isotherms.

5.2.2.3 P-V-T apparatus: Proposed Set-up and Description

Figure 5.3 shows the schematic of the setup for doing P-V-T studies. All pipes, fitting and sample chamber will be made of stainless steel rated to at least 1360 bar pressure and 400 ^{o}C which can be obtained from High Pressure Co. (HiP). A nickel or aluminum based anti-seize will be applied to all fittings during assembly. The device will consist of a pressure generating section and a sample chamber. The pressure generating section includes high pressure pump that applies desired pressure on the confining fluid (Galinstan-liquid alloy of Gallium, Indium and Tin). The pressure will be precisely controlled by an automated pressure regulator that is capable of holding a constant pressure and ramping pressure at controlled rates. The sample chamber will be placed within an environmental chamber capable of controlling the temperature precisely. A thermocouple will read the internal temperature inside the sample chamber. The temperature controller and the pressure regulator will be LabVIEW compatible and will be connected to the computer through a NI card. The dimension change of the sample and the confining fluid combined will be measured by an LVDT coil that will surround a non-magnetic steel pipe containing the probe which is a non-magnetic rod fitted with a cylindrical magnet. The LVDT coil will be attached to a NI card and the change in

voltage/dimension change will be recorded using a LabVIEW program. The change in position of the probe can be converted to volume change of the sample as a function of pressure and temperature.

Experiments of interest to this study will include:

- **Isobaric Temperature Sweep:** This set of experiments will measure the specific volume change as a function of temperature at constant pressure. Firstly, this will provide the isobaric thermal expansion co-efficient which is necessary for solubility parameter calculation. Secondly, these experiments will study the effect of hydrostatic pressure on thermal transitions such as glass transition, melting and crystallization.

- **Isothermal Pressure Ramp:** This set of experiments will measure the specific volume change as function of applied pressure at a constant temperature. This will provide the isothermal compressibility which again is necessary to calculate solubility parameters. Further, pressure induced isothermal crystallization can be studied using this class of experiments.

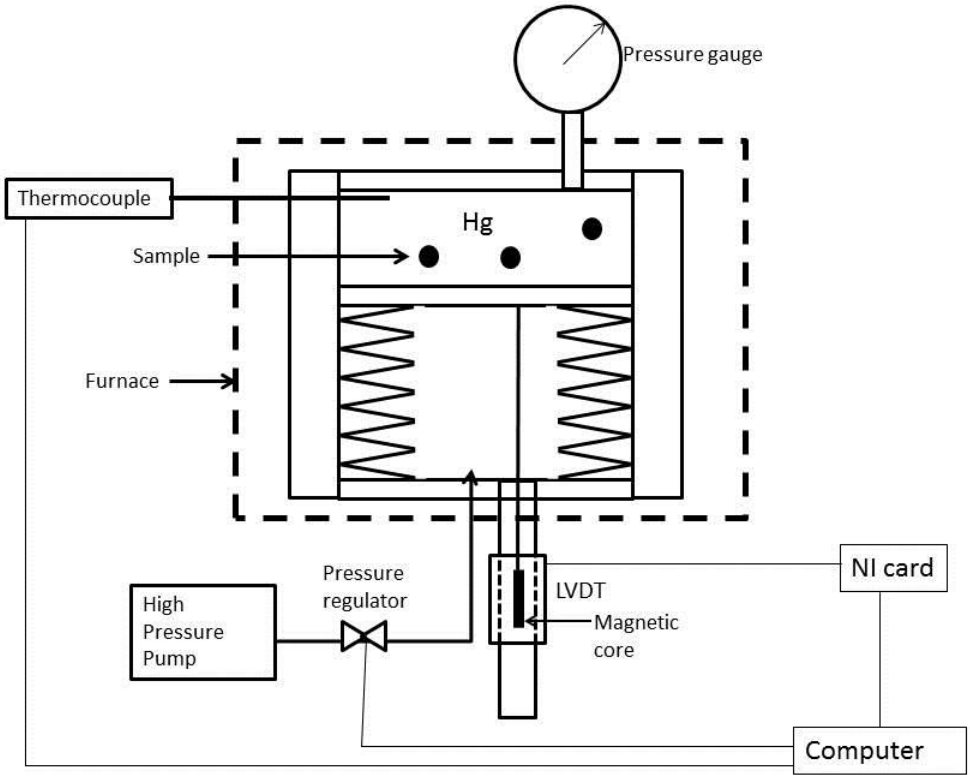

Figure 5-3: Schematic of the set-up for P-V-T studies

BIBLIOGRAPHY

1. S. Ebnesajjad, *Fluoroplastics, Volume 1: Non-Melt Processible Fluoroplastics*, William Andrew, 2000.

2. R. Endo, K. Jounai, H. Uehara, T. Kanamotoand R. S. Porter, *Journal of Polymer Science Part B: Polymer Physics*, **36**, 2551-2562 (1998).

3. A. B. Ariawan, S. Ebnesajjadand S. G. Hatzikiriakos, *Polymer Engineering & Science*, **42**, 1247-1259 (2002).

4. D. M. Bigg, *Polymer Engineering and Science*, **17**, 691-699 (1977).

5. R. J. Crawford, *Polymer Engineering and Science*, **22**, 300-306 (1982).

6. J. P. Jog, *Advances in Polymer Technology*, **12**, 281-289 (1993).

7. K. R. N. J.P. Jog, V.M. Nadkarni, *Int. J. of Materials and Product Technology*, **9**, 155 - 169 (1994).

8. S. S. Hambir, J. P. Jogand V. M. Nadkarni, *Polymer Engineering and Science*, **34**, 1065-1069 (1994).

9. H. Leeand K. Neville, *Handbook of Epoxy Resins*, McGraw-Hill, New York, 1967.

10. A. J. Kinlochand R. J. Young, *Fracture Behaviour of Polymers*, Applied Science Publishers, Northern Ireland, 1983.

11. M. F. Kanninenand C. H. Popelar, *Advanced fracture mechanics*, Oxford University Press, New York, 1985.

12. E. D. Crawfordand A. J. Lesser, *Polymer Engineering and Science*, **39**, 385-392 (1999).

13. X. R. Wangand J. K. Gillham, *Journal of Applied Polymer Science*, **47**, 425-446 (1993).

14. F. F. deNograro, P. Guerrero, M. A. Corcueraand I. Mondragon, *Journal of Applied Polymer Science*, **56**, 177-192 (1995).

15. F. Kusmanto, M. Billhamand P. Hornsby, *Journal of Vinyl and Additive Technology*, **14**, 163-166 (2008).

16. L. Laiarinandrasana, Y. Fuand J. L. Halary, *Journal of Applied Polymer Science*, **123**, 3437-3447 (2012).

17. F. F. deNograro, R. LlanoPonteand I. Mondragon, *Polymer*, **37**, 1589-1600 (1996).

18. F. A. Pfaff. SPI Epoxy Resin Formulators Conference, New Orleans, LA, Nov. 3-5 1996.

19. R. S. Kodyand A. J. Lesser, *Journal of Materials Science*, **32**, 5637-5643 (1997).

20. E. Crawfordand A. J. Lesser, *Journal of Polymer Science Part B-Polymer Physics*, **36**, 1371-1382 (1998).

21. N. C. B. Tan, B. J. Bauer, J. Plestil, J. D. Barnes, D. Liu, L. Matejka, K. Dusekand W. L. Wu, *Polymer*, **40**, 4603-4614 (1999).

22. M. Garcia-Leinerand A. J. Lesser, *Journal of Applied Polymer Science*, **93**, 1501-1511 (2004).

23. K. J. Calziaand A. J. Lesser, *Journal of Materials Science*, **42**, 5229-5238 (2007).

24. D. Lahlali, M. Naffakhand M. Dumon, *Polymer Engineering and Science*, **45**, 1581-1589 (2005).

25. G. Yang, S. Y. Fuand J. P. Yang, *Polymer*, **48**, 302-310 (2007).

26. A. T. Detwilerand A. J. Lesser, *Journal of Materials Science*, **47**, 3493-3503 (2012).

27. I. M. McAninch, G. R. Palmese, J. L. Lenhartand J. J. La Scala, *J. Appl. Polym. Sci.*(2013).

28. Z. H. Yang, A. T. Detwilerand A. J. Lesser, *Journal of Materials Science*, **47**, 4251-4261 (2012).

29. L. Bonnaud, J. P. Pascaultand H. Sautereau, *European Polymer Journal*, **36**, 1313-1321 (2000).

30. S. J. Parkand J. R. Lee, *Journal of Materials Science Letters*, **20**, 773-775 (2001).

31. J. P. Gong, Y. Katsuyama, T. Kurokawaand Y. Osada, *Advanced Materials*, **15**, 1155-1158 (2003).

32. M. Huang, H. Furukawa, Y. Tanaka, T. Nakajima, Y. Osadaand J. P. Gong, *Macromolecules*, **40**, 6658-6664 (2007).

33. R. E. Webber, C. Creton, H. R. Brownand J. P. Gong, *Macromolecules*, **40**, 2919-2927 (2007).

34. R. S. Hoyand M. O. Robbins, *Journal of Polymer Science Part B-Polymer Physics*, **44**, 3487-3500 (2006).

35. E. Ducrot, Y. Chen, M. Bulters, R. P. Sijbesmaand C. Creton, *Science*, **344**, 186-189 (2014).

36. R. N. Haward, Ed. *The Physics of Glassy Polymers*, Chapman & Hall, London, 1997.

37. L. E. Nielsen, Landel, R. F., *Mechanical properties of polymers and composites*, Marcel Dekker, New York, 1994.

38. A. T. Detwilerand A. J. Lesser, *Journal of Applied Polymer Science*, **117**, 1021-1034 (2010).

39. S. Hambirand J. P. Jog, *Bulletin of Materials Science*, **23**, 221-226 (2000).

40. K. M. Kulkarni, L. J. Broutman, S. Kalpakjianand D. B. Emery, *Polymer Engineering and Science*, **16**, 15-24 (1976).

41. A. Pandey, A. Todaand S. Rastogi, *Macromolecules*, **44**, 8042-8055 (2011).

42. J. Frenkel, *J. Phys. (USSR)*, **9**, 385-391 (1945).

43. B. Rosi-Schwartzand G. R. Mitchell, *Polymer*, **35**, 3139-3148 (1994).

44. R. Lovell, G. R. Mitchelland A. H. Windle, *Faraday Discussions of the Chemical Society*, **68**, 46 (1979).

45. J. Yang, K. L. Petersen, R. A. Williams, P. H. Geil, T. C. Longand P. Xu, *Chinese Journal of Polymer Science*, **23**, 123-135 (2005).

46. S. Ebnesajjadand V. Lishinsky, *Machine design*, **71**(1999).

47. H. W. Starkweather, *Journal of Polymer Science: Polymer Physics Edition*, **23**, 1177-1185 (1985).

48. H. Sun, R. S. Cooke, W. D. Batesand K. J. Wynne, *Polymer*, **46**, 8872-8882 (2005).

49. S. Shenoy, D. Woerdeman, R. Sebra, A. Garach-Domechand K. J. Wynne, *Macromolecular Rapid Communications*, **23**, 1130-1133 (2002).

50. S. L. Shenoy, T. Fujiwaraand K. J. Wynne, *Macromolecules*, **36**, 3380-3385 (2003).

51. S. L. Shenoy, T. Fujiwaraand K. J. Wynne, *Macromolecular Symposia*, **201**, 171-178 (2003).

52. M. Lee, C. Tzoganakisand C. B. Park, *Polymer Engineering and Science*, **38**, 1112-1120 (1998).

53. M. Lee, C. Tzoganakisand C. B. Park, *Advances in Polymer Technology*, **19**, 300-311 (2000).

54. Z. Zhangand Y. P. Handa, *Macromolecules*, **30**, 8505-8507 (1997).

55. P. J. Flory.

56. A. Pandey, Y. Champouretand S. Rastogi, *Macromolecules*, **44**, 4952-4960 (2011).

57. T. Suwa, M. Takehisaand S. Machi, *Journal of Applied Polymer Science*, **17**, 3253-3257 (1973).

58. D. A. Ellis, S. A. Mabury, J. W. Martinand D. C. Muir, *Nature*, **412**, 321-324 (2001).

59. L. Melilloand B. Wunderlich, *Colloid & Polymer Science*, **250**, 417-425 (1972).

60. P. H. Geil, J. Yang, R. A. Williams, K. L. Petersen, T. C. Longand P. Xu, **180**, 89-159 (2005).

61. H. G. H. van Melick, L. E. Govaertand H. E. H. Meijer, *Polymer*, **44**, 2493-2502 (2003).

62. R. N. Hawardand G. Thackray, *Proc. R. Soc. A*, **302**(1968).

63. R. N. Haward, *Polymer*, **28**, 1485-1488 (1987).

64. C. Y. C. Leeand W. B. Jones, *Polymer Engineering and Science*, **22**, 1190-1198 (1982).

65. J. A. Hinkley, *Journal of Applied Polymer Science*, **32**, 5653-5655 (1986).

66. L. E. Govaert, H. G. H. van Melickand H. E. H. Meijer, *Polymer*, **42**, 1271–1274 (2001).

67. J. T. A. Kierkels, Dona, C.-L., Tervoort, T. A.,Govaert, L. E., *J. Polym. Sci. B Polym. Phys.*, **46**, 134-147 (2008).

68. A. Peterlin, *Journal of materials science*, **6**, 490-508 (1971).

69. R. Popliand L. Mandelkern, *Journal of Polymer Science Part B: Polymer Physics*, **25**, 441-483 (1987).

70. R. Seguelaand F. Rietsch, *Journal of materials science letters*, **9**, 46-47 (1990).

71. D. Walshand P. Zoller, *Standard pressure volume temperature data for polymers*, CRC Press, 1995.

72. M. Lei, C. Reidand P. Zoller, *Polymer*, **29**, 1784-1788 (1988).

73. P. Zollar, I. H. Mark, N.Bikales, C. Overbergerand G. Mengers, *Encyclopedia of Polymer Science and Engineering* Wiley New York, 1986.

74. S. J. Han, D. J. Lohse, P. D. Condoand L. H. Sperling, *Journal of Polymer Science Part B: Polymer Physics*, **37**, 2835-2844 (1999).

75. J. H. Hilderbrandand R. L. Scott, *The Solubility of Non-Electrolytes*, Van Nostrand Reinhold: Princeton, NJ, 1950.

76. G. A. G. Geeand G. J. Wilson, *Polymer*, **1**, 456-466 (1960).

77. G. Allen, G. Gee, D. Mangaraj, D. Simsand G. J. Wilson, *Polymer*, **1**, 467-476 (1960).